

Preface

Molecular Imaging

Molecular imaging, deals with all the noninvasive imaging techniques that are able to detect and characterize biological processes, at the cellular and/or molecular level, thus allowing higher insights to be achieved from them. It is based on the single or combined use of different techniques as, optical imaging (bioluminescence and fluorescence), ultrasounds, photoacoustic imaging (PAI), magnetic resonance imaging (MRI), magnetic resonance spectroscopy (MRS), nuclear medicine positron emission tomography (PET) or single photon emission computed tomography (SPECT) [1-3].

PET and SPECT are the most sensitive imaging techniques and use a high number of radioactive tracers that are already available for experimental and clinical applications. However patients exposure to ionizing radiation is a major drawback that, together with its inherent low spatial resolution, makes it less favorable than other imaging tools such as Magnetic Resonance Imaging (MRI). Unfortunately, the gain in resolution associated with MRI is accompanied by a loss in sensitivity which is a problem that has been tackled with the use of contrast agents, endowed with very high relaxivity, or resorting to

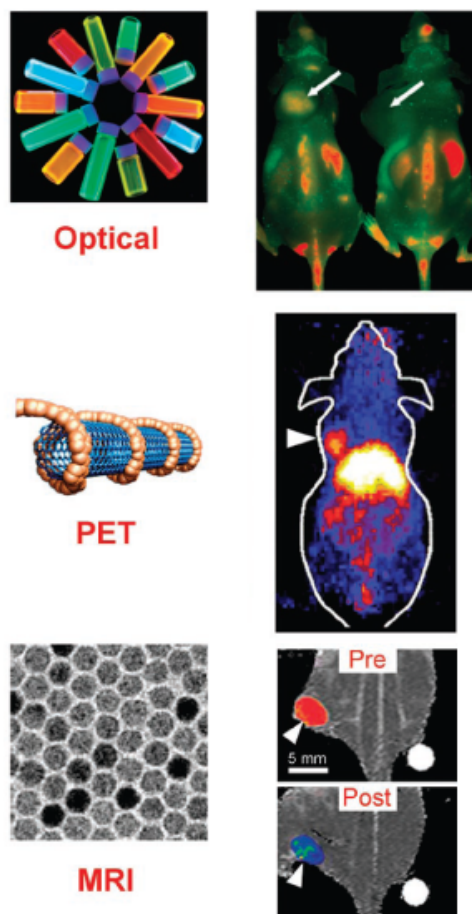


Figure 11 Images of different modalities as representative examples of the use of imaging probes that can serve as platforms for molecular imaging *in vivo* (adapted from [1]).

nanotechnological tools [4].

A recent improvement in imaging modalities is the development of hybrid systems, where the use of multimodality probes exploits the best characteristics of each modality. Nowadays, imaging scanners tend to house different modalities, combining PET/CT and even PET/MRI. Together with the design of new purposely tailored imaging probes, the hybrid scanners overcome the drawbacks and limitations of a single technique, thus considerably improving the overall diagnostic potential of the procedure (Figure 1).

The major characteristics of the most relevant imaging modalities used nowadays are reported in Table 1. Over the last ten years, models derived from nanotechnology have been used to overcome the limitations of conventional modalities, thus improving the sensitivity and accuracy of the diagnosis. Moreover, advances in nanoparticle technology have given rise to theragnostics platforms, defined as the combination of therapeutic and diagnostic agents in a single particle. These techniques unite early diagnosis and possible higher efficiency treatment methods. Typical platforms include liposomes, polymeric micelles, and dendrimers that generally accommodate surface functionalization with hydrophilic polymers and targeting ligands.

Table II Main features of the most relevant imaging modalities (adapted [4]).

Imaging Technique	Source of radiation	Spatial Resolution (mm)	Sensitivity (mol/L)	Probe concentration
PET	High-energy γ rays	1 - 2	10^{-11} - 10^{-12}	pM
SPECT	Lower-energy γ rays	1 - 2	10^{-10} - 10^{-11}	pM
Optical Imaging	Visible light	3 - 5	10^{-15} - 10^{-17}	nM to pM

MRI	Radiowaves	0.025 - 0.1	$10^{-3} - 10^{-5}$	mM to nM
CT	X-rays	0,05 - 0.2	Not characterized	Not well defined
Ultrasound	High-frequency sound	50-500 μm	Not characterized	μM to nM

Aim and outline

Despite success in evaluating the expression of molecular markers, the imaging of the same with MRI remains a challenge mainly due to the technique's low sensitivity. Considerable endeavor has been made in order to overcome this drawback and the encapsulation of MRI contrast agents in nanocarriers emerges as a strategy great potential.

The PhD thesis presented herein emphasizes the importance of MRI as an imaging tool and periodically some insights from optical imaging. The aim of the project is to develop novel probes for enhanced MR imaging via the use of particles as carriers for conventional Gadolinium-based contrast agents. Furthermore, we have aimed at preparing new highly sensitive nanosystems which are able to report on some particular characteristics of pathological tissues, namely enzyme overexpression, pH changes and chemoattractant agents.

Chapter 1 provides a general description of Magnetic Resonance Imaging and an updated revision of the recent improvements in MRI contrast agents and nanoparticles used in pre-clinical and clinical research. In **Chapter 2** a first approach to improving the relaxivity in a given region of interest is presented. The main goal here has been to prepare paramagnetic liposomes which encapsulate the clinically approved Gd-HPDO3A complex and release the imaging probe in the presence of a specific enzyme that is characteristic of a given disease. The resulting liposomal MRI agent has been tested *in vitro* and *in vivo*. In **Chapter 3** we present a distinct methodology for the assessment of enzymatic activity. This

occurs via the disruption of low relaxivity liposome-protein aggregates that are selectively cleaved by the enzyme of interest. This cleavage is associated with an overall relaxation enhancement as the liposome membrane recovers its original permeability to water molecules which was previously impaired by the protein. The *in vivo* exploitation of this technique relies on the entrapment of micron-sized particles into an alginate matrix that has been often used as a biocompatible device in cell-based therapies.

This search for highly sensitive nanoparticles prompted us to consider the micron-sized platform of yeast cell wall particles (YCWPs) whose preparation and characterization are discussed in **Chapter 4**. The peculiar chemical stability of yeast walls enables a new loading protocol to be performed in which the particle inner cavity acts as a micro-reactor for the formation of paramagnetic emulsions of water insoluble Gd-complexes. The high affinity of YCWP to immune system cells led us to exploit the *ex vivo* labeling of immune cells with this type of particles and further track them down into an inflamed region, as presented in **Chapter 5**.

Finally, in **Chapter 6** the principal results of the previous chapters are summarized.

Introduction

1| Magnetic Resonance Imaging

Magnetic Resonance Imaging (MRI) is an outstanding non-invasive technology which allows the acquisition of anatomic images with exceptional spatial resolution. The acquisition of images using the properties of Nuclear Magnetic Resonance (NMR) were first proposed by Raymond Damadian, in 1971, when he discovered that tumor tissues and healthy tissues had different water proton relaxation times [5]. By the same time, Paul Lauterbur had developed the first NMR imaging technique and obtained a "zeugmatogram", a cross-sectional image of two NMR tubes containing pure water (Figure 1) and his work was later published in 1973 [6]. Later on, in 1977, Damadian's group performed the first MRI scan of a human body. Lauterbur, together with Peter Mansfield, were awarded the Nobel Prize for Medicine, in 2003, for their pioneering research in MRI.



Figure 1| First MRI image, denominated zeugmatogram, by Paul Lauterbur, performed in 1971 (adapted from [6]).

Of all the NMR active nuclei (such as ^{13}C , ^{19}F , ^{31}P , ^{15}N , ^{29}Si), ^1H is the element most commonly used in routine MRI due to its high abundance in the human body, essentially, as hydrogen atoms in water molecules.

According to the NMR principle, when a group of spins is under the effect of a given magnetic field, each proton spin aligns

either parallel (low energy state) or anti-parallel (high-energy state) with the magnetic field. However, slightly more protons occupy the low energy state, thus establishing a small net magnetization in the direction of the magnetic field. The number of protons in each energy level is given by the Boltzmann equation:

$$\frac{N_{\text{anti-parallel}}}{N_{\text{parallel}}} = \exp\left[-\frac{\Delta E}{kT}\right] = \exp\left[-\frac{\gamma h B_0}{2\pi k T}\right] \quad \text{eq. 1}$$

where ΔE is the energy gap between the two energy levels, k is Boltzmann's constant (1.3805×10^{-23} J/Kelvin), T is the absolute temperature in Kelvin, B_0 is the magnetic field strength, and h is Planck's constant.

The intensity of the NMR signal is proportional to the energy difference between the two energy states and, therefore, the strength of the magnetic field and the absolute temperature, are factors that affect the MR image.

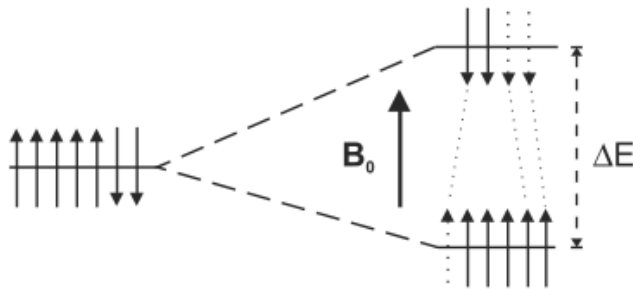


Figure 2I The difference in the energy ΔE between the two energy levels is proportional to the strength of the magnetic field (adapted from [7]).

With an increase in the magnetic field strength there is an increase in the signal to noise ratio (SNR) and, consequently, an higher signal per voxel allows the achievement of better spatial resolution and this leads to the final outcome of high-quality images.

MR signal intensity is affected by three major parameters, namely the proton density (PD) in a given region, the longitudinal relaxation time T_1 , and the transverse relaxation time T_2 . Proton density concerns the concentration of protons in a given region and T_1 and T_2 relaxation times are the time constants of the processes by which the longitudinal and transverse magnetization components, respectively, return to their equilibrium values as protons revert to their resting state, after a stimulatory radiofrequency (RF) pulse. These proton characteristics may change according to the tissue nature and can be different in healthy or pathological regions. The differences in those parameters can be used to create image contrast in the region of interest (ROI).

1.1.1 Contrast Enhancement

Although PD, T_1 and T_2 are primary determinants of the contrast, it can be enhanced by means of applying proper pulse sequences. There are several pulse sequences available for imaging, however the Spin Echo pulse sequence, however, is the most frequently employed (Figure 3). During the spin echo sequence, a first 90° RF pulse is applied and as result, the magnetization vector flips into the transverse plane (x-y). Due to inhomogeneities in the magnetic field, spins start to dephase. The Larmor frequency of a nucleus spin is mainly influenced by the strength of the magnetic field and in an inhomogeneous area the precession is altered (higher magnetic field strength increases the Larmor frequency, while lower strength decreases the frequency). This fact

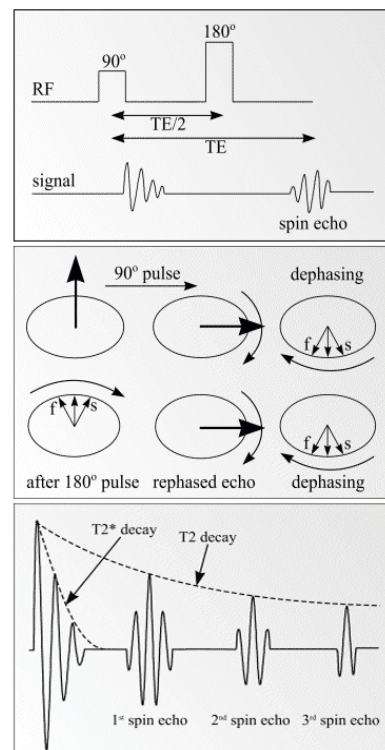


Figure 3 Schematic representation of the Spin Echo pulse sequence and FID decay.

causes signal loss and consequently loss of contrast. To compensate this, a certain time, τ , after the 90° pulse a 180° refocusing pulse is applied, with sufficient energy to flip the magnetization into the (x-y) plane. Then, after the same time, τ , the magnetization components are in phase, as the refocusing pulse produces the so-called "spin echo" [7-11].

Manipulating certain operational parameters (such as the repetition time – T_R and the echo time – T_E), it is possible to acquire three principle types of MR images, namely proton density, T_1 -weighted and T_2 -weighted images (Figure 4).

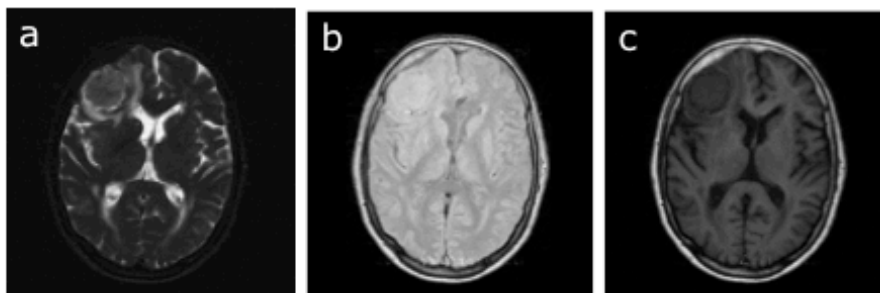


Figure 4I T_2 -w, PD and T_1 -w images of an axial section of human brain (a - T_2 -w: $T_E = 200$ ms, $T_R = 5000$ ms; b - Proton Density: $T_E = 1$ ms, $T_R = 5000$ ms; c - T_1 w: $T_E = 1$ ms, $T_R = 200$ ms)

In a T_1 -weighted image the contrast is mainly due to differences in the T_1 values of tissues. To create this effect, both short T_E and T_R are necessary (Figure 5). When long T_R is used, the tissues in a given region (e.g. water vs. fat) would have already totally recovered their magnetization over the period, and so no contrast is observed. Thus, when using short values of T_R the signal in regions with short T_1 is more intense (brighter image) than in regions with long T_1 (darker image). On the other hand, in a T_2 -weighted image, T_E controls the contrast. Consequently, to perceive contrast, which depends on the transverse relaxation mechanism, a long T_E must be employed thus allowing the different T_2 decays of the spins to

be discriminated. If a short T_E is used, almost no decay takes place and consequently no differences are detected. Thus, when short values of T_E are used, the signal coming from regions with short T_2 is less intense (darker image) than that in regions with long T_2 (brighter image). Finally, in a proton density image, the effects of T_1 and T_2 are minimized and the contrast is solely dependent on the number of protons in the region of interest. Therefore, a sequence with long T_R (minimizing the T_1 -weighting) and short T_E (reducing the T_2 effect) is used. In this case, almost all the regions of a brain are colored the same way, with the exception of the skull (Figure 4) which presents lower proton density. T_1 -weighted, T_2 -weighted and proton density image conditions are summarized in Table II.

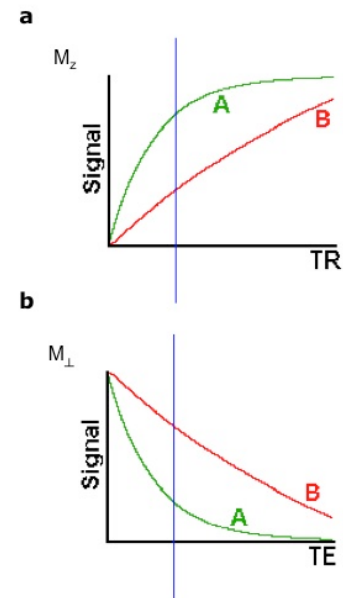


Figure 51 Effect of altering pulse intervals on the T_1 and T_2 contrast (example of water and fat). In a $(T_1)A < (T_1)B$; in b $(T_2)A < (T_2)B$.

Table III Main parameters that influence contrast weighting in a spin echo sequence (adapted from [10, 11]).

TR	TE	Weighting	Stronger Signal
Short (<750 ms)	Short (shortest possible)	T_1	Shorter T_1
Long (>2000 ms)	Short (15-30 ms)	PD	Higher Proton concentration
Long (>2500 ms)	Long (100-200 ms)	T_2	Longer T_2

Sometimes, the inherent contrast in the MR image is insufficient for the proper characterization of the tissue, even after applying the proper pulse sequences. Therefore, in these

cases the application of contrast agents (CAs) is required in order to amplify the contrast differences between healthy and pathological regions, with the final achievement of improved diagnosis and, consequently, the outcome for the patient health.

1.2I Contrast Agents

MRI contrast agents (CAs) are paramagnetic substances which are able to modify signal intensity by altering the relaxation times of water protons in the area where they distribute. Contrast agents are in general referred as T_1 - or T_2 - agents according to whether they predominantly affect the longitudinal or on the transverse relaxation time.

The concept of molecules that are able to change water relaxation times comes from the early times of MRI, when Bloch showed that $\text{Fe}(\text{NO}_3)_3$ had the ability to decrease water proton T_1 and T_2 [12]. Later in 1978, Paul Lauterbur considered paramagnetic ions as contrast agents, showing the potential of manganese chloride in myocardial infarction imaging, in rats and dogs [13]. However, by this time, the toxic effect of free metal ions was already known and therefore the use of stable chelate complexes was indicated as the way to reduce this effect. Actually, in the mid 80's, $\text{Gd}(\text{III})\text{-DTPA}$ was proposed as a contrast agent for

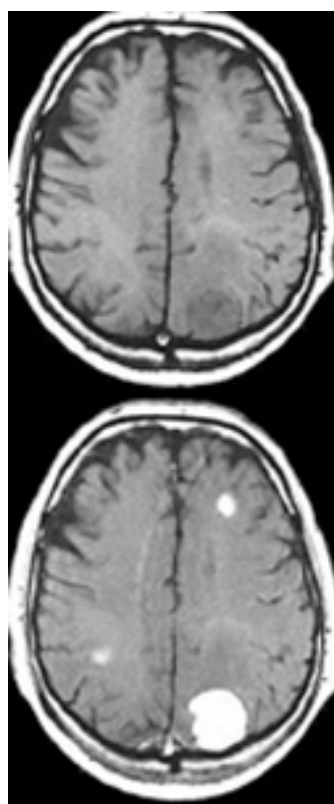


Figure 6I T_1 -weighed images of the brain of a patient with brain tumor. The metastases are detected after the administration of Gd-DTPA (lower image) (adapted from [15]).

clinical studies [14].

The efficiency of a particular contrast agent is expressed by its relaxivity, r_i , which corresponds to its capacity to shorten the relaxation rates $R_i = 1/T_i$ of the water protons and is usually normalized to one millimolar contrast agent concentration, $[CA]$ (eq. 2) [15]:

$$R_i = R_{dia} + r_i[CA] \quad (i=1, 2) \quad \text{eq.2}$$

where R_{dia} is the contribution measured for the system containing the same medium and a diamagnetic analogue of the contrast agent, and $[CA]$ is the contrast agent concentration.

1.2.1I T_1 Contrast Agents

Contrast agents that affect T_1 relaxation time are also called positive contrast agents, due to their ability to virtually increase the signal intensity in the T_1 -weighted images. After Lauterbur's *in vivo* experiments [13], it has become clear that free Mn^{2+} was highly toxic to living beings and so other paramagnetic metal ions, since then, have been considered for MR imaging. Other paramagnetic ions such as Gd^{3+} , Fe^{3+} , among others, are still being continuously studied. Gadolinium (III) (Gd^{3+}) is one of the most frequently used lanthanides due to its particularly favorable characteristics. With seven unpaired electrons and long electron spin relaxation, it has a high effect on nuclei T_1 relaxation times (Figure 7). Nevertheless, as is the case

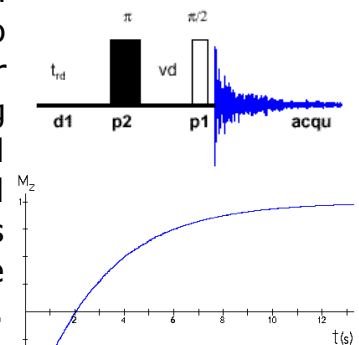
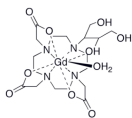
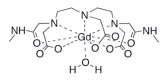
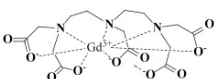
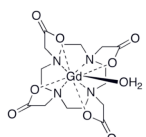


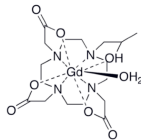
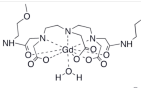
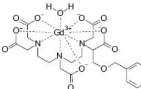
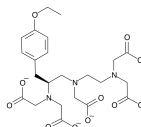
Figure 7I Inversion Recovery pulse sequence for the measurement of T_1 relaxation time.

with all others lanthanides, the use of this metal ion in its free form is not compatible with *in vivo* use, as it is extremely toxic, even in low doses.

In 1984, Leinado [16] reported the first *in vivo* use of a Gadolinium complex the Gd(III)-DTPA (DTPA = diethylenetriaminepentaacetic acid), a contrast agent that was approved for clinical use in 1988. Nowadays, complexes containing the element Gadolinium are amongst the most popular contrast agents used regularly in medicine, and the ligands that complex the metal ion are mainly DTPA or DOTA derivatives (DOTA = tetraazacyclododecanetetraacetic acid). In Table III the major characteristics of several clinically approved CAs are represented.

Table III Characteristics of some clinically approved extracellular fluid and hepatobiliary contrast agents (adapted from [17]).

Generic Name	Registered Name	Abbreviation	Manufacturer	T ₁ -Relaxivity in plasma (s ⁻¹ ·mM ⁻¹ , 1.5T)	Schematic Representation
Gadobutrol	Gadovist	Gd-BT-DO3A	Bayer	5.2	
Gadodiamide	Omniscan	Gd-DTPA-BMA	GE Healthcare	4.3	
Gadopentate dimeglumine	Magnevist	Gd-DTPA	Bayer	4.1	
Gadoterate meglumine	Dotarem	Gd-DOTA	Guerbet	3.6	

Gadoteridol	ProHance	Gd-HPDO3A	Bracco	4.1	
Gadoversetamine	Optimark	Gd-DTPA-BMEA	Mallinckrodt	4.7	
Gadobenate dimeglumine	MultiHance	Gd-BOPTA	Bracco	6.3	
Gadoxetate disodium	Eovist	Gd-EOB-DTPA	Bayer	6.9	

As mentioned above, the efficiency of a particular contrast agent is expressed by its relaxivity, r_i ($i = 1, 2$). To measure the r_1 relaxivity of a specific contrast agent, an Inversion Recovery pulse sequence is applied to determine the water proton T_1 value of a CA aqueous solution. In this type of sequence (Figure 7), a first 180° pulse (π) is applied (that flips the magnetization into the negative half of the z axis) and, after a given time, τ (vd), a 90° ($\pi/2$) pulse is applied in order to flip the magnetization into the x - y plane where the detection coil is located. During τ the magnetization starts to recover towards equilibrium. The dependence of the magnetization on time can be evaluated by applying different τ values and at the end of the experiment a mono-exponential curve is obtained (Figure 7) which can be fitted according to the equation 3, where $M_z(0)$ is the longitudinal magnetization at time 0 and T_1 is the longitudinal relaxation time [10].

$$M_z(TI) = M_z(0) * [1 - 2e^{(-\tau/T_1)}] \quad \text{eq.3}$$

The T_1 value corresponds to the time required to recover 63% of the original magnetization value.

Commercially available Gd^{3+} contrast agents have relaxivities of ca. $4\text{-}5\text{ s}^{-1}\cdot\text{mM}^{-1}$ at typical clinical magnetic field strengths (e.g. 1.5 T, Table II), consequently inducing poor enhancement in a MR image. Thus, the principle challenge presented to chemists in the field has been to design contrast agents with higher relaxivities which are able to be disperse in specific regions of the body or to respond to certain stimuli. A good contrast agent should be highly stable and have the capacity to enhance the relaxation rate of the solvent protons to their potential maxima. The total relaxivity of a Gd(III) complex consists of the additive contributions from the inner-sphere, outer-sphere and, sometimes, second-sphere water molecules (Figure 8). Contrast agent relaxivity optimization can be achieved by increasing the efficiency of several of the molecular parameters that determine the relaxivity of its inner-sphere contribution. These include the number of water molecules coordinated to the metal ion (q), the exchange lifetime of those water molecules (τ_M) and the re-orientational correlation time (τ_R) of the complex, as represented in appendix A.

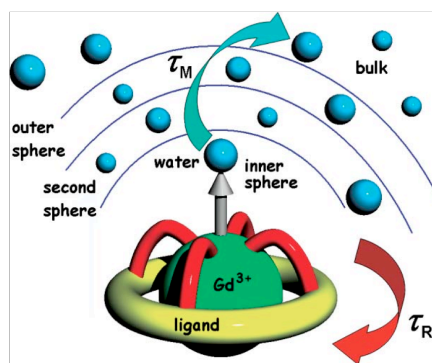


Figure 8I Illustration of the molecular parameters that influence the relaxivity of a small Gd(III) complex as a CA .

The number of water molecules, q , is typically equal to one due to the octadenticity of the ligands normally used and the fact that Gd^{3+} ion generally hosts nine donor atoms in its coordination sphere. This type of coordination scheme allows the formation of highly stable complexes that prevent the leakage of the metal ion [18]. Several groups have been extensively working on the preparation of coordination cages with that form Gd^{3+} complexes with a higher q number and,

consequently, improved relaxivity. Examples of these highly sensitive contrast agents have been prepared by Raymond's group using the hexadentate HOPO (tripodal hydroxypyridinone ligand) or related ligands (eg. HOPO-TAM), with six oxygen donor atoms thus allowing the coordination of two (and even three) water molecules. Other solutions are represented by the use of ligands such as PCTA-[12] (3,6,9,15-tetraaz-abicyclo [9.3.1]pentadeca-1(15),11,13-triene-3,6,9-triacetate), DO3A (1,4,7,10-tetra-azacyclododecane-tris acetic acid) or AAZTA (6-amino-6-methylperhydro-1,4- diazepinetetraacetic acid), as shown in the Figure 10 [15, 18-22].

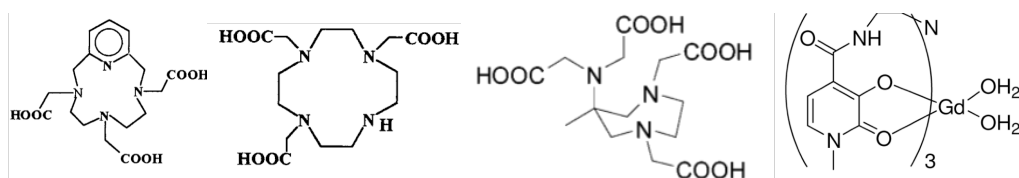


Figure 9 Schematic structure of some ligand cages used to prepare highly sensitive Gadolinium based contrast agent with $q = 2$. From left to right: PCTA-[12], DO3A, AAZTA, TREN-1-Me-3,2-HOPO.

The molecular rotational correlation time, τ_R , mainly depends on the molecular radius of the complex and thus (if extensive internal flexibility is not presented) higher molecular weight induces a lengthening of the τ_R and consequently the relaxivity is higher at 0.5-1.5 Tesla fields (Figure 10).

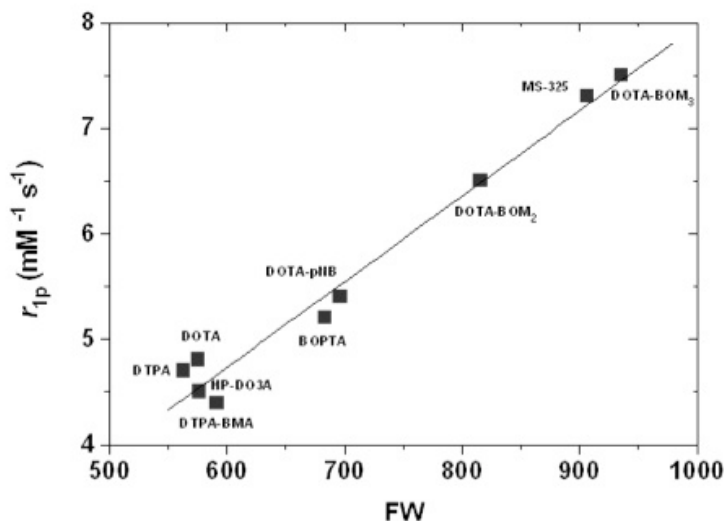
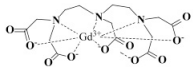
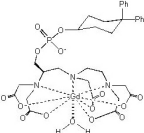


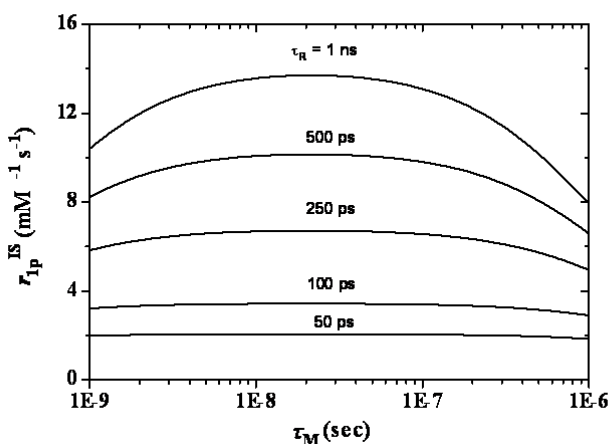
Figure 10I Correlation of the r_1 relaxivity (20 MHz) with the molecular weight of several Gd(III) complexes (adapted from [15]).

A great deal of effort has been made in order to increase the T_R parameter, for instance, by covalently or non-covalently binding the complexes to macromolecules. Vasovist® (Bayer Schering Pharma AG, Berlin/Germany, code name MS-325) was the first clinically approved contrast agent which can boast this characteristic. This probe consists of a Gd(III)-DTPA cage functionalized with a diphenylcyclohexylphosphate group that confers a strong affinity to human serum albumin (HSA). Hence, after intravenous injection, Vasovist strongly and non-covalently binds to the serum protein, resulting in a significant increase in the relaxivity (Table IV) [23, 24].

Table IVI Comparison of Gd-DTPA and Vasavovist relaxivity values (adapted from [24]).

		Field Strength		
		0.47T	1.5T	3.0T
Gd-DTPA		3.8	4.1	3.7
Vasovist		28-47	19-28	10-19

Finally, the exchange lifetime of the water molecules, τ_M , is also a crucial parameter that affects the observed relaxivity. As shown in Figure 11, an excessively slow τ_M has a detrimental effect on r_1 (essentially because the effect of the paramagnetism is inefficiently passed to the bulk water), whereas a fast water exchange has the same effect on r_1 , as the water molecules are not in contact to the lanthanide ion long enough and so do not experience its paramagnetic effect [15, 19, 25].

**Figure 11I** Relationship between the effects of τ_M and water exchange rate on the r_1 relaxivity (adapted from [25]).

Water exchange lifetime is strongly affected by several factors that influence the water exchange mechanism. These include the nature of the coordination arms (e.g. carboxamide vs. carboxylate), the overall charge of the complex and the presence of bulky substituents which destabilize the complex

structure relative to its transition state and thus promote a water dissociative mechanism [15, 26]. The τ_M value can be calculated from the fitting of the temperature dependence profiles of the transverse relaxation rate of ^{17}O labeled water.

Nowadays, some of the most sensitive contrast agents are substituted Gd-calix[4]arenes, whose r_1 relaxivity of around $70 \text{ s}^{-1}\cdot\text{mM}^{-1}$ increases up to $100 \text{ s}^{-1}\cdot\text{mM}^{-1}$ when conjugated to HSA [27]. Despite their high relaxivity, it is necessary to inject several grams of contrast agent into the blood stream to obtain satisfactory contrast, and non-specific CAs are systematically and rapidly cleared through the kidneys. An ideal contrast agent should also be specific to a certain body region so that the amount of probe injected into the patient could be significantly decreased. A way to overcome this problem is upon using systems which are able to work as carriers for the contrast agents. Currently, different types of carriers are reported in the literature as ways of increasing the concentration of the probe in the area of diagnostic interest. This aspect will be further discussed in section 2.

1.2.2I T₂ Contrast Agents

A successful way of decreasing T_2 is the use of iron oxide-based contrast agents which, besides their ability to decrease the transverse relaxation time, are also able to cause local field inhomogeneities, thus leading to even faster NMR signal decay [28]. Consequently, in a T_2 -weighted image, the region where the probe is accumulated becomes darker. However, it has recently been demonstrated that, using the proper sequence, iron oxide-based contrast agents can also enhance the T_1 contrast in a MR image [29, 30]. In this way, it is still possible to observe the effect of superparamagnetic iron oxide nanoparticles (SPIO), in regions without any signal, thus overcoming one of the major drawbacks of negative contrast agents. SPIOs usually consist of a magnetite (Fe_3O_4) or

maghemite ($\gamma\text{Fe}_2\text{O}_3$) core, coated with a natural or synthetic polymer and can be characterized according to their mean size, and are divided in three main categories – Oral SPIO, Standard SPIO (SSPIO) and Ultrasmall SPIO (USPIO), as shown in Table V.

Table VI Name and characteristics of commercial superparamagnetic iron oxide nanoparticles.

Classification	Trade name	Coating material	Hydrodynamic diameter
Oral SPIO	Lumirem	Silicon	300 nm
	Abdoscan	Sulphonated styrene	3.5 μm
SSPIO	Endorem	Dextran	80-180 nm
	Resovist	Carboxydextran	60 nm
USPIO	Clariscan	Pegylated Starch	20 nm
	Supravist	Carboxydextran	30 nm
	Sinerem	Dextran	15-40 nm

The low toxicity of SPIOs allows their application in imaging procedures, such as macrophage infiltration in inflammatory regions, cancer diagnosis and the early detection of cardiovascular diseases. Nevertheless, the most promising application of this type of contrast agents concerns the detection of the fate of cells in vivo, after their previous labeling [31, 32].

Paramagnetic liposomes can also be included in the class of T_2 agents and their effect mainly depends on the magnetic moment of the paramagnetic complexes, on the amount of agent entrapped in the vesicle as well as on its dimensions and the magnetic field. Still, few reports are available in the literature on such systems [33, 34].

1.3I Classification of contrast agents

The search for the ideal contrast agent has led to the appearance of a massive number of potential candidates and to the need for a proper classification based on their chemical properties, mechanism of action or biological distribution. For instance, most typical Gadolinium-based contrast agents (Magnevist, Dotarem, and others) distribute in the extracellular compartment. On the other hand, hepatobiliary system agents tend to accumulate in the hepatocytes, as represented in Table VI.

Table VII Classification of contrast agents (adapted from [35, 36]).

Classification	Characteristics	Examples
Non-specific extracellular agents	<p>After intravenous injection, leak from the blood pool into the interstitial space due to their small molecular weight.</p> <p>These agents do not have the ability to cross an intact blood-brain barrier. They provide visualization of regions with abnormally high permeability, such as tumors or lesions.</p>	<p>Magnevist®, Dotarem®, Omniscan®, ProHance®, Gadovist®, MultiHance® and OptiMARK®.</p>
Blood pool agents	<p>Agents in this class have higher molecular weight than those in the previous class, a fact that prevents their release into the interstitial space and so they remain for longer periods in the blood stream.</p> <p>This characteristic allows for the imaging of the vasculature.</p>	<p>Vasovist®, Vistarem®, Sinerem®, Combidex® and Supravist®.</p>

Organ-specific agents	<p>Some existing contrast agents have a natural tendency to be internalized by a specific cell type.</p> <p>Several sub-classes could be considered but as an example one could take, for instance, some derivatives of Gd-DTPA which are already in clinical use as a tool for the diagnostic of hepatic lesions, after it was demonstrated that they are entrapped by the hepatocytes.</p>	<p>Primovist®, Eovist®, Tealascan®, Feridex®, Endorem®, Resovist®,</p>
Targeting agents	<p>These agents are able to recognize specific moieties on the cell surface.</p> <p>Although this is a rather elegant methodology, it suffers from low target area concentration, making it difficult to achieve sufficient contrast. Nevertheless, targeted nanoparticles seem to be a way of overcoming this major drawback.</p>	<p>Liposomes with RGD moiety associated, for neiovasculature targeting; Liposomes functionalized with folate, etc [47, 48].</p>
Responsive agents	<p>These so-called “smart agents” are sensitive to certain stimuli that include pH, enzymatic activity, redox potential, etc, allowing the characterization of the microenvironment of the region of the interest to be achieved.</p> <p>A typical example of this type of CAs is Egad, a Gd-DOTA derivative. In this molecule, a sugar moiety blocks the access of the water molecule to its coordination site. Upon enzyme activation, the sugar is released and allows the coordination of H₂O to the paramagnetic center. In this case, the increase in the water relaxivity is directly correlated to the activity of β-galactosidase (the enzyme studied), a commonly used gene marker.</p>	<p>Egad, Gd-DOTA-serotonin, etc.</p>

2I Nanocarriers

The interest in nanosystems (Figure 12) arose from the need to enhance the *in vivo* efficiency of many drugs once it was proven that the optimal concentration of the therapeutic agents in cell cultures

needs to be increased to higher concentrations *in vivo*, resulting in more intense side effects. Actually, several pharmaceuticals display poor solubility, instability or short half lifetimes in blood,

resulting in inefficient treatment and higher toxicity risks. Indeed, nanocarriers offer several advantages when working as drug delivery vehicles and an extensive number of nanoparticles have been reported in the literature of which liposomes are one of the most cited types. Nowadays, more than 20 nanosystems are in clinical use and several more under clinical trials or pre-clinical development [37].

More recently, the ability of nanoparticles to work as carriers for a variety of molecules has come into play, in a new strategy in which therapeutics and diagnostics are combined in a single particle, giving rise to new theragnostic agents. The word theragnostics is derived from the Greek words *therapeia* (to treat) and *gnosis* (knowledge) referring to the monitorization of the response to a specific treatment and, for this reason, molecular imaging is providing new opportunities in the preclinical and clinical development of new and improved therapies.

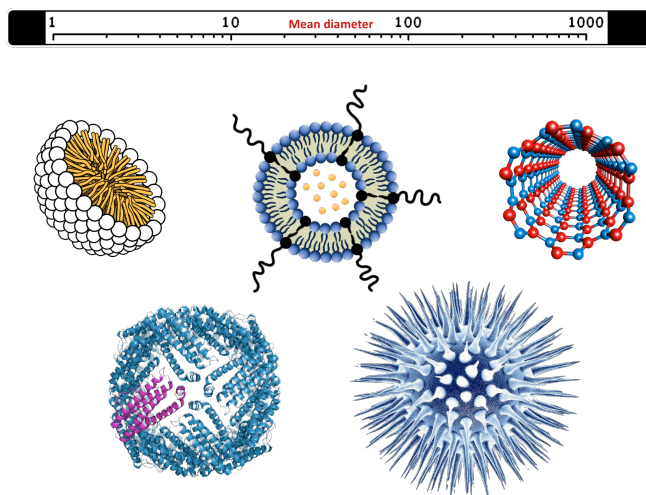


Figure 12I Schematic representation of several particulate systems (scale in nm).

2.1I Paramagnetic Lipid-Based Particles

Lipid-based nanoparticles are among the most intensively studied groups of nanoparticles and liposomes are the vehicles most frequently used. The diversity present within this type of systems is illustrated in Table VII.

Table VIII Characteristics of lipid-based nanoparticles (adapted from [38, 39]).

Carrier	Size Range	Composition	Common preparation technique
Liposomes	25 nm-few microns	Natural or synthetic phospholipids	Passive and active loading
Solid Lipid Nanoparticles	50-1000 nm	Fats with high melting points of natural origin	High pressure homogenization, microemulsion formation and precipitation
Oily Suspensions	10 nm-few microns	Natural or synthetic oils	Dispersion technique
Lipid Microbubbles	Few microns	Lipids, phospholipids polymers and proteins	Sonication
Lipid Microspheres	0.2-100 μm	Lipids or phospholipids with high melting points	Melt method, multiple microemulsions, preincorporation into lipophilic carriers.

Bangham first referred to them in 1964, while he was studying red blood cell membranes' and often these particles are "affectionately" called "Bangasomes". Liposomes can be described as nanosized artificial unilamellar vesicles of a commonly spherical shape, prepared with either natural or

chemically modified lipids, which can be loaded with a variety of water-soluble or insoluble drugs [38].

Several liposome preparation procedures have been reported and they contain some common steps, which include the hydration of the lipidic film, a sizing stage and their purification from non-entrapped materials. In brief, as is represented in Figure 13, the appropriate lipids must first be dissolved and mixed in an organic solvent in order to form a homogeneous mixture of all the membrane components. Once the proper mixture is obtained, the organic solvent is removed, usually by rotary evaporation, yielding a thin lipid film. This lipidic film is then hydrated via the simple addition of an aqueous solution and, as amphiphilic phospholipids self-associate into bilayers, the outcome are multilamellar vesicles (MLVs) whose size can be controlled by either sonication or extrusion. During the extrusion, liposomes are forced through a polycarbonate filter with a defined pore size, yielding particles with a mean size around that of the pore diameter. Alternatively, during the sonication, high energy in the ultrasound range is applied, inducing a mechanic force that agitates the particles in a sample, breaking intermolecular interactions and creating a population of smaller liposomes [40].

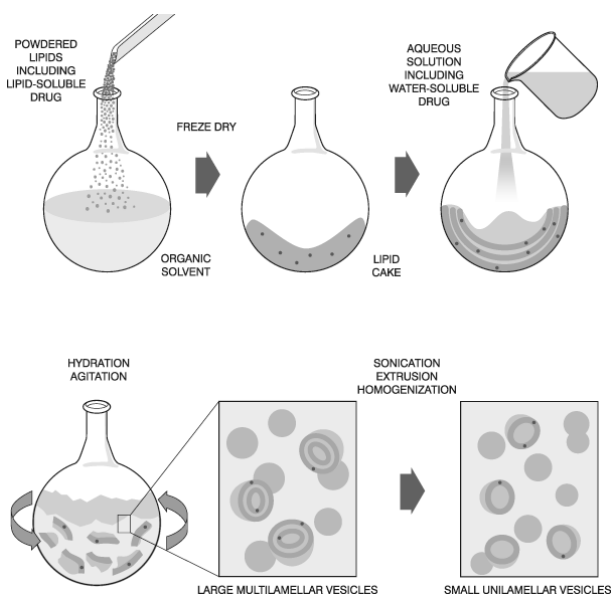


Figure 13I Schematic representation of liposome preparation steps (adapted from [40]).

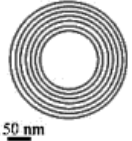
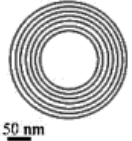
usually by rotary evaporation, yielding a thin lipid film. This lipidic film is then hydrated via the simple addition of an aqueous solution and, as amphiphilic phospholipids self-associate into bilayers, the outcome are multilamellar vesicles (MLVs) whose size can be controlled by either sonication or extrusion. During the extrusion, liposomes are forced through a polycarbonate filter with a defined pore size, yielding particles with a mean size around that of the pore diameter. Alternatively, during the sonication, high energy in the ultrasound range is applied, inducing a mechanic force that agitates the particles in a sample, breaking intermolecular interactions and creating a population of smaller liposomes [40].

The entrapment of the chosen drug can also be achieved through several different processes, including (i) the

incorporation of the drug in the aqueous solution, (ii) the use of lipophilic drugs, (iii) active entrapment methods such as pH gradient protocols and (iv) electrostatic interactions between drug and the liposome membrane.

The characteristics of the liposome membrane can be tuned by changing the lipid composition, thus achieving certain physico-chemical properties, as size, surface charge (defined by the zeta potential), stability, bilayer rigidity and permeability. In this way, liposomes can be classified according to their structural properties, i.e., size and number of lamellae or charge. For instance, in Table VIII, liposomes are classified according to their size and membrane morphology.

Table VIII Liposome classification and nomenclature.

Abbreviation	Denomination	Diameter	Morphology
SUV	Small unilamellar vesicles	20-100 nm	
LUV	Large unilamellar vesicles	>100 nm	
GUV	Giant unilamellar vesicles	>1 μm	
OLV	Oligolamellar vesicles	0.1-0.5 μm	
MLV	Multilamellar large vesicles	>0.5 μm	

The fate of liposomes after their intravenous injection is determined by a subset of properties. Shortly after they were proposed as drug carriers, it became apparent that liposomes were rapidly recognized and removed from the circulation by

the reticuloendothelial system (RES). To avoid detection by the immune system, “stealth liposomes” were purposed. These are functionalized with a hydrophilic coating on the outside of the liposome membrane, which enables longer blood half-life times. The first approach consisted in preparing liposomes with characteristics similar to red blood cells by adding monosialoganglioside (GM1) to the liposome surface. Later, liposomes coated with a synthetic lipid derivative of poly (ethylene glycol) (PEG) were also proposed and this is nowadays the most widely used method of increasing the circulation time of liposomes [41-43]. However, although poly (ethylene glycol) is able to decrease the extent of liposomal uptake by the reticuloendothelial system, recent reports have shown evidence that after a second dose, PEG-coated liposomes were rapidly cleared from the blood [44].

Typically tumor blood vessels are prone to leakage due to the lack of tight junctions between endothelial cells, giving rise to the so-called enhanced permeability and retention (EPR) effect. Liposomes are thus able to enter tumor interstitium. However, at level, the presence of poly(ethylene glycol) impairs the uptake of liposomes by the tumor cells. Taking this fact into account and to facilitate the capture by cells, “detachable” PEG conjugates (DSPE-S-S-PEG5000) were proposed in which the PEG is released due to the tumor redox microenvironment [45]. A distinct method of increasing liposomal accumulation in the region of interest relies on the covalent attachment at the extremity of PEG of a ligand targeting an internalizing receptor. This is done in a similar way to what has already been referred to contrast agents in the section 1.3.

Several liposome formulations have already been clinically approved, numerous others are under clinical trial (Table IX).

Table IXI Examples of liposomal formulations clinically approved or under clinical trials (adapted from [37, 46]).

Composition	Trade name	Company	Indication	Administration
Clinically approved liposomal formulations				
Liposomal amphotericin B	Abelcet	Enzon	Fungal Infections	I.V
Liposomal cytarabine	Depocyt	SkyePharma	Malignant lymphomatous meningitis	I.T
Liposomal daunorubicin	Daunoxome	Gilead Sciences	HIV-related Kaposi's Sarcoma	I.V
Liposomal doxorubicin	Myocet	Chephalon (EU) and Sopherion Therapeutics (USA)	Metastatic Breast cancer	I.V.
Liposome-PEG doxorubicin	Doxil/Caelyx	Ortho Biotech, Schering-Plough	HIV-related Kaposi's Sarcoma, Metastatic breast and ovarian cancer	I.V.
Liposomal IRIV vaccine	Inflexal V/ Epaxal	Berna Biotech	Influenza/ Hepatitis A	I.M.
Liposomal morphine	DepoDur	SkyePharma, Endo	Postsurgical analgesia	Epidural
Micellular estradiol	Estrasorb	Novavax	Menopausal therapy	Topical

Liposome formulations under clinical trials

Liposomal annamycin	L- Annamycin	Callisto	Phase I – Acute lymphocytic leukemia, acute myeloid leukemia Phase II - Progressive osteogenic sarcoma	I.V.
Liposomal cisplatin	SLIT Cisplatin	Transave	metastatic to the lung	Aerosol
Liposomal doxorubicin	Sarcodoxom e	GP-Pharm	Phase I/II – Soft tissue sarcoma	I.V.
Liposomal fentanyl	AeroLEF	Delex Therapeutics	Phase II – Postoperative analgesic	Aerosol
Liposomal Iurtotecan	OSI-211	OSI Pharmaceuticals	Phase II - Ovarian cancer	I.V.
Liposomal Vincristine	Onco TCS	Inex, Enzon	Non- Hodgkin's lymphoma	I.V.

Besides liposomes, other particles are being exploited, namely polymeric micelles, dendrimers, carbon nanotubes and quantum dots, with potential application in a wide variety of areas such as gene therapy, photodynamic therapy and cancer theragnostics, among others [37].

Nanotechnology plays an extraordinary role in the development of imaging, diagnosis and drug delivery tools. Newly developed systems offer the possibility of achieving an improved knowledge of their interaction with biological systems. Moreover, there the hope that the increasing research in this

field will contribute to the translation of the technology to the clinics.

References

1. Cai, W. and X. Chen, Nanoplatforms for targeted molecular imaging in living subjects. *Small*, 2007. 3(11): p. 1840-54.
2. Frullano, L. and T.J. Meade, Multimodal MRI contrast agents. *J Biol Inorg Chem*, 2007. 12(7): p. 939-49.
3. Wang, X., et al., Photoacoustic imaging with a commercial ultrasound system and a custom probe. *Ultrasound Med Biol*. 37(3): p. 484-92.
4. Massoud, T.F. and S.S. Gambhir, Molecular imaging in living subjects: seeing fundamental biological processes in a new light. *Genes Dev*, 2003. 17(5): p. 545-80.
5. Damadian, R., Tumor detection by nuclear magnetic resonance. *Science*, 1971. 171(976): p. 1151-3.
6. Lauterbur, P.C., Image formation by induced local interactions. Examples employing nuclear magnetic resonance. 1973. *Clin Orthop Relat Res*, 1989(244): p. 3-6.
7. Brown, M.A. and R.C. Semelka, *MRI: Basic Principles and Applications*. 2010: Wiley, John & Sons.
8. Westbrook, C., C.K. Roth, and J. Talbot, *MRI in Practice Vol. 3rd Edition*. 2007: Wiley, John & Sons.
9. Hashemi, R.H. and W.G. Bradley, *MRI - THE BASICS*. 1997: Williams & Wilkins.
10. Rinck, P.A., *Magnetic Resonance in Medicine*. 2001: Wiley-Blackwell.
11. McRobbie, D.W., et al., *MRI from Picture to Proton*. 2007: Cambridge University Press.
12. Bloch, F., W. Hansen, and M. Packard, The Nuclear Induction Experiment. *Physical Review*, 1946. 70(7-8): p. 12.
13. Mendonca-Dias, M.H., E. Gaggelli, and P.C. Lauterbur, Paramagnetic contrast agents in nuclear magnetic resonance medical imaging. *Semin Nucl Med*, 1983. 13(4): p. 364-76.
14. Carr, D.H., Paramagnetic contrast media for magnetic resonance imaging of the mediastinum and lungs. *J Thorac Imaging*, 1985. 1 (1): p. 74-8.

15. Aime, S., M. Botta, and E. Terreno, Gd(III)-based contrast agents for MRI. *Advances in Inorganic Chemistry - Including Bioinorganic Studies*, Vol 57, 2005. 57: p. 173-237.
16. Laniado, M., et al., First use of GdDTPA/dimeglumine in man. *Physiol Chem Phys Med NMR*, 1984. 16(2): p. 157-65.
17. Aime, S. and P. Caravan, Biodistribution of gadolinium-based contrast agents, including gadolinium deposition. *J Magn Reson Imaging*, 2009. 30(6): p. 1259-67.
18. Bottrill, M., L. Kwok, and N.J. Long, Lanthanides in magnetic resonance imaging. *Chem Soc Rev*, 2006. 35(6): p. 557-71.
19. Terreno, E., et al., Challenges for molecular magnetic resonance imaging. *Chem Rev*. 110(5): p. 3019-42.
20. Aime, S., et al., NMR relaxometric studies of Gd(III) complexes with heptadentate macrocyclic ligands. *Magn Reson Chem.*, 1998. 36: p. S200-S208.
21. Aime, S., et al., [Gd-AAZTA]-: a new structural entry for an improved generation of MRI contrast agents. *Inorg Chem*, 2004. 43(24): p. 7588-90.
22. Pierre, V.C., et al., Substituent effects on Gd(III)-based MRI contrast agents: optimizing the stability and selectivity of the complex and the number of coordinated water molecules. *Inorg Chem*, 2006. 45(20): p. 8355-64.
23. Fink, C., M. Goyen, and J. Lotz, Magnetic resonance angiography with blood-pool contrast agents: future applications. *Eur Radiol*, 2007. 17 Suppl 2: p. B38-44.
24. Goyen, M., Gadofosveset-enhanced magnetic resonance angiography. *Vasc Health Risk Manag*, 2008. 4(1): p. 1-9.
25. Caravan, P., Strategies for increasing the sensitivity of gadolinium based MRI contrast agents. *Chem Soc Rev*, 2006. 35(6): p. 512-23.
26. *The Chemistry of Contrast Agents in Medical Magnetic Resonance Imaging*, ed. A. E. Merbach and E. Toth, 2001: John Wiley & Sons.
27. Schuhle, D.T., et al., Calix[4]arenes as molecular platforms for magnetic resonance imaging (MRI) contrast agents. *Chemistry*, 2009. 15(13): p. 3290-6.
28. Makowski, M.R., et al., Molecular imaging with targeted contrast agents. *Top Magn Reson Imaging*, 2009. 20(4): p. 247-59.

29. Saleh, A., et al., In vivo MRI of brain inflammation in human ischaemic stroke. *Brain*, 2004. 127(Pt 7): p. 1670-7.
30. Bjornerud, A. and L. Johansson, The utility of superparamagnetic contrast agents in MRI: theoretical consideration and applications in the cardiovascular system. *NMR Biomed*, 2004. 17(7): p. 465-77.
31. Mahmoudi, M., et al., Magnetic resonance imaging tracking of stem cells in vivo using iron oxide nanoparticles as a tool for the advancement of clinical regenerative medicine. *Chem Rev*. 111(2): p. 253-80.
32. Huang, C., et al., Surface functionalization of superparamagnetic nanoparticles for the development of highly efficient magnetic resonance probe for macrophages. *Contrast Media Mol Imaging*. 6 (4): p. 298-307.
33. Castelli, D.D., et al., Evidence for in vivo macrophage mediated tumor uptake of paramagnetic/fluorescent liposomes. *NMR Biomed*, 2009. 22(10): p. 1084-92.
34. Delli Castelli, D., et al., In vivo MRI multicontrast kinetic analysis of the uptake and intracellular trafficking of paramagnetically labeled liposomes. *J Control Release*. 144(3): p. 271-9.
35. Bellin, M.F., MR contrast agents, the old and the new. *Eur J Radiology*, 2006. 60(3): p. 314-323.
36. Geraldes, C.F.G.C. and S. Laurent, Classification and basic properties of contrast agents for magnetic resonance imaging. *Contrast Media Mol Imaging*, 2009. 4(1): p. 1-23.
37. Zhang, L., et al., Nanoparticles in medicine: Therapeutic applications and developments. *Clinical Pharmacology & Therapeutics*, 2008. 83 (5): p. 761-769.
38. Mulder, W.J.M., et al., Lipid-based nanoparticles for contrast-enhanced MRI and molecular imaging. *NMR Biomed*, 2006. 19(1): p. 142-164.
39. Rawat, M., et al., Lipid carriers: A versatile delivery vehicle for proteins and peptides. *Yakugaku Zasshi-Journal of the Pharmaceutical Society of Japan*, 2008. 128(2): p. 269-280.
40. Lasic, D.D., *Liposomes in Gene Delivery*. 1997: CRC-Press.
41. Drulis-Kawa, Z. and A. Dorotkiewicz-Jach, Liposomes as delivery systems for antibiotics. *Int J Pharm*. 387(1-2): p. 187-98.

42. Gabizon, A. and D. Papahadjopoulos, Liposome formulations with prolonged circulation time in blood and enhanced uptake by tumors. *Proc Natl Acad Sci U S A*, 1988. 85(18): p. 6949-53.
43. Allen, T.M., et al., Liposomes containing synthetic lipid derivatives of poly(ethylene glycol) show prolonged circulation half-lives in vivo. *Biochim Biophys Acta*, 1991. 1066(1): p. 29-36.
44. Ishida, T., et al., Accelerated blood clearance of PEGylated liposomes following preceding liposome injection: effects of lipid dose and PEG surface-density and chain length of the first-dose liposomes. *J Control Release*, 2005. 105(3): p. 305-17.
45. McNeeley, K.M., et al., Masking and triggered unmasking of targeting ligands on nanocarriers to improve drug delivery to brain tumors. *Biomaterials*, 2009. 30(23-24): p. 3986-95.
46. Immordino, M.L., F. Dosio, and L. Cattel, Stealth liposomes: review of the basic science, rationale, and clinical applications, existing and potential. *Int J Nanomedicine*, 2006. 1(3): p. 297-315.
47. Sipkins, D.A., et al., Detection of tumor angiogenesis in vivo by alphaVbeta3-targeted magnetic resonance imaging. *Nat Med*, 1998. 4(5): p. 623-6.
48. Winter, P.M., et al., Molecular imaging of angiogenesis in nascent Vx-2 rabbit tumors using a novel alpha(nu)beta3-targeted nanoparticle and 1.5 tesla magnetic resonance imaging. *Cancer Res*, 2003. 63(18): p. 5838-43.

MRI visualization of release from liposomes triggered by enzymes

Abstract

We have envisaged an approach to design enzyme-responsive agents based on the use of Gd(III)-loaded liposomes. Vesicles exposing a peptide acting as a MMP substrate and encapsulating a clinically approved Gd(III) agent were prepared and tested *in vitro* by measuring the relaxivity over time in the presence of collagenase. We demonstrate that the enzyme triggers the release of the imaging probe through a destabilisation of the liposome membrane, thus causing a relaxivity enhancement. *In vivo* kinetic experiments following the intratumor injection of the lipopeptide-containing liposome in a melanoma mouse model indicated a rapid washout of the imaging probe from the tumor. This finding is consistent with a release of the MRI probe in the extracellular tumor fraction, where MMPs accumulate. In the future, a system as this one could be used as a theragnostic agent in which an anti-tumoral drug could be co-encapsulated with the MRI probe, allowing monitoring *via* MRI the drug delivery/release process.

Introduction

When Magnetic Resonance is the imaging modality of choice, it is necessary to design highly sensitive systems in order to overcome the relatively low sensitivity of the technique. This issue can be tackled by using nanosystems that are able to deliver to the target a very high number of imaging agents. Among them, liposomes have attracted much attention due to their favorable pharmacokinetic and pharmacodynamic properties and the relative easiness they can be tailored to fit the biological features of the target pathology and the agent to be delivered. These self-assembling lipid-based soft nanovesicles are primarily used as drug-delivery carriers, and, recently, there has been a growing interest to set-up protocols for imaging guided drug delivery [1-3].

The release of a liposomal payload within a localized area can be triggered upon destabilization of the liposome membrane, following external (e.g. heat, light, and ultrasound) or internal stimuli (e.g. enzymatic activity or pH), and exploiting peculiar characteristics of diseased tissue (e.g. enzymes that are up-regulated and changes in pH) [4-8]. On this basis, the exploitation of the activity of specific enzymes could be used as an approach for the diagnosis of a several types of pathologies. Recently, some reports have presented enzymatically cleavable lipids, which are specifically cleaved by enzymes overexpressed in the extracellular space in tumor tissues [9-11]. Nihar Sarkar and co-workers presented an interesting example, where a lipopeptide containing a cleavage site for Matrix Metalloproteinase-9 (MMP-9) was incorporated into the liposome membrane [12-16]. In the presence of the enzyme, the lipopeptide was cleaved and, as consequence of the induced destabilization of the liposome membrane, its content was released.

Matrix Metalloproteinases (MMPs) are a family of zinc-dependent endoproteases, up-regulated in many pathologies (e.g. cancer, atherosclerotic plaques, multiple sclerosis, etc.), that degrade proteins in the extracellular matrix (ECM). They are key players in many physiological processes, such as

embryonic development, morphogenesis, reproduction, among others, and their expression is regulated by growth factors, hormones and cytokines [17]. For instance, oncogenic cellular transformation induces expression of high levels of MMPs in tumor cells that are later secreted to the extracellular space, with major roles in tumor progression, specifically interfering with angiogenesis, invasion and metastasis. Under these circumstances, the over-expression of MMPs can therefore be explored for site-specific triggered release of imaging probes encapsulated in nanoparticles. For this purpose, standard peptide sequences, namely Proline-Leucine-Glycine-Leucine-Tryptophane-Alanine-Arginine (PLG*LWAR) and Leucine-Tryptophane-Leucine-Alanine-Proline-Glycine-Arginine (LWLAPGR) [9, 11], which have been demonstrated to act as MMPs substrates, have been incorporated in the membrane of nanoparticles.

Aiming at assessing the potential of MRI for the visualization of enzymatic-triggering release of drugs from liposomes, the goal of this work is to design paramagnetic liposomes encapsulating the clinically approved complex Gadoteridol (Chart 1), able to release the imaging probe in the presence of MMP using a novel amphiphilic lipopeptide.

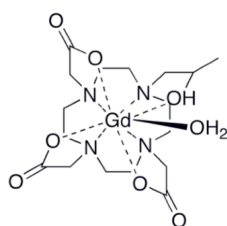


Chart 11 Representation of Gadoteridol (Gd-HPDO3A) complex, the registered trademark of ProHance.

To evaluate the *in vivo* activity of matrix metalloproteinases, a “smart” MRI imaging probe must be designed, with an optimized release of its content in response to the

microenvironment MMP activity. The ideal probe, in the absence of the MMP activity, should be silent from the MRI point of view, i.e. it must display a reduced relaxivity. Several peptide motifs were proposed for the detection of MMPs and are commonly composed of standard peptide sequences, as the (PLG*LWAR) and LWLAPGR [9], which are cleaved by MMPs. Due to the low sensitivity of MRI, a crucial point is to maximize the availability of nanoparticles at the target tissue, where the stimuli should induce the release of the contrast agents. Thus, the aim of this work is to prepare paramagnetic liposomes encapsulating a high amount of the clinically approved Gadoteridol complex and exposing a novel amphiphilic lipopeptide on their surface, and to evaluate the ability of such systems to release the imaging probe in the presence of MMPs. When the Gd chelate is confined in the liposome, the water mobility across the lipidic bilayer is reduced, thus quenching the effect of the paramagnetic metal. The probe release triggered by the enzyme will result in a r_1 relaxivity and T_1 contrast enhancement.

Hereby, we present the synthesis and optimization of the designed lipopeptide, whose peptidic part (an octapeptide) was properly selected in order to act as substrate for collagenases. The peptide was linked to a stearic acid chain, and then incorporated into the bilayer of liposomes encapsulating Gadoteridol, in order to expose the peptidic substrate to the exterior of the nanovesicle. The ability of the MRI nanoprobe to report the activity of MMPs from the class of Collagenases was assessed first *in vitro* using relaxometric techniques, and then *in vivo* by MRI in a mouse bearing a B16-F10 melanoma syngeneic tumor. The proposed system could have the potential ability to work as a theragnostic agent if in addition to the contrast agent, the particle is loaded with a proper drug.

Material and Methods

Materials

Reagents and solvents for solid-phase peptide synthesis (SPPS) were purchased from ABI Chemicals (Seveso, MI, Italy), and Rink Amide resin was received from Merck Chemicals Ltd, Nottingham, UK). All other reagents, including Fmoc protected amino acids, were received from Sigma-Aldrich (Milan, Italy). Dipalmitoyl-glycerophosphatidylcholine (DPPC) and Dipalmitoyl-glycerosuccinate (DPGS) were purchased from Avanti Polar Inc. (Alabaster, AL, USA). ProHance (Gd-HPDO3A) was kindly provided by Bracco Imaging S.p.A. (Milan, Italy, Partner 21). All the other chemicals were purchased from Sigma-Aldrich, namely Collagenase from *Clostridium histolyticum*, Matrix metalloproteinase 1, stearic acid and cholesterol.

Synthesis of the amphiphilic lipopeptides (LP₁ and LP₂)

The amphiphilic lipopeptides LP₁ (PLGLWAR, MMPs substrate) and LP₂ (LWLAPGR, used as negative control) were synthesized by a standard solid phase synthesis using an automated peptide synthesizer (Liberty CEM automated microwave peptide synthesizer) equipped with a microwave-enhanced reactor. Briefly, the Fmoc-protected arginine was linked to Rink Amide resin (loading 0.64 mmol/g, double-coupling) and the other aminoacids were subsequently added. Finally, the stearic acid moiety was attached to proline, the last aminoacid of the peptide sequence (double-coupling). All the synthesis steps were performed in the presence of Pybop and DIPEA as the coupling agent and 40% piperidine in Dimethylformamide (DMF) to release the Fmoc protection groups. After the synthesis was concluded, the lipopeptide was removed from the resin, in a cleavage accomplished by 5% Trifluoroacetic acid (TFA) and 95% triisopropylsilane, and final deprotection of tryptophan was achieved by 10% acetic acid. LP₁ and LP₂ were purified by Reverse Phase chromatography (Xterra®Prep RP18, 5 µm particle size) on a gradient of H₂O/0.1% TFA and CH₃CN/

0.1% TFA as eluents. The obtained products were characterized on a Waters 3100 Mass Detector.

Liposome preparation and characterization

Liposomes were prepared using the well-established procedure based on the hydration of a thin lipidic film. The following lipid formulations were prepared (total lipid amount 20 mg): Lipo-LP₁: DPPC/Chol/DPGS/LP1 (32.5/32.5/5/10 molar ratio), Lipo-LP₂: DPPC/Chol/DPGS/LP2 (32.5/32.5/5/10) and Lipo-SA: DPPC/Chol/DPGS/SA (32.5/32.5/5/10). The lipids were dissolved in chloroform and the organic solvent was then removed under reduced pressure using a rotary evaporator until a thin film of dry lipid was formed on the wall of the flask. After completing the solvent removal (sample under vacuum pump for ca. 2 hours), one mL of a 200 mM isotonic solution of ProHance (the marketed formulation of Gadoteridol), whose osmotic pressure was adjusted to 300 mOsm by using HEPES/NaCl buffer, was added to the film and the hydration was accomplished by a gentle vortexing at 338 K. The obtained multilamellar vesicles (MLV) were sequentially extruded (4 times) through polycarbonate membranes with a pore size of 400 and 200 nm, using a Lipex high-pressure extruder (Northern Lipids, Vancouver, Canada). The non-encapsulated Gadoteridol was removed by dialysis (two cycles of 4 h each, at 277 K) against isotonic buffer (HEPES 10 mM/NaCl 140 mM) at pH 7.4. The mean size and polydispersity of the resulting unilamellar liposomes was assessed by dynamic light scattering (Zetasizer NanoZS, Malvern, UK).

The effective Gd(III) concentration (C_{eff}) in the total liposome suspension volume was estimated by the NMR bulk magnetic susceptibility method [18] using tert-butyl alcohol as inert reference. The chemical shift measurements were carried out on a Bruker Avance 600 NMR spectrometer (Bruker Biospin, Rheinstetten, Germany).

Relaxometric characterization and enzymatic assay

¹H relaxation rate measurements

The longitudinal water proton relaxation times T_1 were measured at 298 K on a Stelar Spinmaster FFC (Stelar, Mede, Pavia, Italy) NMR relaxometer operating at 20 MHz, using the standard inversion-recovery sequence. The temperature was controlled by a Stelar VTC-91 air flow heater equipped with a copper-constantan thermocouple. The actual temperature was checked inside the probe head (uncertainty of ± 0.1 K) by using a digital thermometer. The relaxation rates R_1 were normalized to a millimolar concentration of Gd(III) through the following equation:

$$r_1 = \frac{R_1 - R_{1dia}}{[Gd]} \quad \text{eq. 1}$$

where R_{1dia} is the relaxation rate of a liposomal sample not loaded with any paramagnetic Gd(III) complex. The enzyme kinetic effect on the liposomes was studied by incubating the liposomes at 310 K under gentle stirring. The R_1 values were measured as a function of the incubation time.

Animal models

B16-F10 murine melanoma cells were grown in DMEM medium supplemented with 10% FBS, 2 mM glutamine, 100 U/ml penicillin and 100 $\mu\text{g/ml}$ streptomycin. Six to 10-week-old female C57Bl6 mice (Charles River Laboratories, Calco, Italy) were inoculated subcutaneously with 1×10^6 B16-F10 cells suspended in phosphate buffer saline.

MRI measurements

Longitudinal (T_1) and transverse (T_2) water proton relaxation times were measured on a Bruker Avance 300 NMR

spectrometer (Bruker Biospin, Karlsruhe, Germany) operating at 7.05 T, equipped with a Micro 2.5 micro-imaging probe. T_1 values were measured using a spin echo sequence preceded by an inversion pulse. T_2 values were measured using a spin multi-echo sequence (50 echoes, echo time 3.3 ms). The in vivo MR images were obtained at the same instrument using a coil with an inner diameter of 30 mm. A series of axial spin-echo T_1 -weighted images (echo time 3.3 ms, repetition time 250 ms) were acquired over time after intra-tumor injection of the liposomal suspension. The T_1 contrast was calculated as enhancement percentage ($T_1^{\text{enh}\%}$) using the following expression:

$$T_1^{\text{Enh}\%} = \frac{I_{\text{post}} - I_{\text{pre}}}{I_{\text{pre}}} \times 100 \quad \text{eq. 2}$$

where I_{PRE} and I_{POST} are the MR signal intensities of a region of interest within the tumor before and after the intra-tumor injection of the liposomes, respectively. Such intensities were normalized with respect to an external reference represented by a 5 mm tube filled with an aqueous solution of Gadoteridol.

Results and Discussion

Preparation and characterization of the paramagnetic liposomes

The amphiphilic lipopeptides LP₁ and LP₂ (Figure 1) were synthesized in order to have a MMP substrate and a non-cleavable control, able to be readily incorporated in a liposome bilayer. As the aim is to trigger a destabilization of the nanovesicle upon the enzyme action, a slightly less stable incorporation of the substrate could be favorable, so a single C₁₈ alkylic chain was selected as hydrophobic portion of the substrate.

The relaxivity of Lipo-LP₁ (0.47 T, 298 K) normalized to the millimolar concentration of the encapsulated paramagnetic complex was $1.2 \text{ s}^{-1}\cdot\text{mM}^{-1}$, i.e. about three-fold lower than the one of the non-encapsulated Gd-complexes ($4.2 \text{ s}^{-1}\cdot\text{mM}^{-1}$). This relaxivity “quenching” is due to the very slow water exchange across the liposome membrane. Such effect decreases the transfer efficiency of the paramagnetic relaxation induced by the metal complex to the bulk water protons. From the extent of this “quenching”, the water permeability across the liposome bilayer can be estimated through a simple calculation [20]. Assuming that the intraliposomal concentration of ProHance corresponds to that one of the solution used for hydrating the lipid film, a water permeability of $1.5 \text{ mm}\cdot\text{s}^{-1}$ was calculated for Lipo-LP₁. This number is ca. 7-fold larger than the one reported for DPPC-based liposomes ($0.2 \text{ mm}\cdot\text{s}^{-1}$) [20], thus suggesting that the incorporation of LP₁ leads to a partial destabilization of the bilayer structure. As support to this hypothesis, the relaxivity of Lipo-SA was much lower ($0.34 \text{ s}^{-1}\cdot\text{mM}^{-1}$) and the corresponding water permeability was very close ($0.4 \text{ mm}\cdot\text{s}^{-1}$) to the value observed for DPPC-based liposomes. On the same basis, the relaxivity of the other control formulation Lipo-LP₂ is also quite reduced ($0.41 \text{ s}^{-1}\cdot\text{mM}^{-1}$) as well as its water permeability ($0.3 \text{ s}^{-1}\cdot\text{mM}^{-1}$), suggesting that indeed only LP₁ somehow interacts with the liposome membrane, influencing the membrane stability. The equations used for the calculation of the liposome water permeability are represented in Appendix B.

Testing the liposomes performance in vitro

The release properties of the developed liposomes in the presence of collagenases were first assessed in vitro by relaxometric measurements. As the imaging probe has a lower relaxivity when encapsulated, its release from the vesicle will be accompanied by a relaxivity enhancement. In a typical experiment, collagenases were added to the three liposomal preparations (Lipo-LP₁, Lipo-LP₂ and Lipo-SA), followed by the r_1 measurements over time.

In the presence of collagenases (a mixture of several enzymes), the liposome formulation containing LP₁ released part of its contents, and the release was slightly higher in the presence of MMP1, a pure enzyme, likely due to a partial, small instability of the liposome. However, it is noteworthy that the final relaxivity is lower (3.0 vs. 4.2 s⁻¹·mM⁻¹) than the value expected in the case of a complete release of the imaging probe from the vesicle.

Nevertheless, the relaxivity of Lipo-LP₁ in the presence of the enzymes increases much more rapidly with respect to the small enhancement observed without adding the proteases, reaching an enhancement of ca. 150 % in less than one hour. However, the liposome alone is not completely stable, presenting a slow background leakage. It has to be noticed that even in the absence of the enzyme the relaxivity increases by ca. 60 % after 3 h, thus indicating a rather low stability of this formulation. In fact, with the control formulations (with the scrambled peptide and the stearic acid) the collagenases had no detectable effect, thus confirming that the enhancement observed is related to the enzyme activity. Furthermore, the initial relaxivity of these formulations is lower than the relaxivity of the formulation with the MMP substrate, suggesting that the presence of this lipopeptide is influencing the permeability of the membrane (Figure 3).

The aforementioned result has been confirmed by a MRI experiment performed at 7.05 T (Figure 4), where the T₁w-images showed clear differences in MR T₁ contrast due to the triggered-release of the probe by the enzyme activity.

In order to demonstrate that the observed relaxation enhancement was really due to a release of the probe and not related to an increase of the water permeability of the liposome membrane, the transverse relaxivity (r₂) was measured. It is known that the compartmentalization of a paramagnetic chelate inside the nanovesicle can generate an additional and specific contribution to the T₂ relaxation, especially at high magnetic fields [21]. Hence, it is expected that the release of the probe is accompanied by a r₂ decrease, whereas an increase of the

water permeability should not affect (or eventually enhance) the r_2 value. Figure 5 reports the r_2 and r_1 values measured, at 7.05 T, at time 0 and after 24 h for Lipo-LP₁ liposomes with and without 1% collagenases. The r_2 reduction after 24 h for the untreated liposome confirms the low stability of this formulation, whereas the decrease observed as soon the enzyme was added indicates that the T_1 enhancement is primarily caused by the release of the probe from the vesicle.

Concerning the mechanism underlying the release, the most reliable hypothesis would involve the “uncorking” of the lipopeptide from the vesicle bilayer induced by the enzyme-substrate binding. A similar mechanism has been proposed for accounting the release observed in serum for liposomes incorporating fatty acids in their bilayer [8]. In that case, it was demonstrated that the release was induced by the high affinity displayed by serum albumin towards fatty acids. Such binding allowed the extraction of the bilayer component with the consequent destabilization of the nanovesicle. Analogously, the high affinity between LP₁ and the proteases investigated could be the key-factor responsible for the release of the imaging agent from Lipo-LP₁ sample.

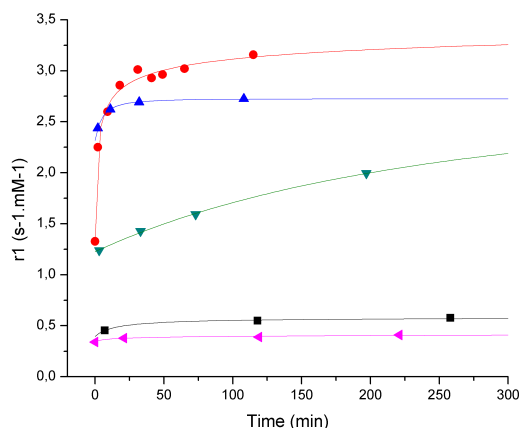


Figure 31 Kinetic timeframe of the relaxivity for the investigated liposomes at 0.47 T and 298 K: pink – Lipo-SA + Coll 1%, black – Lipo-LP₂ + Coll 1%, green – Lipo-Lp₁, blue – Lipo-LP₁ + Coll 1% and red – Lipo-LP₁ + 1 μM MMP1.

Testing the liposomes performance in vivo

The three liposomal formulations were also tested *in vivo*, and in order to better appreciate the release features of such systems, they were directly injected in mice bearing syngeneic B16-F10 melanoma tumors. Just after the injection (10 μ L) of the liposomal suspension, the evolution of the T_1 contrast was monitored over time. Figure 6 reports the temporal evolution of the T_1 contrast for the three liposomal formulations, whereas Figure 7 illustrates the kinetic variation of the tumor T_1 contrast. Using the formulation containing the MMP substrate (Lipo-LP₁) it was possible to observe a decrease in the signal over time consistent with the release of the probe from the liposome and consequent excretion. With both control formulations one could detect a delayed enhancement not observed with the lipopeptide.

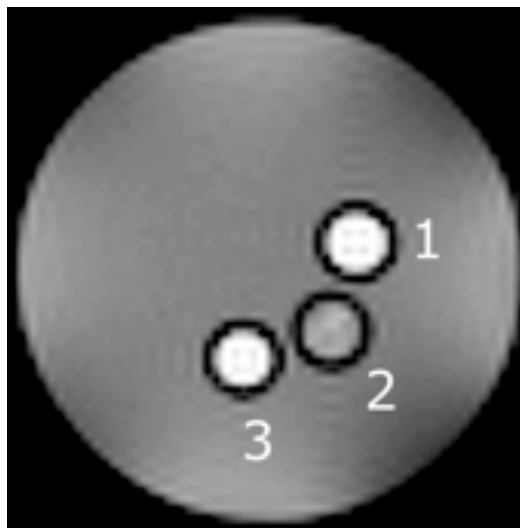


Figure 41 MR T_1 -weighted image of a phantom containing 1 – a solution of Gadoteridol, 2 – a suspension of Lipo-LP₁ and a 3 - suspension of Lipo-LP₁ + Coll 1%.

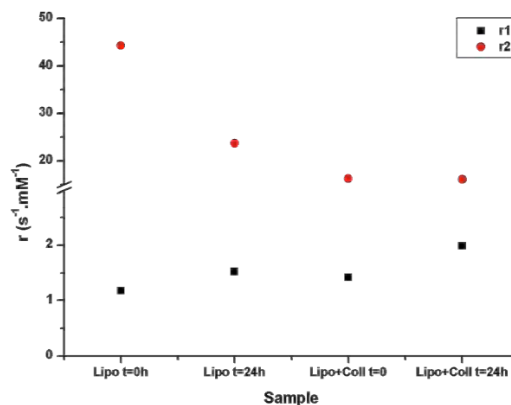


Figure 51 Longitudinal and transverse relaxivity for Lipo-LP₁ with and without 0.1% Collagenase at time 0 h (just after the addition of the enzyme) and after 24 h.

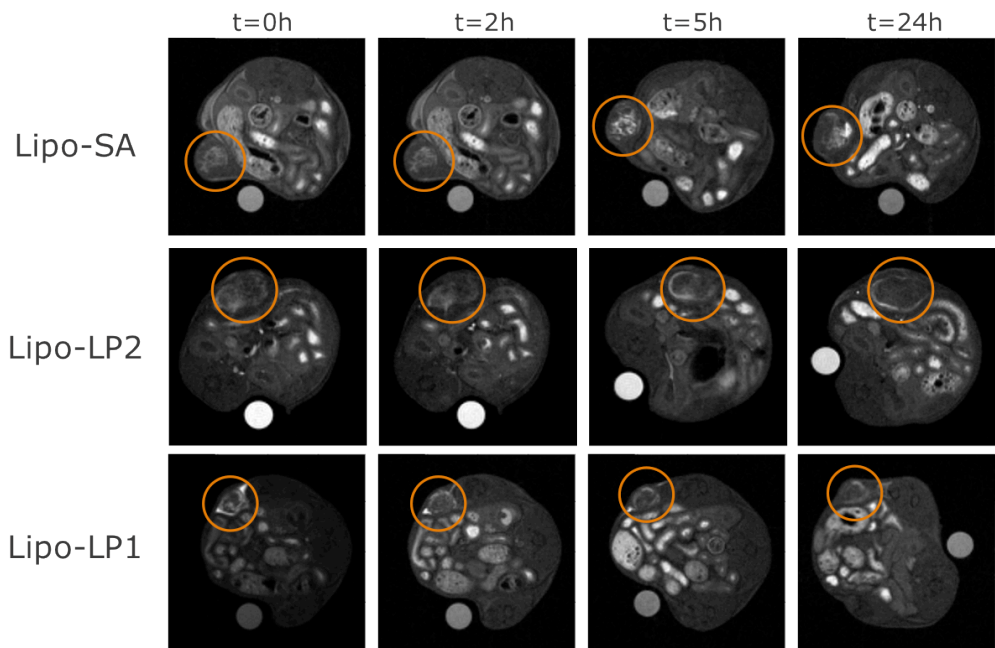


Figure 6I Axial MR images of mice bearing syngeneic B16-F10 melanoma tumors (labeled with the red circle) after intra-tumor injection of Lipo-SA (upper row), Lipo-LP₂ (middle row) and Lipo-LP₁ (bottom row).

The T_1 contrast was calculated as enhancement percentage using eq.2 and the result plotted as a function of the time (Figure 7). The main difference between the two kinetics is the late T_1 enhancement observed for both controls (Lipo-LP₂ and Lipo-SA), that is completely missing for the kinetic of the liposome containing the lipopeptide acting as an MMP substrate (Lipo-LP₁).

The delayed T_1 enhancement is consistent with results observed for other liposomal formulations, including conventional stealth and pH sensitive liposomes [22], which were described as an intracellular release of the imaging probe following the vesicle degradation. The lack of this feature for the LP₁-based formulation, whose kinetics is similar to that observed after injection of the free Gd-agent, could be an indication of the early release of the complex in the extracellular fluid where MMPs are present. Consequently, this finding suggests that *in*

vivo, the enzymatic kinetics appears to be faster (or at least competitive) than the cellular uptake. Thus, the results hereby presented seem to corroborate the indication that the release of the imaging probe is taking place extracellularly, being quickly washed out by the tumor vasculature (Figure 8). For the control formulations, at the beginning of the experiment, right after the injection of liposomes in the tumor, the paramagnetic metal is entrapped in the liposomes, and dispersed in the extracellular compartment. This step is then followed by the cellular internalization of the liposomes that leads to the localization of liposomes into endosomes. Once there, due to the characteristics of these intracellular organelles, liposomes start losing their integrity, causing the release of their payload. At this stage, the rate of the release depends on the stability of the liposome membrane (liposomes with stearic acid have higher stability than those with Lipo-LP₂). Later on, the paramagnetic metal is released back from the cells to the extracellular space, from where it is washed out by the blood stream.

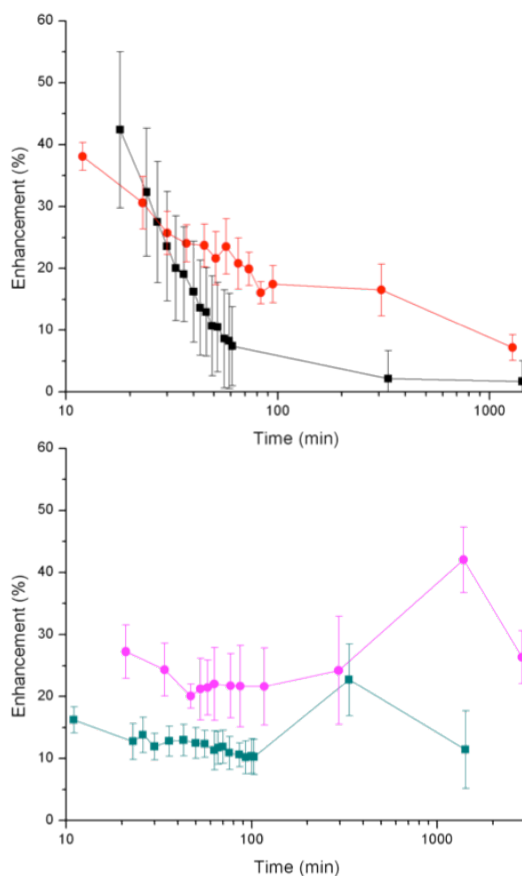


Figure 71 Time evolution of the T₁ contrast in the tumor for ProHance (in black), Lipo-Lp₁ (in red), Lipo-SA (in pink) and Lipo-LP₂ (green).

Conclusions

A novel liposomal formulation, designed for the MRI visualization of drug-delivery by enzyme triggered release by MRI, has been developed and characterized. Though the stability of the formulation in the absence of the triggering stimulus still needs to be optimized, the *in vivo* results on a mouse syngeneic tumor model are quite encouraging and demonstrate the good potential of these nanocarriers to accumulate and release the drug in the extracellular space of the tumor. In order to proceed with a potential clinical application for these systems, there is the need to give them stealthiness, a process usually done by the incorporation of hydrophilic polymers like PEG (polyethylene glycol) in the membrane of the liposomes. There are several reports in the literature that indicate that PEG does not interfere with enzyme kinetics (due to a potential stereotactic impedance) [23, 24].

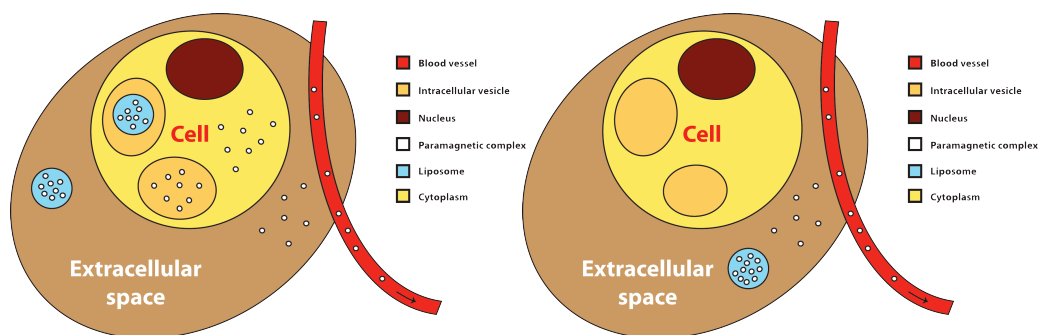


Figure 8I Schematic representation of the proposed intra-tumor fate of Lipo-LP₂/Lipo-SA (right) and Lipo-LP₁ (left).

In summary, the results obtained suggest that the liposomal formulation hereby presented has potential for future *in vivo* therapeutic preclinical studies.

References

1. Lammers, T., et al., Nanotheranostics and image-guided drug delivery: current concepts and future directions. *Mol Pharm.* 7(6): p. 1899-912.
2. Hynynen, K., MRI-guided focused ultrasound treatments. *Ultrasonics.* 50(2): p. 221-9.
3. Shubayev, V.I., T.R. Pisanic, 2nd, and S. Jin, Magnetic nanoparticles for theragnostics. *Adv Drug Deliv Rev*, 2009. 61(6): p. 467-77.
4. Hanahan, D. and R.A. Weinberg, The hallmarks of cancer. *Cell*, 2000. 100(1): p. 57-70.
5. Hanahan, D. and R.A. Weinberg, Hallmarks of cancer: the next generation. *Cell.* 144(5): p. 646-74.
6. Lee, E.S., Z. Gao, and Y.H. Bae, Recent progress in tumor pH targeting nanotechnology. *J Control Release*, 2008. 132(3): p. 164-70.
7. Stubbs, M., et al., Causes and consequences of tumour acidity and implications for treatment. *Mol Med Today*, 2000. 6(1): p. 15-9.
8. Torres, E., et al., Improved paramagnetic liposomes for MRI visualization of pH triggered release. *J Control Release.* 154(2): p. 196-202.
9. Gialeli, C., A.D. Theocharis, and N.K. Karamanos, Roles of matrix metalloproteinases in cancer progression and their pharmacological targeting. *FEBS J.* 278(1): p. 16-27.
10. Amalinei, C., et al., Matrix metalloproteinases involvement in pathologic conditions. *Rom J Morphol Embryol.* 51(2): p. 215-28.
11. Scherer, R.L., J.O. McIntyre, and L.M. Matrisian, Imaging matrix metalloproteinases in cancer. *Cancer Metastasis Rev*, 2008. 27(4): p. 679-90.
12. Banerjee, J., et al., Release of liposomal contents by cell-secreted matrix metalloproteinase-9. *Bioconjug Chem*, 2009. 20(7): p. 1332-9.
13. Banerjee, J., et al., Liposome-mediated amplified detection of cell-secreted matrix metalloproteinase-9. *Chem Commun (Camb).* 46(18): p. 3209-11.

14. Elegbede, A.I., et al., Mechanistic studies of the triggered release of liposomal contents by matrix metalloproteinase-9. *J Am Chem Soc*, 2008. 130(32): p. 10633-42.
15. Sarkar, N.R., et al., "Uncorking" of liposomes by matrix metalloproteinase-9. *Chem Commun (Camb)*, 2005(8): p. 999-1001.
16. Sarkar, N., et al., Matrix metalloproteinase-assisted triggered release of liposomal contents. *Bioconjug Chem*, 2008. 19(1): p. 57-64.
17. Nagase, H. and J.F. Woessner, Jr., Matrix metalloproteinases. *J Biol Chem*, 1999. 274(31): p. 21491-4.
18. Peters, J.A., et al., Determination of paramagnetic lanthanide(III) concentrations from bulk magnetic susceptibility shifts in NMR spectra. *Magn Reson Chem*, 2001. 39(11): p. 723-726.
19. Stack, M.S. and R.D. Gray, Comparison of vertebrate collagenase and gelatinase using a new fluorogenic substrate peptide. *J Biol Chem*, 1989. 264(8): p. 4277-81.
20. Terreno, E., et al., Determination of water permeability of paramagnetic liposomes of interest in MRI field. *J Inorg Biochem*, 2008. 102(5-6): p. 1112-9.
21. Castelli, D.D., et al., Evidence for in vivo macrophage mediated tumor uptake of paramagnetic/fluorescent liposomes. *NMR Biomed*, 2009. 22(10): p. 1084-92.
22. Delli Castelli, D., et al., In vivo MRI multicontrast kinetic analysis of the uptake and intracellular trafficking of paramagnetically labeled liposomes. *J Control Release*. 144(3): p. 271-9.
23. Penate Medina, O., et al., Liposomal Tumor Targeting in Drug Delivery Utilizing MMP-2- and MMP-9-Binding Ligands. *J Drug Deliv*. 2011: p. 160515.
24. Hatakeyama, H., et al., Systemic delivery of siRNA to tumors using a lipid nanoparticle containing a tumor-specific cleavable PEG-lipid. *Biomaterials*. 32(18): p. 4306-16.

"SMART" MRI contrast agents: Enzyme Responsive Nanosystems

Abstract

A new approach to enzyme-responsive MRI agents based on the use of liposomes loaded with a high number of paramagnetic metal complexes (Gd-HPDO3A) is presented. It relies on the disruption of low relaxivity aggregates formed by liposomes and a macromolecular substrate that is selectively cleaved by the enzyme of interest. The interaction of anionic liposomes composed of POPC:CHOL:DPGS and the cationic peptide protamine yields a poorly soluble supramolecular assembly endowed with a low relaxivity. The action of the serine protease trypsin causes the digestion of protamine and the consequent de-assembly of the supramolecular adduct. The process is accompanied by an overall relaxation enhancement of solvent water protons as consequence of the recovery of the original permeability of the liposome membrane to water molecules. The observed increase of relaxivity is linearly dependent on the enzyme concentration.

An illustrative example of the possible use of the herein presented responsive agent has been reported. It consists of the entrapment of the supramolecular assembly in alginate vesicles that have often been used as gaskets for in vivo applications of stem cells and pancreatic islets. The change in the observed longitudinal relaxation rate R_1 (i.e. the increased hyper-intensity in the corresponding MR images) may act as a sensor of the protease activity in the biological environment in which the cells containing gasket is located.

Adapted from

Supramolecular protamine/Gd-loaded liposomes adducts as relaxometric protease responsive probes. Sara Figueiredo, João Nuno Moreira, Carlos F.G.C. Geraldes, Silvio Aime, Enzo Terreno, *Bioorganic & Medicinal Chemistry*, 2011, Feb 1;19(3):1131-5.

Introduction

Magnetic Resonance Imaging (MRI) is a well-established diagnostic imaging technique based on the visualization of the very intense ^1H NMR water signal. The contrast in MR images arises mainly from differences in T_1/T_2 of tissue protons and can be improved by the use of paramagnetic contrast agents (CAs), which shorten the longitudinal (T_1) and transverse (T_2) relaxation times of water protons [1-3]. The most widely used class of MRI CAs is represented by paramagnetic chelates of the Gd^{3+} ion [4, 5]. Their efficiency in enhancing the water proton relaxation rates ($1/T_1$ and/or $1/T_2$) is usually expressed by the longitudinal and transverse relaxivity values, r_1 and r_2 , respectively (in s^{-1} per mM of Gd^{3+}), measured at a given Larmor frequency and temperature [1, 6].

As far as Molecular and Cellular Imaging applications are concerned, MRI, despite its high spatial resolution (μm), is limited by the low sensitivity of its probes [7]. Due to this limitation, addressing molecular events at the cellular level by MRI requires large local concentrations of the CA in order to achieve a detectable contrast change. This is usually not feasible with targeted CAs containing as imaging reporter one or even a small number of Gd^{3+} chelates [8]. Thus, it is necessary to design amplification procedures that lead to the accumulation of a high number of imaging reporters at the site of interest. Among several possibilities, one route deals with the use of vesicular systems, like liposomes, that may be loaded with many Gd-containing complexes [9-11].

Liposomes are nanovesicles made of naturally-occurring or synthetic phospholipids widely used as biocompatible systems for drug delivery [4, 9, 12-14]. The high versatility of such systems enables them to carry drugs with different physico-chemical properties, as well as MRI contrast agents [15]. Hydrophilic molecules can be easily encapsulated in the aqueous cavity of the vesicle, whereas hydrophobic compounds can be incorporated in the membrane bilayer. Thus, liposomes offer a solution to the low sensitivity of MRI, by increasing the local payload of Gd^{3+} chelates as reporter groups [12].

So far the main applications of the liposome-based agents in MRI have been in the field of tumor targeting either by exploiting the passive targeting of the vesicle (through the Enhanced Permeability and Retention - EPR effect) [16, 17] or by active targeting through the conjugation of a specific vector on the surface of the liposome [9, 14, 17-19]. Thus, liposomes loaded with paramagnetic metal complexes yield an amplification of the MR response because the solvent water molecules have access to the intraliposomal compartment containing a high number of paramagnetic complexes. Concentrations up to hundreds millimolar of paramagnetic complexes in the aqueous cavities can be obtained, thus providing a powerful relaxation "sink" for the "bulk" solvent molecules [4, 12, 20, 21]. The efficiency in transferring the paramagnetic effect to the bulk water is dependent on the permeability of the liposomal membrane to the water molecules. It is well established that the permeability of the membrane of liposomes is dependent on the formulation of the membrane components (i.e. through a proper modulation of the relative amounts of saturated and unsaturated phospholipids and cholesterol).

As far as the design of a responsive agent is concerned, in analogy to what is done with simple molecular systems, the relaxivity of Gd(III)-loaded liposomes has to be modulated by the specific parameter of interest that affects one or more of its determinants.

In principle, the relaxometric response of a Gd-loaded liposome can be made dependent of processes like association, collapsing, degradation or precipitation. Any of these modifications is expected to have a profound effect on the relaxation enhancement brought by the paramagnetic metal complexes included or encapsulated in the liposomes. Whereas a change in the permeability may affect the accessibility of external water molecules to the paramagnetic centers, a tight association of liposomes may lead to an almost complete silencing of the paramagnetic effect on the longitudinal relaxation time of water protons. Conversely, it maintains and

even increases the effects on transverse relaxation rates as a result of the effect on the magnetic susceptibility brought about by compartmentalized systems. Conversely, the disruption of the liposomes integrity may lead to the complete release of the paramagnetic payload, thus leading to a situation, as far the *in vivo* MRI application is concerned, ruled only by the biodistribution properties of the paramagnetic chelates [14, 17].

This work deals with the design of an enzyme responsive probe based on the aggregation/de-aggregation processes. Aggregation of liposomes to form micro-sized particulates is obtained through the action of the cationic protamine that tightly binds at the surface of anionic liposomes. The de-aggregation step is operated by trypsin, as a representative example of proteases (Figure 1).

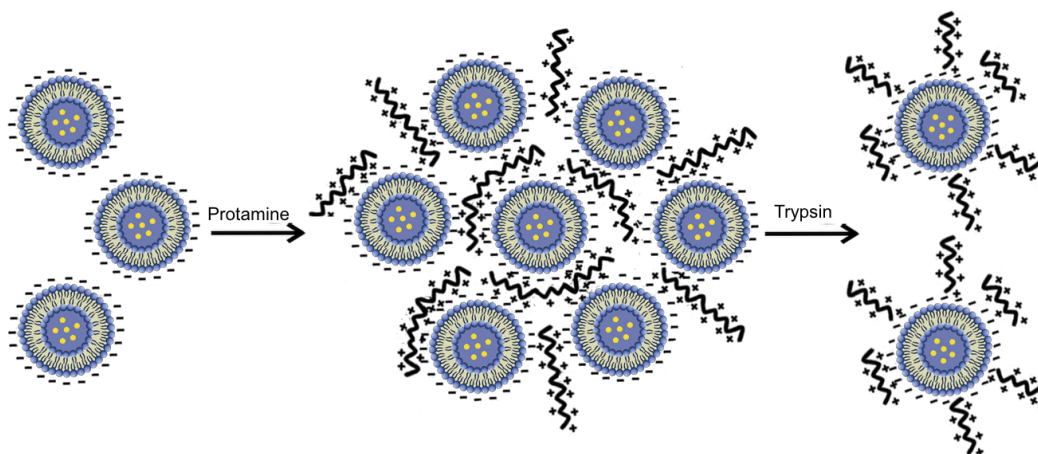


Figure 1 Illustration of the liposome aggregation induced by protamine and subsequent degradation of the supramolecular assembly by the action of trypsin.

Material and Methods

Preparation of paramagnetic liposomes

The lipids used in the liposomal membranes were purchased from Avanti Polar Lipids. They are 1-palmitoyl-2-oleoyl-sn-glycero-3-phosphocholine (POPC), cholesterol (CHOL), 1,2-dipalmitoyl-sn-glycero-3-succinate (DPGS) and 1,2-distearoyl-sn-glycero-3-phosphoethanolamine-N-[amino (polyethyleneglycol) 2000] (DSPE-PEG). Gd-HPDO3A (HPDO3A = 1,4,7-tris(carboxymethyl)-10-(2'-hydroxypropyl)-1,4,7,10-tetraaza-cyclododecane) is commercially available from Bracco Imaging under the trade name of ProHance®.

Liposomes have been prepared by the thin lipid film method. Briefly, the proper lipids mixture (POPC:CHOL:DPGS at a 2:2:1 molar ratio or POPC:CHOL:DPGS:DSPE-PEG at a 2:2:0.9:0.1 molar ratio) was dissolved in the volatile solvent chloroform, which was slowly evaporated until a thin film was formed. This lipidic film was left under vacuum until total evaporation of chloroform and then hydrated with a 200 mM aqueous solution of the paramagnetic complex Gd-HPDO3A (ProHance). The suspension was then extruded through polycarbonate membranes with a pore diameter of 200 nm (Northern Lipids, USA) and the final suspension was purified from the non-encapsulated metal complex by dialysis carried out against an isotonic buffer HBS (5 mM HEPES, 0.15 M NaCl, pH 7.4). Mean size diameter of the particles was measured by dynamic light scattering.

Preparation of samples for relaxometric experiments.

Protamine sulfate salt from salmon was purchased from Sigma-Aldrich. The protamine solutions used to aggregate the negatively charged liposomes were prepared at the proper concentration in PBS buffer.

Trypsin from bovine pancreas was purchased from Sigma-Aldrich (TPCK-treated, essentially salt-free, lyophilized powder,

$\geq 10,000$ BAEE units/mg protein). Trypsin solutions were prepared at the appropriate concentration in PBS buffer.

The association of anionic liposomes and protamine was performed always in the same order of addition, with the purpose of obtaining the highest reproducibility possible. Briefly, in several different vials, liposomes and protamine were incubated achieving the final concentration of 4 mg/mL and 2 mg/mL, respectively. To this suspension, from now on named the particulate suspension, trypsin was added at several concentrations. Another set of experiments was performed using the same concentration of liposomes (4 mg/mL) but a lower protamine quantity, accomplishing the final concentration of 0.2 mg/mL. The incubation with trypsin took place at a constant temperature of 310 K under continuous stirring, in an Eppendorf Thermomixer.

Entrapment of the supramolecular protamine-Gd-liposome adducts into alginate vesicles was performed following a previously reported experimental set-up [22]. Briefly, the supramolecular assembly to be encapsulated was resuspended in low viscosity alginate, obtaining the final concentration of 1.5% (w/v) of alginate and 10 mg/mL of liposomes. The suspension was then dripped into a 1.3% (w/v) solution of CaCl_2 , and after that washed with HEPES buffer.

The water proton longitudinal relaxation times of anionic liposomes and particulate suspensions have been measured using the inversion-recovery technique, on a Stelar Spinmaster spectrometer (Stelar, Mede, Italy), at 20 MHz and 298 K. The dimensions of the anionic liposomes and the particulates were measured by dynamic light scattering on a Malvern Zetasizer Nano ZS instrument (Malvern, UK). The measured T_1 value (T_1 and $R_1=1/T_1$) is the result of both paramagnetic and diamagnetic contributions, as shown by the equation 1:

$$r_1 = \frac{R_1 - R_{1dia}}{[Gd]} \quad \text{eq. 1}$$

where the relaxivity r_1 is the paramagnetic relaxation rate enhancement per mM concentration of the Gd(III) species.

Results and Discussion

Anionic liposomes loaded with Gd-HPDO3A have been obtained by means of the film hydration methodology. At 298 K and 20 MHz, the relaxivity (per Gd³⁺ ion) of the obtained suspension is 1.1 s⁻¹·mM⁻¹. This finding is an unambiguous indication that the solvent water molecules do not permeate freely across the liposome membrane. In fact, in the presence of the free water exchange between inner and outer liposome compartments, a relaxivity of ca. 4.2 s⁻¹·mM⁻¹ would have been measured, i.e. the one corresponding to the aqueous 1 mM solutions of Gd-HPDO3A. Through light scattering and electrophoretic mobility measurements it has been possible to determine the size and appropriate charge (Z-potential) of these Gd-loaded liposomes, which resulted to be ca. 165 nm (diameter) and -35 mV, respectively. From the knowledge of the liposome size (under the assumption of a 200 mM intraliposomal concentration of Gd-complex) one may conclude that each vesicle contains ca. 2.35×10⁵ Gd(III) complexes and the relaxivity per liposome is ca. 2.5×10⁵ s⁻¹·mM⁻¹.

The supramolecular protamine-Gd-liposome adducts were obtained by adding aliquots of a solution of protamine (positively charged, ca. 66 residual positive charge per protein molecule) to the anionic liposomes suspension. The addition of protamine to the liposome suspension resulted in the immediate formation of micron-sized particles. Their size ranged from ca. 2.5 to 7.0 μm according to the relative ratio between the negative charges brought by the anionic liposomes and the positive charges brought by the protamine. Larger sizes were obtained in the presence of an excess of positive charges (i.e. on going from 1:2 to 1:4 +/- charge ratios). Conversely, upon the addition of protamine no precipitation is observed upon introducing 2 mol% of DSPE-PEG in the composition of the membrane. In the latter case, the liposomal suspension did

not show aggregation phenomena neither r_1 changes, demonstrating that the increased hydrophilicity and the steric hindrance of the DSPE-PEG component is able to prevent the formation of a strong electrostatic interaction between the liposomes and the cationic protamine.

The particles were almost silent from the relaxometric point of view. The small contribution to the relaxation enhancement of their suspensions ($0.2 \text{ s}^{-1}\cdot\text{mM}^{-1}$) is likely due to the occurrence of few liposomes that partly escape the tight binding interactions that characterize the whole aggregate. The protein acts as a glue towards the negatively charged liposomes, thus creating a further barrier to the exchange of water molecules across the liposomes' membranes. The particles appear quite stable as their size and the longitudinal relaxation enhancement of solvent water protons do not change over a period of several weeks.

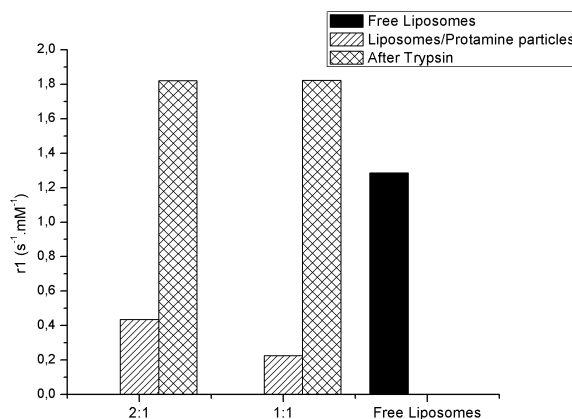


Figure 2I Effect of liposome:protamine ratio (represented by -/+ charge ratio) on the r_1 relaxivity of aggregates formed between negatively charged liposomes encapsulating Gd-HPDO3A and protamine. The effect of trypsin (1 mM, 1 h incubation under continuous agitation at 310 K) is also presented. Both effects are compared with those obtained for the liposomes in the absence of protamine. The liposomal membrane is formed of a mixture of POPC:CHOL:DPGS in the proportion 40:40:20.

To assess whether the particles are responsive in terms of changes of water proton relaxation rate upon progressive cleavage of peptide bonds of the protein, the particles' suspensions were added with variable amounts of trypsin, a common serine protease. This enzyme predominantly cleaves peptide chains at the carboxyl side of the amino acids lysine and arginine, except when they are followed by proline. After

the addition of trypsin to the substrate, the size of the adducts decreases to ca. 300 nm diameter, i.e. to a value close to the size of free Gd-loaded liposomes. Conversely, no effect is observed when trypsin is added to free liposomes. Thus, trypsin, through the cleavage of protamine, yields a progressive reduction of liposomes-protamine aggregates.

Figure 2 shows the effect of the addition of protamine on the r_1 values of liposomes' suspensions at two $-/+$ charge ratios (negative charges are the residual charges on the liposome surface; positive charges are provided by protamine) and the effect of subsequent addition of trypsin.

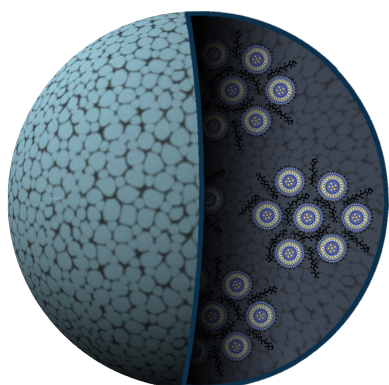


Figure 41 Sketched representation of entrapped micron-sized particles into an alginate matrix.

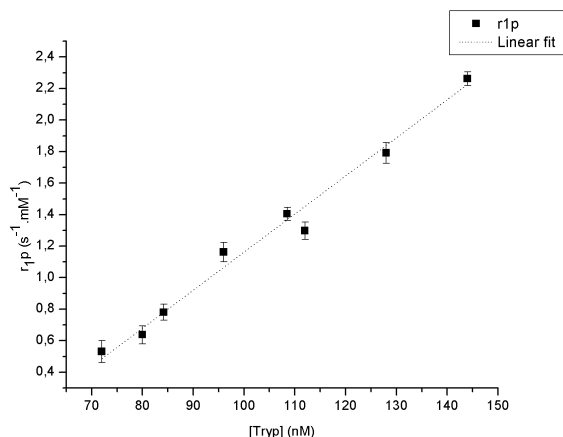


Figure 31 Linear dependence of the r_1 relaxivity of the complexes formed between negatively charged liposomes encapsulating Gd-HPDO3A and protamine, after incubation (6 h under continuous agitation at 310 K) with different concentrations of trypsin. The liposomal membrane is formed of a mixture of POPC:CHOL:DPGS in the molar ratio 2:2:1.

One hour after the addition of trypsin, the resulting Gd-relaxivity markedly increased and was even slightly higher than the one measured for free liposomes ($1.8 s^{-1} \cdot mM^{-1}$ and $1.5 s^{-1} \cdot mM^{-1}$, respectively). These data support the view that trypsin, through the cleavage of protamine, restores the conditions existing before the addition of the cationic protein. Actually, the slight increase in the observed r_1 values reflects a small

increase in the water permeability that may arrive from minor misalignments in the phospholipid components of the liposomes' membrane resulting from the interaction with products arising from the degradation of protamine.

Figure 3 reports the relationship between the observed r_1 values and trypsin concentration (from 60 to 150 nM) for liposome suspensions containing 4.8 mM concentration of Gd-HPDO3A. The r_1 values were measured (at 20 MHz and 298 K) after 6 h from the addition of the enzyme to the particles' suspension. The enzymatic degradation of protamine occurs at the enzyme optimum temperature (310 K) and a good linearity has been observed between r_1 values and the concentration of the enzyme.

This finding demonstrates that it is possible to determine protease activity by a simple relaxometric assay that may be translated into the design of a MRI-based method to determine local enzyme concentrations *in vivo*. The size of these protamine/liposomes aggregates is not compatible with *in vivo* uses based on their intravenous administration, as for such uses one needs to deal with particles that have to be (max) in the hundred(s) of nanometer dimension. However the herein reported particles may find potential application as *in vivo* MRI sensors of protease activity when they are suitably enclosed in given devices and located at the biological site of interest. For instance, the herein developed responsive agents may report the protease activity in the surroundings of transplanted cells such as stem cells or pancreatic islets. To get more insight into this potential application, the particles have been encapsulated into an alginate matrix, a vehicle that is currently under intense scrutiny in the field of transplantation and cell-based therapy. An analogous approach might be tackled to assess enzymatic activities in the microenvironment of a scaffold designed for homing and differentiating stem cells.

The protamine/liposomes particles, generated as described above, were then trapped in an alginate matrix, following the same procedure as previously reported for cells' and liposomes' entrapment (Figure 4). The size of the pores of the alginate

matrix can be tailored according to the environment to be engineered. The herein formed matrix contains pores that are large enough to allow trypsin to enter the intravesicular space and small enough to prevent the release of liposomes once the particles have been de-assembled.

Figure 5 reports the observed R_1 values of alginate-entrapping particles upon trypsin addition to the alginate

suspending medium. In the presence of trypsin (4 and 0.4 mM) R_1 increases to reach the saturation value after approximately 5 h from the addition of the enzyme to the alginate suspending medium. Overall, the observed behavior closely parallels what is described above for the particles suspended in aqueous medium.

The performance of the proposed concept was also assessed in vitro on an imaging scanner. To this purpose, the T_1 contrast of a preparation of alginate capsules entrapping aggregated liposomes externally added with 4 mM of trypsin was compared with a control sample added with PBS. The two systems were put in two 5 mm glass tubes surrounded by agarose gel and imaged at 7.05 T at room temperature. The result shown in Figure 6 clearly indicates the significant contrast enhancement detected in the sample treated with the enzyme.

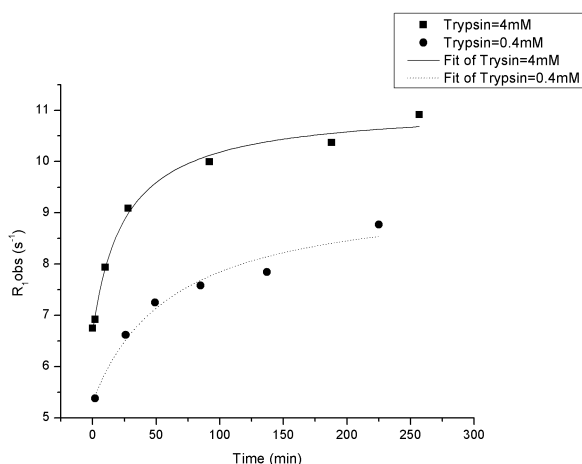


Figure 5I Observed R_1 values of a suspension containing particles in the alginate matrix, upon trypsin addition (4 and 0.4 mM). The curves represent a simple hyperbolic fit for guiding-eye.

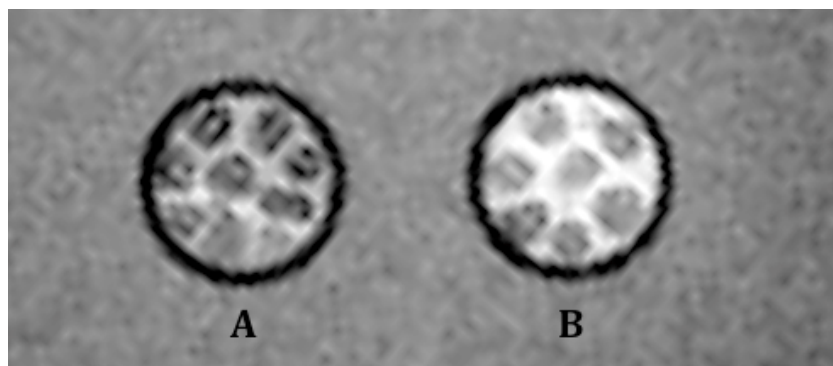


Figure 6I MRI-T₁-weighted image of two capillaries ((A) and (B)) containing alginate gaskets entrapping liposomal particles. B) Report about the trypsin action on the Protamine/Gd-loaded liposome supramolecular adducts entrapped in the alginate matrix. The image was obtained using a standard T₁-weighted multislice multiecho sequence (TR/TE = 250/3.3).

Conclusion

The main existing methods used to determine enzyme activity are based on the rate of a reaction catalyzed by the enzyme, using either natural or synthetic substrates, such as BAEE (N-Benzoyl-L-Arginine Ethyl Ester) or the Biuret reagent. For these rate measurements, the concentration of protein is determined by ultraviolet spectrophotometric absorption, as it has been described extensively over the years by several research groups [23]. As a proof of concept, a new relaxometric approach is hereby presented, which allows the determination of an enzyme concentration using as substrate a complex formed between negatively charged liposomes and a small cationic protein, available for both MRI and *in vitro* assessments. It is known that the concentration of several proteases of biological and pathological relevance is comprised within a range that can be considered with the herein reported method. For instance, human prostatic epithelial cells continuously secrete prostate-specific antigen (PSA), a kallikrein-like serine protease, to the seminal plasma, constituting one of the most abundant proteases in this fluid, in a concentration of about 1.0 mg/ml (~30 nM) [24]. Another protein that may be taken into account is trypsinogen, the precursor of trypsin. It has been reported

that the concentration of two different types of trypsinogen is 26 mg/L (~ 1.1 nM) for trypsinogen-1 and 50 mg/L (~ 2.1 nM) for trypsinogen-2 in transplanted patients having cholangiocarcinoma [25].

Overall, the methodology presented here appears suitable for a conventional in vitro quantification of protease enzymes, being based on the capacity of protamine to bind a negatively charged liposomal formulation. Upon complexation with the negatively charged liposomes, this small cationic protein causes their association, which may finally lead to their precipitation, reducing the r_1 relaxivity of the solution. The ability to enhance water proton relaxation rates is recovered once the macromolecular association is cleaved by the serine protease trypsin, leading to a relaxivity enhancement. Another point of interest concerns the versatility of the method hereby presented. Selecting the appropriate substrate, the work presented here could be expanded to any enzyme of interest. Moreover, the limiting concentration of serine protease that can be detected is dependent mainly on the substrate concentration (small cationic protein protamine).

Finally, an in vivo exploitation of the herein described particles has been proposed. It relies on the possibility of entrapping micron-sized particles into an alginate matrix that has often been considered as a bio-compatible device in cell-based therapies. The protamine/liposomes particles may act as a protease sensor of the local microenvironment in which the device is located. The characteristics of the alginate matrix are such that one can easily modulate the size of the holes in order to get a good control of the way-in/way-out of the substances according to their size.

The herein reported methodology may be easily extended to assess other types of enzymatic activity through the proper selection of the complementary recognition characteristic of the given enzyme-substrate and the liposome outer surface.

References

1. Aime, S., et al., Lanthanide(III) chelates for NMR biomedical applications. *Chem Soc Rev*, 1998. 27(1): p. 19-29.
2. Aime, S., M. Botta, and E. Terreno, Gd(III)-based contrast agents for MRI. *Advances in Inorganic Chemistry - Including Bioinorganic Studies*, Vol 57, 2005. 57: p. 173-237.
3. Strijkers, G.J., et al., MRI contrast agents: current status and future perspectives. *Anticancer Agents Med Chem*, 2007. 7(3): p. 291-305.
4. Aime, S., D.D. Castelli, and E. Terreno, Chapter 10 - Lanthanide-loaded paramagnetic liposomes as switchable magnetically oriented nanovesicles. *Methods Enzymol*, 2009. 464: p. 193-210.
5. Caravan, P., et al., Gadolinium(III) Chelates as MRI Contrast Agents: Structure, Dynamics, and Applications. *Chem Rev*, 1999. 99(9): p. 2293-352.
6. Meade, T.J. and S. Aime, Chemistry of molecular imaging. *Acc Chem Res*, 2009. 42(7): p. 821.
7. Aime, S., et al., Pushing the sensitivity envelope of lanthanide-based magnetic resonance imaging (MRI) contrast agents for molecular imaging applications. *Acc Chem Res*, 2009. 42(7): p. 822-31.
8. Caravan, P., Strategies for increasing the sensitivity of gadolinium based MRI contrast agents. *Chem Soc Rev*, 2006. 35(6): p. 512-23.
9. Esposito, G., S.G. Crich, and S. Aime, Efficient Cellular Labeling by CD44 Receptor-Mediated Uptake of Cationic Liposomes Functionalized with Hyaluronic Acid and Loaded with MRI Contrast Agents. *ChemMedChem*, 2008. 3(12): p. 1858-1862.
10. Terreno, E., et al., From spherical to osmotically shrunken paramagnetic liposomes: An improved generation of LIPOCEST MRI agents with highly shifted water protons. *Angew Chem Int Ed Engl*, 2007. 46(6): p. 966-968.
11. Terreno, E., et al., Osmotically Shrunken LIPOCEST Agents: An Innovative Class of Magnetic Resonance Imaging Contrast Media Based on Chemical Exchange Saturation Transfer. *Chem Eur J*, 2009. 15(6): p. 1440-1448.
12. Mulder, W.J., et al., Lipid-based nanoparticles for contrast-enhanced MRI and molecular imaging. *NMR Biomed*, 2006. 19(1): p. 142-64.

13. Castelli, D.D., et al., Lanthanide-loaded paramagnetic liposomes as switchable magnetically oriented nanovesicles. *Inorg Chem*, 2008. 47 (8): p. 2928-2930.
14. Torchilin, V.P., Affinity liposomes in vivo: factors influencing target accumulation. *J Mol Recognit*, 1996. 9(5-6): p. 335-46.
15. Geraldes, C.F. and S. Laurent, Classification and basic properties of contrast agents for magnetic resonance imaging. *Contrast Media Mol Imaging*, 2009. 4(1): p. 1-23.
16. Maeda, H., G.Y. Bharate, and J. Daruwalla, Polymeric drugs for efficient tumor-targeted drug delivery based on EPR-effect. *Eur J Pharm Biopharm*, 2009. 71(3): p. 409-19.
17. Torchilin, V.P., Drug targeting. *Eur J Pharm Sci*, 2000. 11 Suppl 2: p. S81-91.
18. Mendonça, L.S., et al., Transferrin receptor-targeted liposomes encapsulating anti-BCR-ABL siRNA or asODN for chronic myeloid leukemia treatment. *Bioconjug Chem*. 21(1): p. 157-68.
19. Santos, A.O., et al., Design of peptide-targeted liposomes containing nucleic acids. *Biochim Biophys Acta*. 1798(3): p. 433-41.
20. Strijkers, G.J., et al., Three-compartment T1 relaxation model for intracellular paramagnetic contrast agents. *Magn Reson Med*, 2009. 61(5): p. 1049-58.
21. Terreno, E., et al., Determination of water permeability of paramagnetic liposomes of interest in MRI field. *J Inorg Biochem*, 2008. 102(5-6): p. 1112-9.
22. Dhoot, N.O. and M.A. Wheatley, Microencapsulated liposomes in controlled drug delivery: strategies to modulate drug release and eliminate the burst effect. *J Pharm Sci*, 2003. 92(3): p. 679-89.
23. Bradford, M.M., A rapid and sensitive method for the quantitation of microgram quantities of protein utilizing the principle of protein-dye binding. *Anal Biochem*, 1976. 72: p. 248-54.
24. Webber, M.M., A. Waghray, and D. Bello, Prostate-specific antigen, a serine protease, facilitates human prostate cancer cell invasion. *Clin Cancer Res*, 1995. 1(10): p. 1089-94.
25. Lempinen, M., et al., Enhanced detection of cholangiocarcinoma with serum trypsinogen-2 in patients with severe bile duct strictures. *J Hepatol*, 2007. 47(5): p. 677-83.

Yeast Cell Wall Particles:
a promising class of nature-inspired
microcarriers for multimodal imaging

Abstract

The relatively low sensitivity of paramagnetic MRI probes has instigated the development of systems able to deliver a high number of MR imaging reporters to the biological target site of interest. Several nano-sized carriers have been considered including naturally-occurring systems such as proteins, viruses capsids or lipoproteins. The search for carriers able to carry a large number of paramagnetic units prompted us to consider the recently proposed micron-sized platform of yeast cell wall particles (YCWPs).

We developed a procedure for entrapping paramagnetic emulsions in the inner core of YWCPs using water-insoluble Gd-complexes. The longitudinal relaxivity of Gd-loaded YCWP measured at 20 MHz was ca. 50 % higher than that reported for the same chelate embedded in a liposome membrane. After intramuscular injection of the particles in a mouse bearing a subcutaneously grafted tumor, a clear enhancement of the MRI signal was observed in the tumor and proximal lymph node.

In summary, YCWP may represent a very promising class of carriers for designing highly sensitive MRI probes.

Adapted from

Gd-loaded Yeast Cell Wall Particles: an innovative micron-sized platform for labeling and tracking immune cells by multimodal imaging. Sara Figueiredo, João Nuno Moreira, Carlos F.G.C. Geraldes, Silvia Rizzitelli, Silvio Aime, Enzo Terreno, Chem Comm, 2011 Sep 20;47(38):10635-7.

Introduction

Nature has strongly inspired the search for carriers able to allow a safe delivery of a high number of diagnostic or therapeutic chemicals to a given biological target. For instance, liposomes, one of the most used nanocarriers for drug delivery purposes, are composed of phospholipids that are reminiscent of the natural components of cell membranes. Besides the great benefits primarily related to the improvement of the pharmacokinetic properties and therapeutic index of a drug, the use of naturally-occurring carriers has been also considered for enhancing the detection threshold of imaging agents, especially for those modalities, like Magnetic Resonance Imaging (MRI), which are intrinsically characterized by a relatively poor sensitivity. In addition to liposomes [1], many other nature-like carriers have been investigated so far including proteins [2-6], virus capsids [7, 8], lipoproteins [9, 10] and even whole cells have been used, primarily for cell-tracking purposes [11].

Recently, a novel class of natural carriers has been proposed, the so-called yeast cell wall particles (YCWPs) [12]. Yeasts are cells whose membrane consists of β -1,3-D-glucan polymer associated with mannose-containing proteins and chitin. Such materials are well tolerated by living systems and can be processed into small fragments by macrophages [13]. Moreover, β -1,3-D-glucan is an excellent targeting vector towards dectin-1 receptor, which is exposed on the membrane of several phenotypes of antigen presenting cells [14, 15]. The ability of YCWPs to act as delivery system has been recently reported for nucleic acids [16].

On this basis, it was deemed of interest to explore the use of YCWPs as a versatile carrier of imaging reporters. The hydrophilic nature of the polysaccharidic membrane does not allow the incorporation of amphiphilic chemicals as typically done for lipid-based particles. Moreover, attempts to stably include hydrophilic molecules in the particle core failed due to the high porosity of the wall. Nevertheless, the peculiar chemical stability of yeast walls can be exploited to undertake a new loading procedure in which the inner cavity of the particle

may act as a micro-reactor, thus allowing the formation of large size self-assembling systems (e.g. emulsions) that, once formed, remain entrapped in the particle.

Thus, the aim of this work was to prepare and characterize a system able to carry larger paramagnetic payloads and to test the potential of this new loading approach, the commercially available rhodamine-DPPE (Rh-DPPE) dye was selected as model of water insoluble amphipatic fluorescent probe.

Material and Methods

Preparation of yeast cell wall particles

β -1,3-D-glucan shells were prepared as described elsewhere [10]. Briefly, *Saccharomyces cerevisiae* were suspended in a 1 M solution of NaOH and heated at 353 K for 1 h under continuous magnetic stirring. The insoluble material was then collected by centrifugation and suspended in acidic water (pH 5) and stirred for 1 h at 328 K. The insoluble material was collected again by centrifugation and washed in water, isopropanol and acetone. The product obtained was dried at room temperature to a fine powder.

Labeling of yeast cell wall particles

Dry glucan particles were incubated overnight at room temperature with a chloroform solution containing water insoluble Gd-DOTAMA(C18)₂ or rhodamine-DPPE dye (Avanti Polar Inc, Alabaster, AL, USA), respectively. The resulting labeled particles were washed three times in PBS buffer, re-suspended in the same buffer and counted with a hemacytometer.

Characterization of yeast cell wall particles mean size

The mean size of yeast particles was determined by dynamic light scattering (DLS) on a Malvern Zetasizer Nano ZS instrument (Malvern, UK) and corroborated by the analysis of TEM images, obtained on a Philips CM-10 transmission electron microscope operating at 100 keV.

Confocal Microscopy

Confocal microscopy was performed with a confocal laser scanning microscopy system (CLSM) equipped with an argon-ion laser (Leica TCS SP5 (Leica Microsystems s.r.l.)). All images were acquired using the same exposure time and brightness/contrast settings.

Relaxometric characterizations of yeast cell wall particles

The water proton longitudinal relaxation times of YCWPs were measured using the inversion-recovery technique, on a Stellar Spinmaster Relaxometer operating at variable frequencies between 20 and 80 MHz and on a Stellar Field Cycling Relaxometer in the frequency range 0.01–20 MHz, at 298 K. The water proton longitudinal (T_1) and transverse (T_2) relaxation times of β -1,3-D-glucan shells were measured using, respectively, an inversion-recovery or a Carr-Purcell-Meiboom-Gill sequence. NMRD profiles were obtained over a range of magnetic fields from 0.24 mT to 1.6 T (0.01-70 MHz).

The measured T_1 value (T_1 and $R_1=1/T_{1s}$) is the result of both paramagnetic and diamagnetic contributions, as shown by the equation 1.

$$r_1 = \frac{R_1 - R_{1dia}}{[Gd]} \quad \text{eq. 1}$$

where the relaxivity r_1 is the paramagnetic relaxation rate enhancement per mM concentration of the Gd(III) species. The concentration of gadolinium in YCWPs was determined by ICP-MS after mineralization of the sample.

In vitro MRI experiments

Glass capillaries containing YCWPs were placed in an agar phantom and MRI- T_1 and T_2 -weighted images were performed on a Bruker Avance 300 NMR spectrometer equipped with a microimaging probe operating at 7.05 T and on a portable Aspect M2™ MR imaging scanner (Netanya, Israel) operating at 1 T. The images were obtained using a standard T_1 -weighted multislice multiecho sequence. T_1 -weighted ^1H -MR image acquired at 7.05 T (TR/TE/NEX (250/7.9/10), FOV 1 cm, 1 slice 3 mm), T_2 -weighted ^1H -MR image acquired at 7.05 T (TR/TE/NEX (5000/26.4/10) FOV 1 cm, 1 slice 3 mm), T_1 -weighted ^1H -MR image acquired at 1T (TR/TE/NEX (250/7.2/10), FOV 2 cm, 1 slice, 3 mm) and T_2 -weighted ^1H -MR image acquired at 1 T (TR/TE/NEX (5000/26.4/10), FOV 2 cm, 1 slice, 3 mm).

The T_1 measurement of particles was performed using a saturation recovery sequence and T_2 values were measured using a multiecho sequence (TR/TE/NEX 5000/3.3/1, number of echoes 500).

In vivo MRI experiments

C57BL/6 mice (Charles River Laboratories, Calco, Italy) were inoculated subcutaneously in the left flank with 0.2 ml of a suspension containing 1×10^6 B16-F10 murine melanoma cells. B16-F10 cells were obtained from ATCC (Manassas, VA, USA) and were grown in a DMEM medium supplemented with 10% FBS, 2 mM glutamine, 100 U/ml penicillin and 100 $\mu\text{g}/\text{ml}$ streptomycin. Solid tumors formed in about 7–10 days were used for imaging evaluation. Prior to MRI examination, animals were anesthetized by injecting a mixture of tiletamine/

zolazepam (Zoletil 100, Virbac, Carros, France), 20 mg/kg and xylazine (Rompun, Bayer S.p.a. Milan).

All MR images were acquired on a Bruker Avance 300 NMR spectrometer (7.05 T) equipped with a Micro 2.5 microimaging probe (Bruker BioSpin). The system is equipped with two birdcage resonators with 30- and 10-mm inner diameter, respectively.

T₂-weighted images were acquired using a RARE sequence (TR/TE/NEX 5000/3.3/4 rare factor 64). T₁-weighted, fat suppressed, images were obtained using a multi slice multi echo protocol (TR/TE/NEX 250/3.3/6). Fat suppression was performed by applying a pre-saturation pulse (90° BW = 1400 Hz) at the absorption frequency of fat (-1100 Hz from water). MRI was recorded before administration and 5, 24 and 48 h after administration of contrast to evaluate the biodistribution.

Results and Discussion

Dried YCWPs were prepared according to the published method[12]. Then, the particles were suspended in 5 mL of chloroform containing 20 µg/mL of Rh-DPPE. The suspension was left under stirring overnight in order to allow the dye to equilibrate between inside and outside the yeast shells. Afterwards, the particles were separated by centrifugation and the pellet, represented by the swollen YCWPs, was added with water. The sudden change in the solvent polarity induces the formation of an oil/water microemulsion (behavior observed also in the absence of YCWPs) that entraps the amphiphilic dye inside the

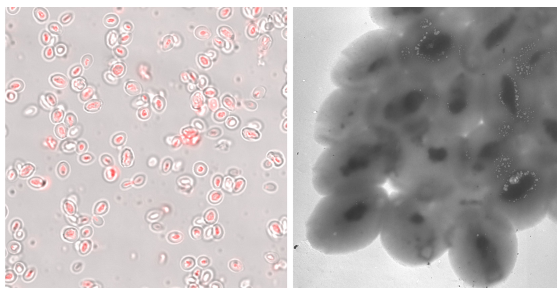


Figure 11 Left: Laser-scanning confocal microscopy of rhodamine-labeled YCWPs. Right: Transmission Electron Microscopy (TEM) image of Gd-loaded YCWPs yeast shells.

particle core. The laser-scanning confocal image reported in Figure 1 (left), overlaid to the phase contrast image, clearly shows the localization of the fluorescent dye inside the yeast shells that appear as pseudo-spherical particles with a hydrodynamic diameter of ca. 6 μm , as determined by Dynamic Light Scattering measurements.

The same loading protocol was used by replacing the fluorescent dye with the water insoluble paramagnetic agent Gd-DOTAMA(C18)₂ (Chart 1) selected as prototype of amphipatic MRI agents [17]. In this case, a ten-fold higher amount of imaging label (2 mg/mL vs. 0.02 mg/mL) was used to balance the difference in the threshold detection between the two imaging techniques.

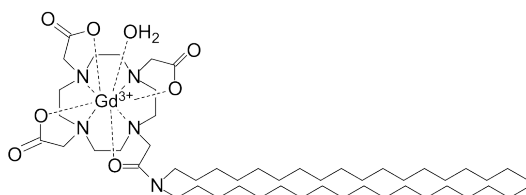


Chart 11 Gd-DOTAMA(C18)₂ complex.

Figure 1. (right) reports a TEM image of the Gd-loaded YCWPs where the vesicle cores appear filled up with the metal-based emulsion.

As far as the MRI potential of this system is concerned, the entrapment of the paramagnetic emulsion inside the particle may have two important benefits: i) an increased paramagnetic density (i.e. mass of Gd/volume particle), and ii) an enhanced relaxivity per paramagnetic center as a consequence of the restricted rotational motion of the paramagnetic agent.

Hence, the Gd-loaded YCWPs were characterized by ¹H-relaxometry measuring first the longitudinal relaxivity at 20 MHz and 298 K. Interestingly, the suspension showed a

relaxivity (per Gd^{3+} ion) of $22.3 \text{ s}^{-1}\cdot\text{mM}^{-1}$, a value ca. 50 % higher than reported for the same chelate embedded in a liposome membrane [18]. On the basis of the Gd^{3+} concentration determined in the suspension and counting the particles, which are visible by optical microscopy, it was estimated that each YCWP is loaded with ca. 16 millions of $\text{Gd-DOTAMA}(\text{C18})_2$ units, which represents the highest paramagnetic payload ever reported for an imaging probe carrier. As a beneficial consequence, the relaxivity of the system per particle concentration reached the unprecedented value of $3.6 \times 10^8 \text{ s}^{-1}\cdot\text{mM}^{-1}$. This finding suggests that solvent water protons have an easy access to the paramagnetic $\text{Gd}(\text{III})$ centers that point outward from the surface of the emulsion. The relaxivity was also measured at 310 K, where a value very close to the one observed at 298 K was obtained ($22.0 \text{ s}^{-1}\cdot\text{mM}^{-1}$ Gd). This result indicates that the relaxivity of the emulsion at 298 K is likely limited by the occurrence of a slow water exchange rate of the metal-coordinated water molecule, as expected for neutral monoamide derivatives of Gd-DOTA with a restricted rotational motion.

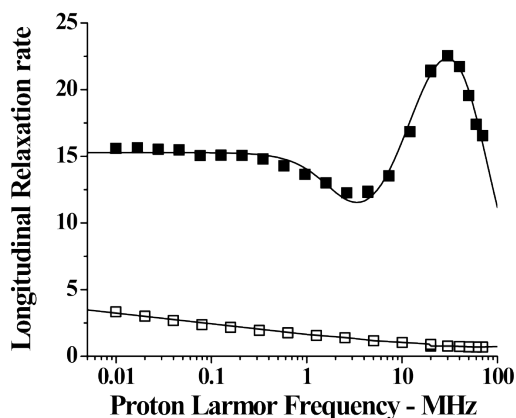


Figure 21 Nuclear Magnetic Relaxation Dispersion profiles for an aqueous suspension of YCWPs empty (open squares) and loaded with $\text{Gd-DOTAMA}(\text{C18})_2$ (normalized to 1 mM concentration of Gd, filled squares) (pH 7.4, 298 K, YCWPs 20 mg/mL).

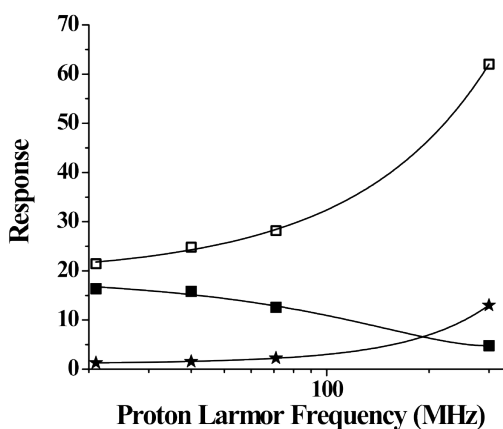


Figure 31 Magnetic field dependence of millimolar r_1 (filled squares), r_2 (open squares) values and their ratio (stars) for an aqueous suspension of YCWPs loaded with $\text{Gd-DOTAMA}(\text{C18})_2$ (pH 7.4, 298 K).

A further characterization of the paramagnetic material was gained through the acquisition of the Nuclear Magnetic Relaxation Dispersion (NMRD) profiles that highlight the great sensitivity of the paramagnetic relaxation towards structure and molecular motions of the metallic centers.

The NMRD profile of YCWPs loaded with Gd-DOTAMA(C18)₂ complex shows the relaxivity peak centered around 20 MHz that is a clear indication of the restricted rotational motion of Gd(III) centers (Figure 2). The NMRD profile of the diamagnetic empty microparticles is characterized by a steady decrease of the relaxation rates from low to high magnetic field strength, paralleling the usual behavior observed in biological specimens, tissue-surrogates, or large macromolecules, where it is accounted for in terms of the rather complex dynamic processes experienced by the protons in these samples [19].

The profile obtained for the paramagnetic system was analyzed using the classical relaxation model that takes into consideration the relaxation contributions arising from water protons in the inner- and outer-spheres of the paramagnetic center [20]. The data were nicely fitted, accordingly with the equations in appendix A, using the following parameters (allowed to vary during the analysis) $\Delta^2 = 1.9 \times 10^{19} \text{ s}^{-2}$, $\tau_V = 28.7 \text{ ps}$, $\tau_R = 7.3 \text{ ns}$, and $\tau_M = 690 \text{ ns}$, whereas the other variables of the model were kept fixed to the typical values of a Gd-based chelate (distance of the inner sphere water protons: 3 Å; distance of closest approach of outer sphere water: 3.8 Å; relative solute-solvent diffusion constant, $2.2 \times 10^{-5} \text{ cm}^2 \cdot \text{s}^{-1}$). The results obtained fit well with the proposed hypothesis of a paramagnetic emulsion made of amphiphilic Gd complexes localized in the inner aqueous cavities of YCWPs with no restriction for the water access from the outer compartment.

Besides generating T_1 enhancement, the paramagnetic emulsion entrapped in the microparticles can yield also a marked contribution to T_2 relaxation. Conversely to T_1 relaxation, T_2 effects steadily increase upon increasing the magnetic field strength. Figure 3 compares the magnetic field

dependence of r_1 and r_2 as well as the r_2/r_1 ratio, which suggests that the MRI agent may preferentially act as T_1 or T_2 agent depending on the magnetic field strength. In particular, the paramagnetic YCWPs could be used as highly sensitive T_1 agents at fields lower than 100 MHz, and display a preferential T_2 effect at higher fields.

To better appreciate the magnetic field-dependent contrasting ability of the investigated particles, a phantom containing a suspension of Gd-loaded YCWPs containing 1 mM of Gd was imaged at 1 T (corresponding to a Larmor Frequency of 40 MHz) and 7.05 T (300 MHz). Figure 4 (left) displays T_1 -w and T_2 -w images of the phantom, whereas the corresponding contrast enhancement, measured using the external agar as reference, is reported on the right. The results highlight the advantage of using the lower field for enhancing T_1 contrast, whereas as far as T_2 contrast is concerned, the signal loss at 300 MHz was only slightly larger than at low field (the lower absolute values in case of T_2 effects is likely related to the use of agar, for which $T_2 \ll T_1$, as reference).

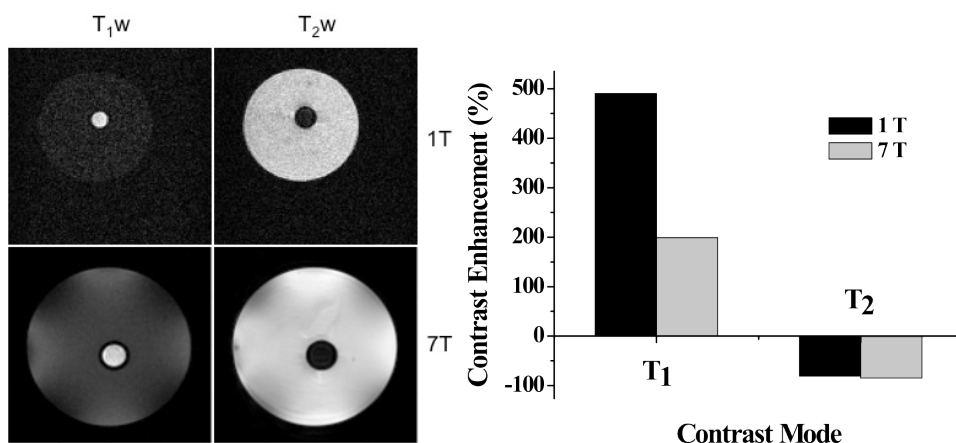


Figure 4 Left: MR- T_1 -w and T_2 -w images of a suspension of Gd-labelled YCWPs (1 mM Gd) at 1 T and 7.05 T (room temperature). Right: corresponding positive (T_1) and negative (T_2) contrast enhancement calculated using the external agar as reference.

An interesting proof-of-concept of the MRI potential of the paramagnetic YCWPs was gained in vivo upon intramuscular injection of 100 μ l of a suspension of Gd-loaded YCWPs (injected dose of Gd = 1.2 mmol/kg) within the leg of a mouse bearing a subcutaneously grafted melanoma B16-F10 tumor. 48 h post-injection a clear brightening was observed in the external rim of the tumor (high density of blood capillaries) and at the lymph node proximal to the tumor (Figure 5), thus suggesting that the microparticles are rapidly taken up by macrophages and delivered to the lymph node.

Conclusions

In summary, YCWPs may represent a promising innovative class of carriers for multimodal imaging. In particular, as far as the use in MRI is concerned, they could find interesting applications considering their extremely high ability to generate T_1 contrast at intermediate fields (0.5-1.5 T) and/or their T_2 effect predominant at high fields. Potential fields of application of paramagnetic YCWPs are in cell-tracking experiments, especially for labeling and visualizing cells of the immune system (antigen presenting cells, macrophages, dendritic cells) for which yeast shells display high affinity.

In addition, and analogously to other particulate systems,

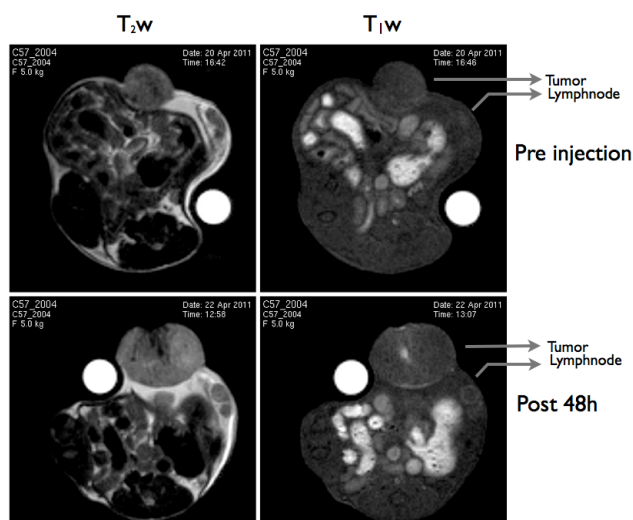


Figure 5 T_2 -weighted and fat-suppressed T_1 -weighted multislice multiecho MR images of C57BL/6 mice grafted subcutaneously with B16 melanoma cells. Images were obtained before and after the injection of Gd-labeled YCWPs (Post 48 h).

YCWPs can be loaded with lipophilic probes for other imaging modalities, and, moreover, β -1,3-D-glucan shells can be suitably functionalized to endow them with targeting abilities.

References

1. Aime, S., et al., Pushing the sensitivity envelope of lanthanide-based magnetic resonance imaging (MRI) contrast agents for molecular imaging applications. *Acc Chem Res*, 2009. 42(7): p. 822-31.
2. Dumas, S., et al., High relaxivity magnetic resonance imaging contrast agents. Part 1. Impact of single donor atom substitution on relaxivity of serum albumin-bound gadolinium complexes. *Invest Radiol*. 45(10): p. 600-12.
3. Lelyveld, V.S., et al., Metal-substituted protein MRI contrast agents engineered for enhanced relaxivity and ligand sensitivity. *J Am Chem Soc*. 133(4): p. 649-51.
4. Aime, S., L. Frullano, and S. Geninatti Crich, Compartmentalization of a gadolinium complex in the apoferritin cavity: a route to obtain high relaxivity contrast agents for magnetic resonance imaging. *Angew Chem Int Ed Engl*, 2002. 41(6): p. 1017-9.
5. Geninatti Crich, S., et al., Magnetic resonance visualization of tumor angiogenesis by targeting neural cell adhesion molecules with the highly sensitive gadolinium-loaded apoferritin probe. *Cancer Res*, 2006. 66(18): p. 9196-201.
6. Kalman, F.K., S. Geninatti-Crich, and S. Aime, Reduction/dissolution of a beta-MnOOH nanophase in the ferritin cavity to yield a highly sensitive, biologically compatible magnetic resonance imaging agent. *Angew Chem Int Ed Engl*. 49(3): p. 612-5.
7. Anderson, E.A., et al., Viral nanoparticles donning a paramagnetic coat: conjugation of MRI contrast agents to the MS2 capsid. *Nano Lett*, 2006. 6(6): p. 1160-4.
8. Vasalatiy, O., et al., Labeling of adenovirus particles with PARACEST agents. *Bioconjug Chem*, 2008. 19(3): p. 598-606.
9. Cormode, D.P., et al., Nanotechnology in medical imaging: probe design and applications. *Arterioscler Thromb Vasc Biol*, 2009. 29(7): p. 992-1000.
10. Briley-Saebo, K.C., et al., High-Relaxivity Gadolinium-Modified High-Density Lipoproteins as Magnetic Resonance Imaging Contrast Agents. *J. Phys Chem*, 2009. 113(18): p. 6283-6289.
11. Long, C.M. and J.W. Bulte, In vivo tracking of cellular therapeutics using magnetic resonance imaging. *Expert Opin Biol Ther*, 2009. 9 (3): p. 293-306.

12. Soto, E.R. and G.R. Ostroff, Characterization of multilayered nanoparticles encapsulated in yeast cell wall particles for DNA delivery. *Bioconjug Chem*, 2008. 19(4): p. 840-8.
13. Chan, G.C., W.K. Chan, and D.M. Sze, The effects of beta-glucan on human immune and cancer cells. *J Hematol Oncol*, 2009. 2: p. 25.
14. Brown, G.D. and S. Gordon, Immune recognition. A new receptor for beta-glucans. *Nature*, 2001. 413(6851): p. 36-7.
15. Brown, G.D., et al., Dectin-1 is a major beta-glucan receptor on macrophages. *J Exp Med*, 2002. 196(3): p. 407-12.
16. Aouadi, M., et al., Orally delivered siRNA targeting macrophage Map4k4 suppresses systemic inflammation. *Nature*, 2009. 458 (7242): p. 1180-4.
17. Anelli, P.L., et al., Mixed micelles containing lipophilic gadolinium complexes as MRA contrast agents. *MAGMA*, 2001. 12(2-3): p. 114-20.
18. Grange, C., et al., Combined delivery and magnetic resonance imaging of neural cell adhesion molecule-targeted doxorubicin-containing liposomes in experimentally induced Kaposi's sarcoma. *Cancer Res*. 70(6): p. 2180-90.
19. Hallenga, K. and S.H. Koenig, Protein rotational relaxation as studied by solvent ^1H and ^2H magnetic relaxation. *Biochemistry*, 1976. 15 (19): p. 4255-64.
20. Aime, S., M. Botta, and E. Terreno, Gd(III)-based contrast agents for MRI. *Advances in Inorganic Chemistry - Including Bioinorganic Studies*, Vol 57, 2005. 57: p. 173-237.

Immune cell tracking with Gd-labeled Yeast Cell Wall Particles

Abstract

The search for vectors able to carry a large number of paramagnetic units prompted us to consider the recently proposed micron-sized platform of yeast cell wall particles (YCWPs). We developed a procedure for entrapping paramagnetic emulsions in the inner core of YWCPs using water-insoluble Gd-complexes, achieving the highest relaxivity ever measured for a Gd-based agent.

The high affinity of YCWPs to cells of the immune system was used to label macrophages with YCWPs and track them in an *in vivo* animal model.

In vitro experiments, performed on murine macrophages, have demonstrated a high and very fast uptake of the paramagnetic particles with good temporal persistence of the contrast and an extremely low cytotoxicity. The obtained *in vivo* results had shown that Gd-labeled YCWPs represent a very promising high sensitive MRI probes for the visualization of inflammation.

In addition, and analogously to other particulate systems, YCWPs can be loaded with lipophilic probes for other imaging modalities, and, moreover, β -1,3-D-glucan shells can be suitably functionalized to endow them with targeting abilities.

Adapted from

Multimodal tracking of macrophages labelled with Yeast Cell Wall Particles, Sara Figueiredo, Juan Carlos Cutrin, Silvia Rizzitelli, Elisa De Luca, João Nuno Moreira, Carlos F. G. C. Geraldes, Silvio Aime and Enzo Terreno, submitted.

Introduction

Tracking specific immune cells during the progression of a disease is a crucial aspect for getting an in-depth view of their role in the pathology and for monitoring the therapeutic outcome. Tracking the migration of cells requires a noninvasive imaging modality that has to be both sensitive and capable of yielding high-resolution images. Optical tomography and magnetic resonance imaging (MRI) are commonly used to observe cell migration in small animals. From the MRI point of view, the most consistent cellular labeling approaches have dealt with the entrapment of Gd-based contrast agents [1-3] or of iron-oxide nanoparticles (USPIO, SPIO, MPIO) [4-6]. The later is the most common one due to its higher sensitivity. A drawback may be represented by negative contrast produced by those superparamagnetic particles, which often generate susceptibility artifacts. Moreover, the cellular toxicity of this type of agents, on a long term basis, has been raised [7, 8]. Based on these considerations, the use of positive contrast agents appears as a promising alternative to overcome these problems, although it requests the entrapment of 10^7 – 10^8 complexes per cell, to achieve a reasonable have enough for the visualization of the labelled cells [3].

Several internalization routes have been explored in order to accumulate large quantities of paramagnetic complexes in the cell. Aiming at achieving a high intracellular concentration of the metal, cell electroporation has been used. However, such procedure results invariably in a high extent of cell death. Some cells have enhanced phagocytic activity, (neutrophils, macrophages and dendritic cells) with the ability of ingesting infectious agents, namely bacteria, virus or even senescent cells, through an actin-dependent mechanism, usually clathrin-independent [9]. Uptake of contrast agents by phagocytosis has been reported extensively for this type of cells [3, 10, 11] Herein, we report an outstanding cellular labeling methodology that allows an extremely fast internalization of large amounts of Gd complexes through the use of Yeast Cell Wall particles (YCWPs) labeled with insoluble Gd complexes.

YCWPs are mainly constituted of β -1,3-D-glucan that are extracted from the common baker's yeast *Saccharomyces cerevisiae*. Phagocytes have dectin-1 receptor that bind β -1,3 and β -1,6-D-glucans and also express other receptors that recognize foreign bodies such as parasites and yeasts. Dectin-1 on macrophages, monocytes, neutrophils and dendritic cells recognize and bind β -1,3-D-glucan, mediating the production of reactive oxygen species (ROS), and of proinflammatory cytokines, by its own signaling pathway. The outcome includes anti-tumor activities of immune cells [12].

In a precedent publication we reported about the development of a new carrier system for Magnetic Resonance Imaging based on yeast cell wall particles, in which we used them as microreactors. After been loaded with an imaging agent, the particles were exposed to a sudden change in solvent polarity therefore inducing the formation of a micro-emulsion inside the YCWPs, entrapping the probe inside their core. When loaded with gadolinium, the particles were found to have an increased paramagnetic density and enhanced relaxivity per paramagnetic centre.

Herein, we report an outstanding cellular labeling methodology that allow an extremely fast internalization of large amounts of Gd complexes through the use of Yeast Cell Wall Particles. Moreover, due to the high efficiency of the labeling technology, we were also able to exploit some potential applications of the particles, as cell tracking towards an inflamed region.

Material and Methods

Cell Preparation, Uptake experiments and MRI analysis

Macrophage (J774A.1), mouse melanoma (B16-F10) and rat hepatoma (HTC) cell lines were obtained from the American Type Culture Collection. J774A.1 and B16-F10 cells were cultured in DMEM supplemented with 2 mM glutamine, 100 U/ml penicillin, 100 mg/ml streptomycin and 10% FBS by volume. HTC cells were grown in DMEM-F12 medium supplemented with

5% fetal bovine serum, 100 U/mL penicillin, and 100 mg/mL streptomycin. The cells were always cultured in a humidified atmosphere at 37°C with 5% CO₂.

At 80% confluence, cells were detached and seeded in 10 cm culture dishes at a density of about 1×10^6 cells and twenty-four hours after seeding, cells were washed and used for the uptake experiment. Cells were incubated either with the labelled YCWPs or simply with ProHance, at 37 °C in the complete medium. After the proper incubation time, cells were washed thrice with phosphate saline buffer (PBS), detached and transferred into glass capillaries placed in an agar phantom for MRI analysis.

MRI-T₁ and T₂-weighted images were performed on a Bruker Avance 300 NMR spectrometer equipped with a microimaging probe operating at 7.05 T and on an Aspect M2™ MRI scanner (Netanya, Israel) operating at 1 T. The images were obtained using a standard multislice multiecho sequence. T₁-weighted ¹H-MR image acquired at 7.05 T (TR/TE/NEX (250/7.9/10), FOV 1 cm, 1 slice 3 mm), T₂-weighted ¹H-MR image acquired at 7.05 T (TR/TE/NEX (5000/26.4/10) FOV 1 cm, 1 slice 3 mm), T₁-weighted ¹H-MR image acquired at 1 T (TR/TE/NEX (250/7.9/10), FOV 2 cm, 1 slice, 3 mm) and T₂-weighted ¹H-MR image acquired at 1 T (TR/TE/NEX (5000/26.4/10), FOV 2 cm, 1 slice, 3 mm). The T₁ measurement of cells was performed using a standard Saturation Recovery Sequence and T₂ values were measured using a multiecho sequence (TR/TE/NEX 5000/3.3/1, number of echoes 500).

Determination of Gd content in cells

Gd content of J774A.1, HTC and B16-F10 was determined using inductively coupled plasma mass spectrometry (ICP-MS) (Element-2; Thermo-Finnigan, Rodano (MI), Italy). Sample digestion was performed with 2 ml of concentrated HNO₃ (70%) under microwave heating (Milestone MicroSYNTH Microwave labstation equipped with an optical fiber temperature control

and HPR-1000/6M six position high-pressure reactor, Bergamo, Italy). After digestion, the volume of each sample was brought to 2 ml with ultrapure water and the sample was analyzed by ICP-MS. Three replicates of each sample solution were analyzed. The protein concentration of each sample was determined from cell lysates by the Bradford method using bovine serum albumin as standard.

Confocal analysis

Cells were seeded in 26 mm coverslips at a density of about 1×10^5 cells and 24 h after seeding, the medium was replaced and cells were treated with the proper stimuli. After the end of the incubation, cells were washed and fixed in 4% paraformaldehyde containing 2% sucrose. Hoechst dye (Sigma) was added for nuclear staining. Confocal microscopy analysis was performed using a Leica TCS SP5 (Leica Microsystems s.r.l.).

Endocytosis inhibition

Cells were prepared as for the previously experiments and then endocytosis inhibitors were added to the complete medium. Concentrations of inhibitors were 10 μ M chlorpromazine, 1 μ g/mL filipin, 300 nM wortmannin and 1.5 mM amiloride. Cells were subjected to appropriate treatments for 2 h prior to the treatment with either Gd-labeled or Rhodamine-PE labeled YCWPs.

The inhibition of the endocytosis was analyzed either by MRI signal intensity, fluorescence intensity, carried out on FluoroMax-4 (HORIBA Jobin Yvon Inc., NY, USA) spectrofluorimeter, or particle location, detected by confocal microscopy, obtained on Leica TCS SP5 (Leica Microsystems s.r.l.).

Measurement of Cell Viability and Proliferation

Apoptosis was evaluated after 24 h by CellTiter-Blue® Cell Viability assay (Promega, Madison, USA). The fluorescent signal was monitored using 530-560 nm excitation wavelength and 590 nm emission wavelength. The absorbance was monitored at 570 nm and 600 nm. The fluorescent or colorimetric signal generated from the assay is proportional to the number of living cells in the sample. Results are expressed as the mean \pm SD of the percentage of viable cells of 3 different experiments performed in triplicate.

Proliferation was assessed by the determination of the cell number in each plate, over 72 h, in the presence or absence of YCWPs.

In vivo studies

All animal experiments were performed according to the guidelines for the care and use of research animals and were approved by the local Ethics Committee.

Acute liver damage was induced by injecting 8-week-old male C57BL/6 mice with CCl₄, 1 mL/kg (1:1 dilution in olive oil) intraperitoneally (ip). MRI was acquired using a T₁-weighted, fat suppressed, multi slice multi echo protocol (TR/TE/NEX 250/3.2/6, FOV 3 cm, 1 slice 1 mm). Fat suppression was performed by applying a pre-saturation pulse (90° BW = 1400 Hz) at the absorption frequency of fat (-1100 Hz from water).

MRI images were recorded before every administration and 5h after cell injection (1x10⁶ cells in 0,2 mL) to evaluate the biodistribution. Prior to MRI examination, animals were anesthetized by injecting tiletamine/zolazepam (Zoletil 100, Virbac, Carros, France), 20 mg/kg and xylazine (Rompun, Bayer S.p.a. Milan). The mean signal intensity values were calculated on region of interest drawn on the liver.

Healthy mice, injected with labeled cells or mice with acute liver

damage, injected with unlabeled cells were used as control groups.

Histological section

Animals from each group were sacrificed, and representative blocks from liver and spleen were removed for histological analysis at either time 5 h or 24 h post injection. The tissues were placed into 4% formalin for a minimum of 16 h. Afterwards, samples were prepared for snap-freezing, as it is believed that this technique preserves adequately cellular and subcellular components. Tissues were placed in saccharose buffer solution at increased concentration and later snap-frozen in liquid nitrogen. Frozen slices were obtained using a cryostat where the tissue had been previously embedded in OCT (Tissue-Tek® OCT™ Compound) prior to cryostat sectioning. Cryostat sections were sliced at 6-8 μm and mounted on gelatin-coated histological slides for hematoxylin and eosin (H&E) staining. All slices were examined either using a standard light microscope or a ZEISS ApoTome fluorescence microscope.

Statistical analysis

The mean signal intensity values were calculated in regions of interest (ROIs) drawn on livers. Analysis of images was performed in ParaVision, version 4.0. Regions of interest were manually defined by drawing contours around the liver area in every image slice and T_2 -weighted images served as reference. The analysis included pixels within the liver ROI that showed significant signal enhancement, i.e., enhancement equal to or greater than 3 times the standard deviation of the pre image.

Results and discussion

Three distinct cell lines, J774A.1, B16-F10 and HTC, were incubated either with Gd-HPDO3A or with Gd-labelled YCWPs, aiming at assessing the extent of cellular uptake of Gd(III). From the obtained results (Figure 1a), one can conclude that, for the same incubation time period, the amount extent of cellular association of paramagnetic agent encapsulated in internalized upon using β -glucan particles is much higher, and in particular for macrophages (J774A.1) is approximately 250-fold much higher (ca. 250-fold) than that found using with the non-encapsulated Gd-HPDO3A. This observation indicates a high affinity of J774A.1 macrophages towards YCWPs. It is also noteworthy that HTC cells internalized a significant amount of YCWPs, an observation that suggests the presence of several glyco-receptors (Glycocalyx, galactoxylomannan, scavenger receptors), known to have the capability to bind several macromolecules. This fact was not observed with B16-F10 melanoma cells (Figure 1b), which is in agreement with data reported in the literature, where it has been claimed that non-phagocytic cells are only able to uptake particles with a maximum mean size of 500 nm [13].

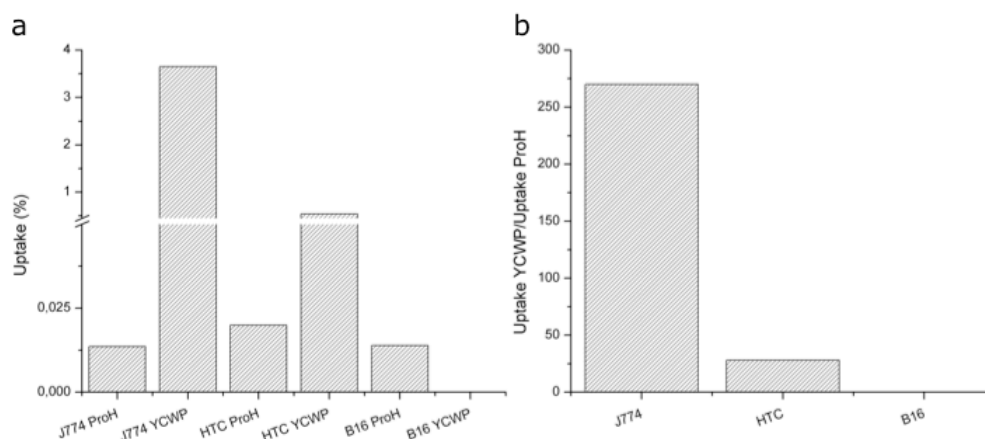


Figure 1 Extent of cellular internalization of Gd-HPDO3A and Gd-loaded YCWPs by cell lines with diverse histological origin. Macrophage (J774A.1), hepatocarcinoma (HTC) or melanoma (B16-F10) cell lines were incubated with at 37 °C for 16 h. In the end of the experiment, Gd³⁺ uptake (%) (a) and the ratio between the Gd³⁺ uptake using YCWPs or ProHance solution (b) was evaluated .

From R_1 measurements taken at different time points, it is clear that J774A.1 cells are able to internalize YCWPs at a rate that is 6 times faster than the Gd-HPDO3A complex. Interestingly, the observed R_1 difference is more significant at 1 Tesla, due to the higher values of the relaxivity of the particles at this field (Figure 2a and b) [14].

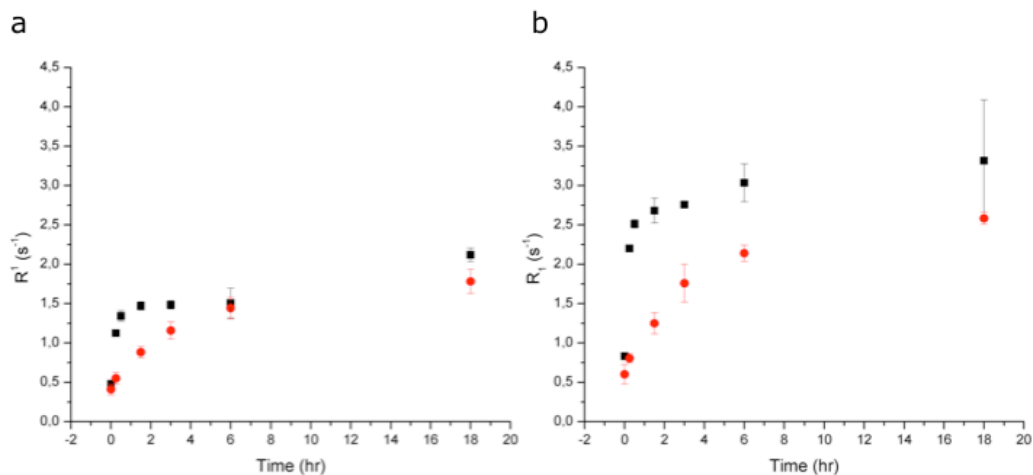


Figure 2I Kinetics of the uptake of Gd-HPDO3A (●) and Gd-labelled YCWPs (■) into J774A.1 cells, detected from the change of the water proton relaxation rates at 7.05 T (a) and at 1 T (b), respectively.

The compartmentalization of the contrast agent in the inner core of the particles results in a heterogeneous distribution of the agent yielding a marked contribution to T_2 -relaxation, thus inducing a significantly higher T_2 -enhancement at 7.05 T than at 1 T, as the T_2 increases as a function of the strength of the magnetic field (Figure 3) [14, 15].

As far as the contrast is concerned, we observed that 24 h after the incubation, the contrast induced by Gd-labelled YCWPs was still observed, both in T_1 - and T_2 -weighting images (Figure 4). However, a significant decrease in both contrast effects was detected from 6 h to 24 h. This observation is accompanied by an increase in the Gd^{3+} content in the culture medium. To get some insights on the occurring processes, confocal microscopy

experiments were carried out using Rhodamine-DPPE-labeled YCWPs (Figure 5). In the generated images, at 24 h, the contrast was dispersed throughout the cell, thus suggesting that the fluorescent payload can be intracellularly released from the β -glucan shells. This fact rationalizes the decrease in the contrast at 24 h post incubation and the distribution of the agent throughout the whole cell.

Afterward, we explored which could be the major routes of internalization of YCWPs into macrophages. upon incubation with inhibitors of the three main routes of internalization: macropinocytosis (amiloride), clathrin-mediated endocytosis (chlorpromazine) and caveolae-mediated endocytosis (filipin). Amiloride was found to be the drug that inhibited the uptake more significantly, showing that macropinocytosis is the major route of internalization used by these particles (Figure 6).

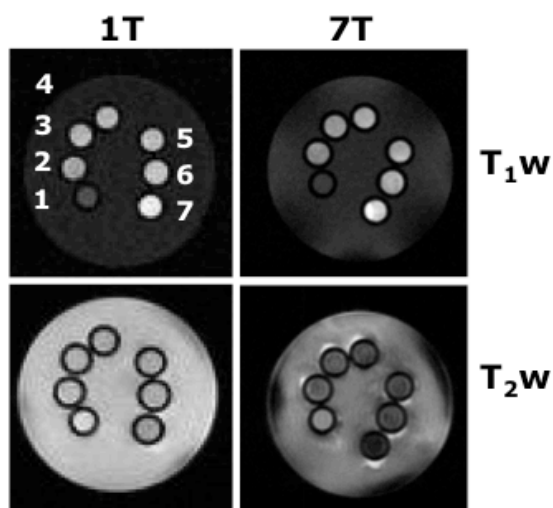


Figure 3I T_1 -w e T_2 -w images at 7.05 T and 1 T of the kinetic of internalization of Gd- labeled YCPWs in J774A.1 cells (1 - unlabeled cells, 2 - incubation time 15 min, 3 - 30 min, 4 - 1 h, 5 - 3 h, 6 - 6 h, 7 - 18 h).

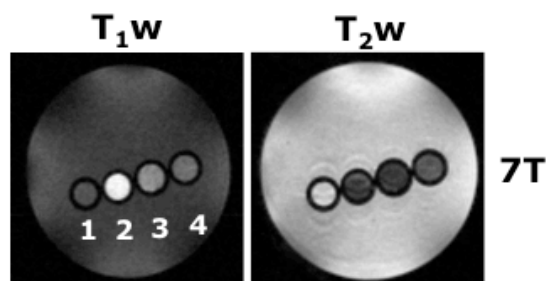


Figure 4I Longevity of MRI contrast in J774A.1 cells incubated with YCPWs (1 - unlabeled cells, 2 - 0 h post incubation, 3 - 6 h post incubation, 4 - 24 h post incubation).

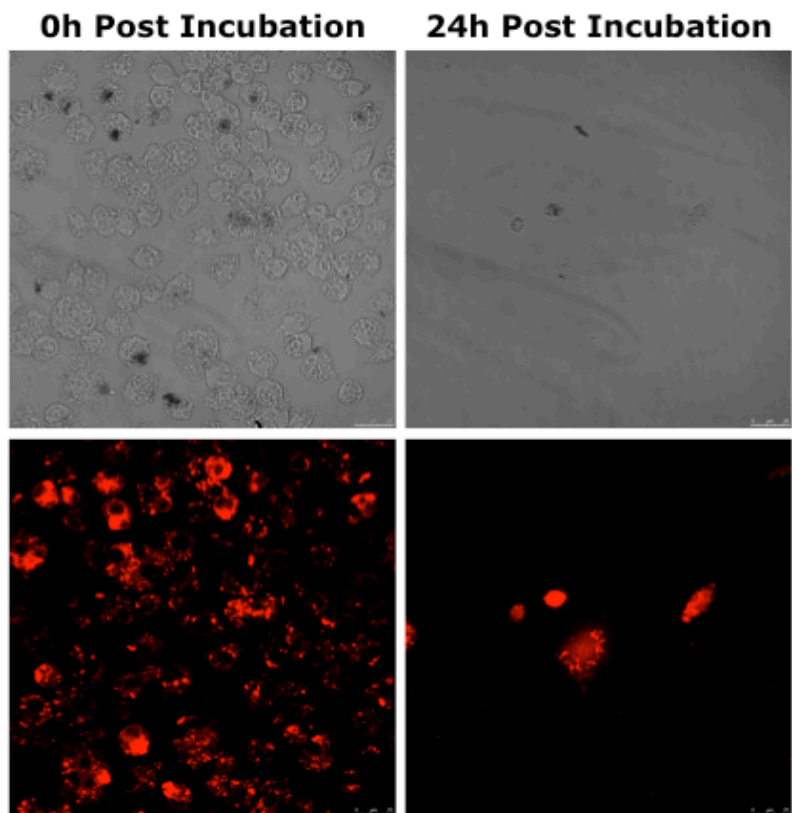


Figure 5I Confocal microscopy analysis of J774A.1 cells incubated with Rhodamine-DPPE-labeled YCWPs, immediately after the incubation and post 24 h.

This observation was confirmed by confocal microscopy experiments that clearly showed an extracellular localization of the particles (Figure 7). It is noteworthy that the interaction of the particles with the cells is likely to occur through binding to Dectin-1 receptors. The same observation could be seen in the MR images, in

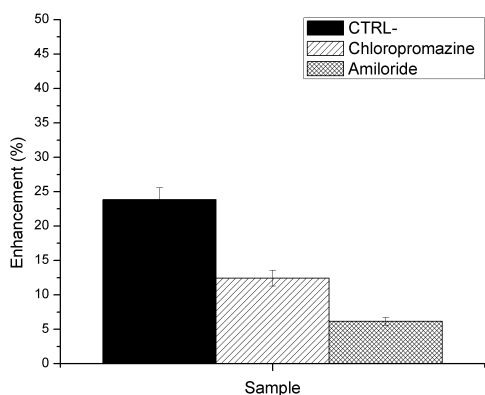


Figure 6I Effect of endocytosis inhibitors on the uptake of YCWPs by J774A.1 macrophages.

which it has been found that, using amiloride, the T_2 effect is significantly reduced, due to a decrease in the compartmentalization of the probe. On the other hand, the T_1 value has no significant difference as probably, previously, quenching effect has not been detected (Figure 8).

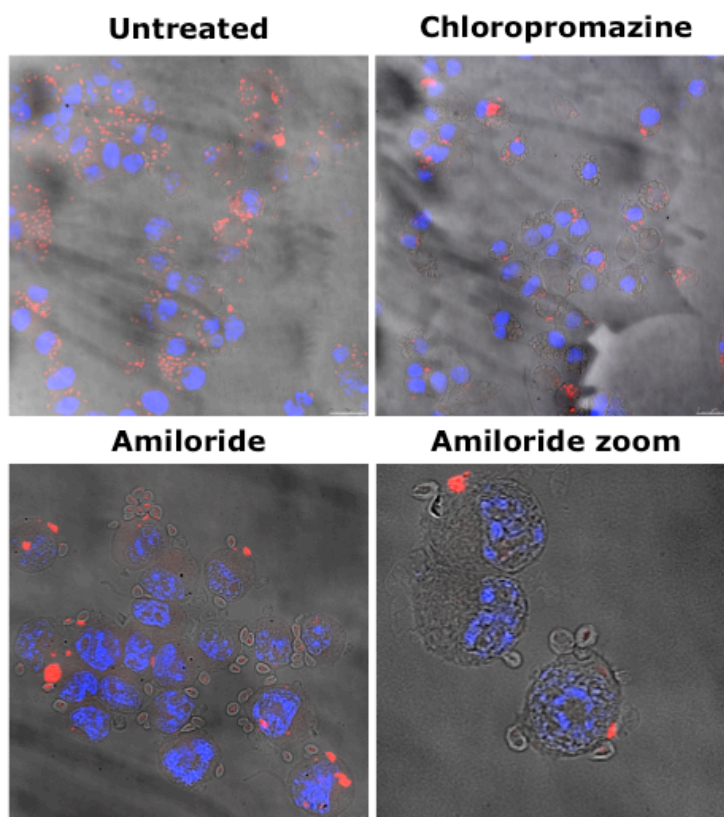


Figure 71 Confocal images of J774A.1 cells incubated with Rhodamine-DPPE labeled YCWPs, either in the presence or absence of endocytosis inhibitors.

Afterwards, the minimum number of labeled cells that could be detected by MRI has been evaluated by diluting the cells labeled with Gd-YWCs with low gelling agar and, subsequently, performing MRI analysis. So far, the minimum number of cells (HTC) detectable by MRI using a Gd^{3+} agent was ca. 500 cells/ μL , using as labeling approach electroporation and ca. 5000

cells/ μL with pinocytosis [16]. By using Gd-YCWPs, a significant contrast was still observable in the presence of ca. 300 cells/ μl (Figure 9a). Additionally, the number of significantly enhanced pixels were calculated and, as expected, more pixels appeared enhanced at 1 Tesla than at 7.05 Tesla, due to the higher efficiency of the probe at lower field (Figure 9b).

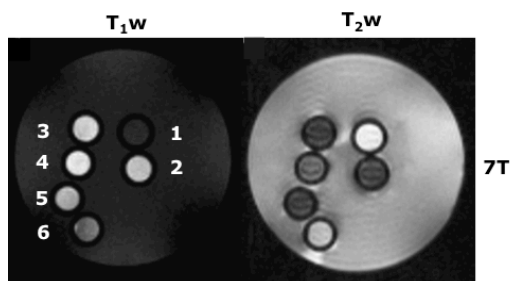


Figure 8I T_1 -w e T_2 -w images at 7.05 T of cells incubated either in the presence or absence of endocytosis inhibitors (1 - negative control, 2 - positive control, 3 - Filipin, 4 - Amiloride, 5 - Chlorpromazine, 6 - Amiloride and Chlorpromazine).

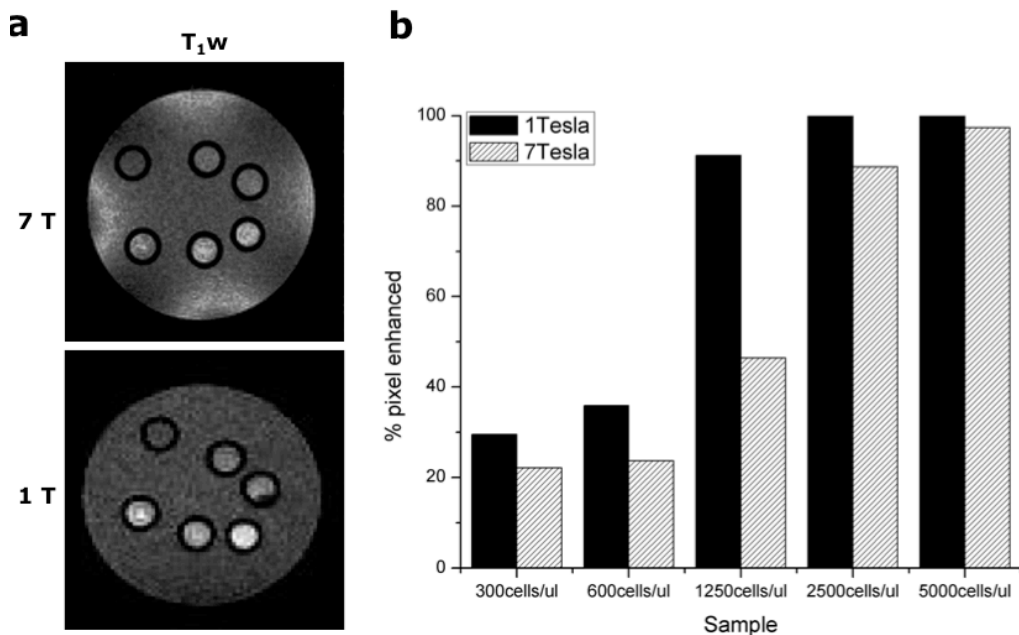


Figure 9I a) T_1 -w image at 7.05 T and 1 T of J774A.1 incubated with Gd-loaded YCWPs and diluted with agar; 1 - unlabeled cells, 2 - 300 cells/ μL , 3 - 600 cells/ μL , 4 - 1250 cells/ μL , 5 - 2500 cells/ μL , 6 - 5000 cells/ μL ; b) representation the number of significantly enhanced pixels for each cell concentration.

Finally, we assessed whether the cell viability of the studied macrophage cell line was affected by the Gd-labeled YCWPs, using a protocol based on the ability of viable cells to convert resazurin (a redox dye) into resorufin, a fluorescent molecule. Noteworthy β -glucans had no effect on the viability of the cell population, even at a concentration normally used for oriental medicinal treatments (Figure 10a). The cell proliferation was also assessed by determining the cell doubling time in the presence or absence of yeast cell wall particles, using two distinct concentrations of β -glucans (Figure 10b). The cell-division rate in the presence of labelled YCWPs resulted unaltered in respect to the untreated cells (Figure 10b). However, using a higher concentration of β -glucan particles, the velocity of duplication decreased, probably due to the overload of cells with the particles.

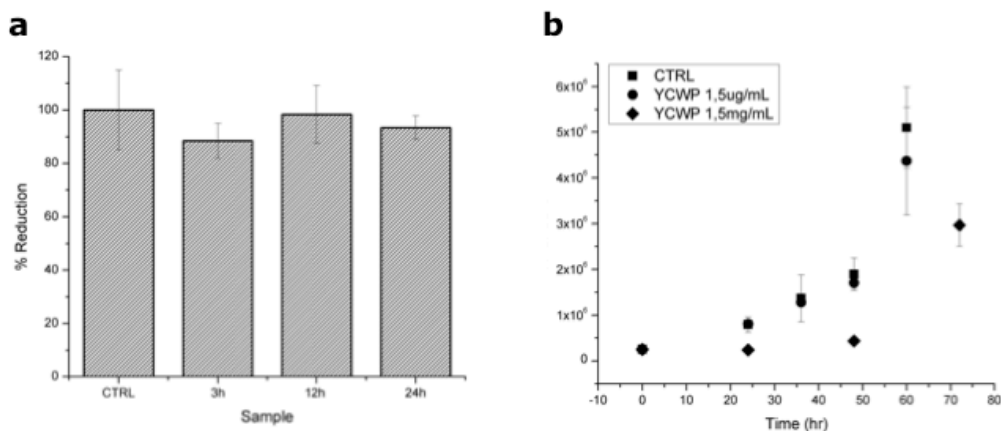


Figure 10 a) Effect of Gd-labeled YCWPs on cell viability. . The results for three different incubation times (3 h, 12 h and 24 h) are shown in histograms.b) Cell doubling time in the absence and presence of two distinct concentrations of YCWPs.

At this point we decided to assess whether it was possible to track *in vivo* macrophages incubated with Gd-labeled yeast cell wall particles. For this propose we used a model based on the intraperitoneal injection of CCl₄, a model of severe

hepatocellular damage frequently used to investigate the response of acute and chronic liver injury. The administration of carbon tetrachloride is associated with necrosis, oxidative stress of hepatocytes, inflammatory response and macrophage recruitment [17]. A recent study from Karlmark and co-workers has demonstrated that within 48h after the hepatotoxic injury there is a burst of infiltrating macrophages [18].

After the injection of Gd-labeled cells, a marked increase in liver signal was observed in a small portion of the liver region, which indicates that the labeled macrophages have successfully reached the inflamed site (Figure 11 a-d). On the other hand, with the control mice no significantly increase in the MRI signal was detected (Figure 11 e-h).

To validate the MRI cell tracking results, the same experiment was performed using fluorescent labeled YCWPs and after the proper incubation time, livers and spleens were harvested for histopathological examination. The organs were fixed and immediately snap frozen in order to maintain the integrity of the tissues. All slices were examined either using a standard light microscope or a ZEISS ApoTome fluorescence microscope, as reported in Figure 12. It is remarkable that the fluorescence detected in both liver (Figure 12 c and d) and spleen (Figure 12 g and h) was higher in the CCl₄ treated mice, represented in the images as bright spots. The high intensity of the fluorescence corresponding to the labeled cells induces a silencing of the background fluorescence of the tissue, as can be seen by comparing those images with the autofluorescence of a healthy liver/spleen (Figure 12 a and e). Also, the fluorescence decreased over time (Figure 12 c and d; g and h), as was also seen in the MRI cell tracking experiment, and that is correlated with the observations in the contrast longevity experiments (Figure 4 and 5). This way, we assume that the cells are able to migrate to the liver, as a response to the recruitment of inflammatory cells.

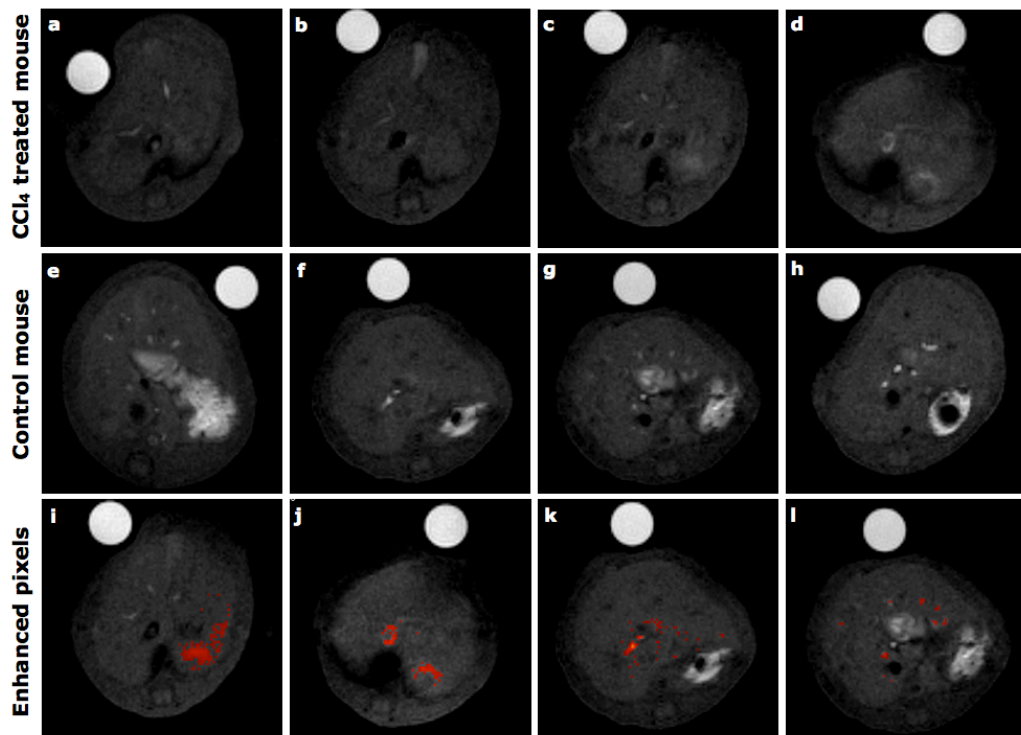


Figure 11 Fat-suppressed T_1 -weighted multislice multiecho MR images of C57BL/6 mice treated with CCl_4 (a-d) or control group (e-h). Images were obtained before (a and e) and after the injection of J774A.1 cells incubated with Gd-labeled YCWPs (b and f post 15 min; c and g - post 5 h; d and h - post 24 h). Red spots in the images from i to l correspond to statistically significant enhanced pixels (i and j are calculated from c and d; k and l are calculated from g and h).

The liver sections were also stained with hematoxylin and eosin (H&E staining). This staining allows the observation of the liver architecture. The image in Figure 13a belongs to a fixed control mouse liver and in this specimen the sinusoidal spaces around a terminal hepatic venule are quite evident. Sinusoids are the vascular spaces between the hepatic cords. It is possible to observe a radial and organized structure, typical of normal liver morphology. On the other hand, the liver parenchyma in the Figure 13b shows extensive steatosis (increase of hepatocyte fatty droplets), massive cords architectural disorganization and hepatocellular necrosis, three of the main hallmarks of the

acute CCl₄ induced hepatitis [19].

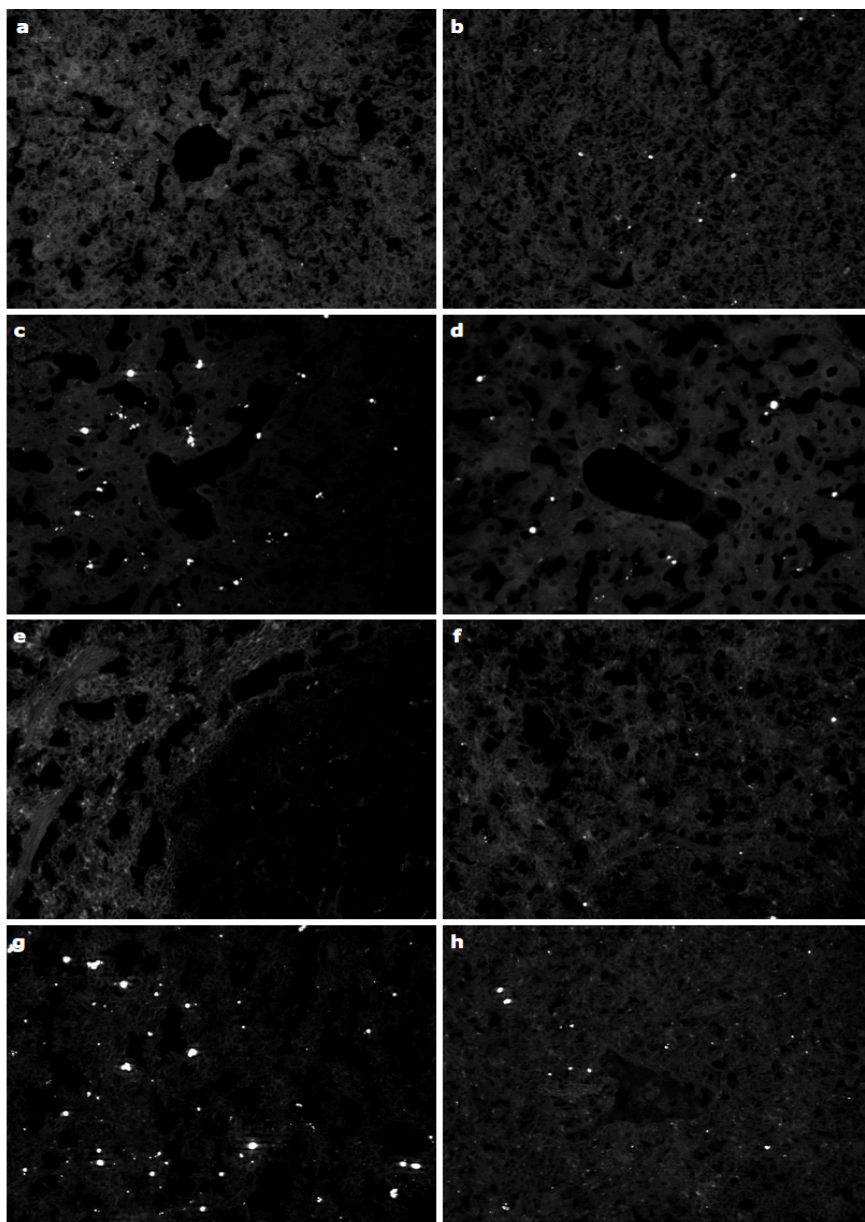


Figure 12. Fluorescence images of liver and spleen section from healthy and CCl₄ treated mice (a - control liver; b - control liver treated with labeled cells; c - CCl₄-treated mice, 5 h post injection of labeled cells; d - CCl₄ treated mice, 24 h post injection of labeled cells; e - control spleen; f - control spleen treated with labeled cells; g - CCl₄ treated mice, 5 h post injection of labeled cells; g - CCl₄-treated mice, 24 h post injection of labeled cells)

Conclusions

Non-invasive cell imaging allows the real-time tracking of transplanted cells, offering insights into several biological processes such as cell function, migration and

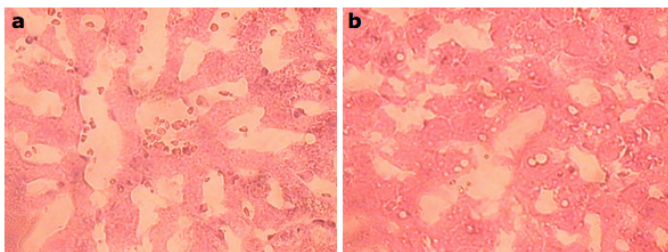


Figure 13. H&E stain of health (a) and CCl₄ treated (b) mice.

engraftment, with special interest for stem cells transplantation in cell based therapies [20]. Also macrophages are presented as potential carriers for contrast agents as they have the ability to rapidly phagocytose foreign particles. This led us to use Yeast Wall Cell Particles (YCWPs) to target this type of immune cells with the aim of using macrophages as inflammation reporters in many diseases, namely acute liver failure. This pathology is characterized by an overwhelming activation of inflammatory cytokines and mobilization of cells from the immune system. To our knowledge, although several liver-specific compounds are available for liver MRI, only superparamagnetic iron oxide particles (SPIOs) have been used to visualize immune cells in liver failure, basically through their uptake by Kupffer cells. However, it has been reported that the use of SPIOs, that generate hypointensity in the MR images, may interfere with endogenous areas of low intensity and thus create artifact issues [21, 22].

Eric Ahrens and co-workers were able to label *in vivo* immune cells with the commercially available perfluoro-15-crown-5-ether (PCE), and track them by means of ¹⁹F MRI to organs experiencing rejection. Although ¹⁹F MRI is able to provide unambiguous detection of fluorine due to the complete absence of background signal, ¹⁹F MRI images may take up to 60 minutes per scan and the detection of low levels of inflammation is still a challenge. Moreover, the proposed *in vivo* cell labeling does not allow the identification of the cell type

involved in the inflammatory process, as it is a non-specific labeling procedure and it is time-consuming, as the animals are imaged 24-48 h post injection [23, 24].

Our approach appears to be extremely efficient to label and detect the accumulation of macrophages in the damaged liver, and it would allow the assessment of the phase of acute liver failure and monitoring the therapeutic treatment. Furthermore, YCWPs can be used as immunomodulator per se or used in combination with several anti-inflammatory drugs, potentiating the effective therapeutic outcome [25].

References

1. Giesel, F.L., et al., Gadofluorine uptake in stem cells as a new magnetic resonance imaging tracking method: an in vitro and in vivo study. *Invest Radiol*, 2006. 41(12): p. 868-73.
2. Schmieder, A.H., et al., Molecular MR imaging of melanoma angiogenesis with alphanubeta3-targeted paramagnetic nanoparticles. *Magn Reson Med*, 2005. 53(3): p. 621-7.
3. Crich, S.G., et al., Improved route for the visualization of stem cells labeled with a Gd-/Eu-chelate as dual (MRI and fluorescence) agent. *Magn Reson Med*, 2004. 51(5): p. 938-44.
4. Lu, C.W., et al., Bifunctional magnetic silica nanoparticles for highly efficient human stem cell labeling. *Nano Lett*, 2007. 7(1): p. 149-54.
5. Shapiro, E.M., et al., Magnetic resonance imaging of the migration of neuronal precursors generated in the adult rodent brain. *Neuroimage*, 2006. 32(3): p. 1150-7.
6. Arbab, A.S., et al., Efficient magnetic cell labeling with protamine sulfate complexed to ferumoxides for cellular MRI. *Blood*, 2004. 104(4): p. 1217-23.
7. Pisanic, T.R., 2nd, et al., Nanotoxicity of iron oxide nanoparticle internalization in growing neurons. *Biomaterials*, 2007. 28(16): p. 2572-81.
8. Farrell, E., et al., Effects of iron oxide incorporation for long term cell tracking on MSC differentiation in vitro and in vivo. *Biochem Biophys Res Commun*, 2008. 369(4): p. 1076-81.
9. Aderem, A. and D.M. Underhill, Mechanisms of phagocytosis in macrophages. *Annu Rev Immunol*, 1999. 17: p. 593-623.
10. Bulte, J.W. and D.L. Kraitchman, Iron oxide MR contrast agents for molecular and cellular imaging. *NMR Biomed*, 2004. 17(7): p. 484-99.
11. Ahrens, E.T., et al., In vivo imaging platform for tracking immunotherapeutic cells. *Nat Biotechnol*, 2005. 23(8): p. 983-7.
12. Chan, G.C., W.K. Chan, and D.M. Sze, The effects of beta-glucan on human immune and cancer cells. *J Hematol Oncol*, 2009. 2: p. 25.

13. Rejman, J., et al., Size-dependent internalization of particles via the pathways of clathrin- and caveolae-mediated endocytosis. *Biochem J*, 2004. 377(Pt 1): p. 159-69.
14. Figueiredo, S., et al., Yeast cell wall particles: a promising class of nature-inspired microcarriers for multimodal imaging. *Chem Commun (Camb)*.2011, 47(38): p. 10635-7.
15. Bjornerud, A. and L. Johansson, The utility of superparamagnetic contrast agents in MRI: theoretical consideration and applications in the cardiovascular system. *NMR Biomed*, 2004. 17(7): p. 465-77.
16. Terreno, E., et al., Effect of the intracellular localization of a Gd-based imaging probe on the relaxation enhancement of water protons. *Magn Reson Med*, 2006. 55(3): p. 491-7.
17. Zhu, R.Z., et al., Protective effect of recombinant human IL-1Ra on CCl4-induced acute liver injury in mice. *World J Gastroenterol*. 16 (22): p. 2771-9.
18. Karlmark, K.R., et al., Hepatic recruitment of the inflammatory Gr1+ monocyte subset upon liver injury promotes hepatic fibrosis. *Hepatology*, 2009. 50(1): p. 261-74.
19. Ramachandran, R. and S. Kakar, Histological patterns in drug-induced liver disease. *J Clin Pathol*, 2009. 62(6): p. 481-92.
20. Hoehn, M., et al., Cell tracking using magnetic resonance imaging. *J Physiol*, 2007. 584(Pt 1): p. 25-30.
21. Ba-Ssalamah, A., et al., Clinical value of MRI liver-specific contrast agents: a tailored examination for a confident non-invasive diagnosis of focal liver lesions. *Eur Radiol*, 2009. 19(2): p. 342-57.
22. Oliva, M.R. and S. Saini, Liver cancer imaging: role of CT, MRI, US and PET. *Cancer Imaging*, 2004. 4 Spec No A: p. S42-6.
23. Hitchens, T.K., et al., ¹⁹F MRI detection of acute allograft rejection with in vivo perfluorocarbon labeling of immune cells. *Magn Reson Med*. 65(4): p. 1144-53.
24. Ahrens, E.T., et al., Rapid quantification of inflammation in tissue samples using perfluorocarbon emulsion and fluorine-19 nuclear magnetic resonance. *Biotechniques*. 50(4): p. 229-34.
25. Novak, M. and V. Vetvicka, Beta-glucans, history, and the present: immunomodulatory aspects and mechanisms of action. *J Immunotoxicol*, 2008. 5(1): p. 47-57.

Concluding Remarks

The main goal of the work presented herein was to develop carriers for conventional contrast agents based on the paramagnetic metal Gadolinium and the generated results have been presented in chapters **2, 3, 4** and **5**.

In **Chapter 2**, aiming at monitoring with Magnetic Resonance Imaging, drug delivery triggered by the activity of a specific enzyme, a novel liposomal formulation was described. To achieve this aim, we proposed the incorporation of a new lipopeptide, LP₁ that could work as a MMP substrate.

Later in the chapter, we were able to present an innovative liposome formulation containing the synthesized amphiphilic lipopeptides and the Gd-HPDO3A MRI contrast agent in its aqueous internal compartment, and assessed, *in vitro*, the probe release in the presence of the enzyme. The relaxivity of Lipo-LP₁, at 20 MHz and 25 °C, normalized to the millimolar concentration of the encapsulated paramagnetic complex was 1.2 s⁻¹·mM⁻¹ and in the presence of collagenases the relaxivity increases to 3.0 s⁻¹·mM⁻¹, corresponding to a r₁ enhancement of ca. 150%.

In vivo results in an syngeneic melanoma tumor have demonstrated the high potential of these nanocarriers to accumulate and release the imaging agent in the extracellular fraction of the tumor as a response to the abnormal expression of MMPs. In summary, the results obtained suggested that the liposomal formulation hereby presented has potential for future *in vivo* therapeutic preclinical studies when also incorporating an adequate drug (theragnostic agent).

In **Chapter 3** was presented the follow-up of the previous chapter. A system was created with the ability to report on any catalytic activity when the proper enzyme-substrate dichotomy is used.

As a proof of concept, a new relaxometric approach was presented in which the determination of enzyme activity was made possible via the use of a complex formed between negatively charged liposomes and a small cationic protein (protamine) as the substrate. In this particular case the protein was protamine.

The association of negatively charged liposomes and protamine led to their precipitation, reducing the r_1 relaxivity of the suspension. Trypsin, as a representative example, is able to cleave the substrate (protamine), inducing the solubilization of the aggregate and thus restoring the relaxivity to its original value. A particular point of interest is the versatility of the method as it could be expanded to work on any enzyme of interest.

Scientists in this field are constantly looking to ways to increase the sensitivity of MRI contrast agents. To achieve this goal, we have decided to go for larger agents, which are able to carry larger amounts of gadolinium chelates. In **Chapter 4** we have presented Yeast Cell Wall Particles as a promising innovative class of carriers for multimodal imaging. YCWPs can undertake a new loading procedure, in which the particle act as a micro-reactor, allowing the entrapment of a probe inside it by inducing a sudden change in the solvent polarity with the formation of an oil/water microemulsion.

Through this loading procedure YCWPs were able to internalize ca. 16 millions of Gd-DOTAMA(C18)₂ units, representing the highest paramagnetic payload ever reported for an imaging probe carrier. This observation has, as consequence, the unprecedented relaxivity of $3.6 \times 10^8 \text{ s}^{-1} \cdot \text{mM}^{-1}$ per particle. Furthermore, YCWPs can undergo a particular loading procedure that allow the loading of any lipophilic probe for any imaging modality to be achieved, thus making multimodal imaging even more powerful.

As the β -1,3-D-glucan polymer is well tolerated by living systems and has been reported as an excellent targeting vector towards macrophages and dendritic cells, we were able to use YCWPs for cell-tracking applications, especially to label and visualize cells from the immune system. This idea was the major point of interest in **Chapter 5**. In fact, we observed the rapid and effective uptake of YCWPs by macrophages and were able to detect, by MRI analysis, ca. 300 cells/ μ l, which is the lowest value ever achieved with a T_1 -based agent. Moreover, we were also able to track macrophages to the liver in a model of acute liver failure and achieved, for the first time, a significant contrast enhancement of the region of interest, using a T_1 -based contrast agent.

Thus, we have presented a new tracking approach to immune cell tracking that can potentially be used, not only for Gd-based MRI, but also for other multimodal imaging tools.

The work performed in the context of this PhD thesis has demonstrated the great potential of MRI as imaging tool. In particular, this work has highlighted its ability to report particular pathological tissue characteristics, namely enzyme expression (**Chapter 2** and **3**) and allow cell to be tracked to damaged regions in an organism (**Chapter 4** and **5**). We hope that the results hereby presented contribute to the translation of this technology towards clinical procedures.

Appendix A

¹H water relaxation rate

The contrast enhancing efficiency of a contrast agent is traditionally expressed as relaxivity, i.e. the increase of the solvent proton longitudinal and transverse relaxation rates normalized to a one millimolar concentration of the paramagnetic metal. Thus, the water proton relaxivity, r_{ip} , is defined as [2, 26, 27]

$$r_{ip} = R_{iobs} - R_{id} \quad i = 1, 2 \quad [1]$$

In eq. 1 r_{ip} corresponds to the longitudinal ($i=1$) or transverse ($i=2$) relaxation rate of the bulk water protons.

The observed relaxivity is a complex phenomenon, involving contributions from the water molecules that bind directly to the metal ion (inner sphere), from the exchangeable protons (second-sphere) and from the water molecules that diffuse near the contrast agent (second sphere). Therefore the total relaxivity is expressed as the sum of the three contributions:

$$r_i = r_{ip}^{IS} + r_{ip}^{OS} + r_{ip}^{SS} \quad i = 1, 2 \quad [2]$$

Inner-sphere contribution to the relaxivity

The inner-sphere contribution arises from the exchange of the water molecule directly coordinated to the paramagnetic metal and is given by:

$$R_{1p}^{is} = \frac{C_{tot}q}{55.6(T_{1M} + \tau_M)} \quad [3]$$

where q is the number of water molecules bounded to the metal, T_{1M} is the longitudinal relaxation time of the bounded water protons and τ_M is the lifetime of the water molecule in the inner-sphere.

The Solomon-Bloembergen theory provides the magnetic field dependence of T_{1M} , given by:

$$\frac{1}{T_{1M}} = \frac{2}{15} \frac{\gamma_H^2 g_e^2 \mu_B^2 S(S+1)}{r_H^6} \left[\frac{3\tau_{c1}}{1 + \omega_H^2 \tau_{c1}^2} + \frac{7\tau_{c2}}{1 + \omega_S^2 \tau_{c2}^2} \right] \quad [4]$$

where S is the electron spin quantum number (7/2 for Gd(III)), γ_H is the proton nuclear magnetogyric ratio, μ_B is the Bohr magneton, g_e is the Landè factor for the free electron, r_H is the distance between the metal ion and the inner-sphere water protons; ω_H and ω_S are the proton and electron Larmor frequencies ($\omega_S = 658 \cdot \omega_H$), respectively and τ_{ci} ($i = 1, 2$) are

the correlation times related to the modulation of the dipolar electron-proton coupling.

This interaction is affected by the reorientation of the paramagnetic species, τ_R , by the residence lifetime, τ_M and by the electronic relaxation times, τ_{iE} :

$$\tau_{ci}^{-1} = \tau_R^{-1} + \tau_M^{-1} + T_{iE}^{-1} \quad [5]$$

Moreover, also the electronic relaxation processes depend on the magnetic field strength.

For Gd(III) complexes τ_{iE} are related to the modulation of the zero field splitting (ZFS) of the electronic spin states due to the dynamic distortions of the ligand field interaction and, according to the Blombergen-Morgan theory, their magnetic field dependence is given by the following equations:

$$T_{1E}^{-1} = \frac{1}{25} \Delta^2 \tau_v \left[4S(S+1) - 3 \right] \left(\frac{1}{1 + \omega_S^2 \tau_v^2} + \frac{4}{1 + 4\omega_S^2 \tau_v^2} \right) \quad [6]$$

$$T_{2E}^{-1} = \frac{1}{50} \Delta^2 \tau_v \left[4S(S+1) - 3 \right] \left(3 + \frac{5}{1 + \omega_S^2 \tau_v^2} + \frac{2}{1 + 4\omega_S^2 \tau_v^2} \right) \quad [7]$$

where Δ^2 is the trace of the square of the transient ZFS tensor and τ_v is the correlation time related to its modulation.

Outer-sphere contribution to the relaxivity.

The component of the relaxivity due to the r_{ip}^{OS} term is commonly estimated by the expression derived by Freed (eqs. 8,9) which takes into account the translational diffusive motion of the water molecules, considered as hard spheres, and incorporate the effects of the electron spin relaxation.

$$R_{1p}^{os} = C^{os} \left(\frac{1}{aD} \right) \left[7J(\omega_S) + 3J(\omega_H) \right] \quad [8]$$

$$J(\omega) = Re \left[\frac{1 + 1/4 \left(i\omega\tau_d + \frac{\tau_d}{T_{je}} \right)^{1/2}}{1 + \left(i\omega\tau_d + \frac{\tau_d}{T_{je}} \right)^{1/2} + 4/9 \left(i\omega\tau_d + \frac{\tau_d}{T_{je}} \right) + 1/9 \left(i\omega\tau_d + \frac{\tau_d}{T_{je}} \right)^{3/2}} \right] \quad [9]$$

with $j = 1,2$; $\tau_d = a^2/D$

In the above equations C^{OS} is a constant ($5.8 \times 10^{-10} \text{ m}^6 \text{ mol}^{-1} \text{ s}^{-2}$) and the non-Lorentzian spectral density functions $J(\omega_i)$ contain the field dependence from $T_{1,2e}$.

At the magnetic fields of interest r_{ip}^{OS} depends primarily on the distance of water closest approach a , related to the molecular dimension and charge distribution of the complex, and on the relative diffusion coefficient of solute and solvent D .

Nuclear Magnetic Relaxation Dispersion (NMRD) profile

The field dependence of r_i by B_0 is represented in the Nuclear Magnetic Resonance Dispersion (NMRD) profile that reports about the changes in $(1/T_1)$ as function of the applied magnetic field strength. The relaxivity depends on the magnetic field either directly, or indirectly through the field dependence of the electronic relaxation times that contribute to the overall correlation time.

In **chapter 4**, the profile obtained for the paramagnetic system was analyzed using the classical relaxation model considering the relaxation contributions arising from water protons in the inner- and outer-spheres of the paramagnetic center, whereas the second hydration sphere of the complex is neglected.

Appendix B

Determination of water permeability of paramagnetic liposomes - P_w determination

In agreement with the model used to describe the relaxation rate in a two-compartment particle, R_{1p} is given by [21]:

$$R_{1p} = \left(\frac{[H_2O]^{intra\ lipo}}{[H_2O]^{total}} \right) \times \frac{1}{\tau^{intra\ lipo} + T_1^{intra\ lipo}} \quad [1]$$

where the $[H_2O]^{intra\ lipo}/[H_2O]^{total}$ ratio represents the molar fraction of water protons in the aqueous core of the particle, and $\tau^{intra\ lipo}$ and $T_1^{intra\ lipo}$ are, respectively, the residence lifetime and the longitudinal relaxation rate of the water protons in the intraliposomal compartment.

Equation 1 is only valid when the molar fraction of the entrapped water is considered very small (< 0.1) and this value can be calculated from the concentration of the Gd(III) complex inside a single vesicle. It is noteworthy that $[Gd]^{intra\ lipo}$ is usually assumed to be equal to the concentration of the complex in the solution used in the preparation of the particles. From the total concentration of the metal chelate in the suspension, $[Gd]^{total}$:

$$\frac{[Gd]^{total}}{[Gd]^{intra\ lipo}} = \frac{[H_2O]^{intra\ lipo}}{[H_2O]^{total}} \quad [2]$$

The value of $T_1^{\text{intra lipo}}$ can be calculated from the concentration of the probe inside the vesicle by neglecting the diamagnetic contribution from the liposome cavity and accordingly to the following equation:

$$T_1^{\text{intra lipo}} = \frac{1}{r_1^{\text{intra lipo}} \times [Gd]^{\text{intra lipo}}} \quad [3]$$

in which $r_1^{\text{intra lipo}}$ and $[Gd]^{\text{intra lipo}}$ are the millimolar relaxivity ($\text{s}^{-1} \cdot \text{mM}^{-1}$) and the millimolar concentration of the Gd(III) complex inside the vesicle, respectively.

$\tau^{\text{intra lipo}}$ is dependent on the diameter of the inner cavity of the vesicle ($d^{\text{inner-lipo}}$) and on the water permeability of the liposome membrane. So, for spherical liposomes:

$$\tau^{\text{intra lipo}} = \frac{d^{\text{inner-lipo}}}{6 \times P_w} \quad [4]$$

Finally, combining eqs 1-4 it is possible to obtain the equation that rules the water permeability in the membrane of a spherical nanoparticle:

$$P_w = \frac{d^{inner-lipo} \times r_1^{intra\ lipo} \times [Gd]^{intra\ lipo} \times R_{1p}}{6 \times \left[\left(r_1^{intra\ lipo} \times [Gd]^{total} \right) - R_{1p} \right]} \quad [5]$$

where both concentrations of the Gd(III) are expressed in millimoles/L.

In **chapter 3** the water permeability of the liposome membrane was determined after measuring the mean hydrodynamic liposome size by dynamic light scattering and considering a bilayer thickness of 5 nm. The millimolar relaxivity of the probe entrapped in the vesicle ($r_1^{intra\ lipo}$) was assumed to be equal to the value measured in aqueous solution at the same experimental condition ($4.2 \text{ s}^{-1} \cdot \text{mM}^{-1}$ at 0.47 T and 298 K).

A value of 0.5 s^{-1} was measured for diamagnetic liposomes, containing precisely the same amount of phospholipids, but in the absence of the Gd(III) complex (R_{1dia} value).

$[Gd]^{intra\ lipo}$ was assumed to be equal to the concentration of Gd-HPDO3A in the hydration solution (200 mM), whereas $[Gd]^{total}$ was experimentally determined by using the "bulk magnetic susceptibility" method.

References

1. Aime, S., M. Botta, and E. Terreno, Gd(III)-based contrast agents for MRI. *Advances in Inorganic Chemistry - Including Bioinorganic Studies*, Vol 57, 2005. 57: p. 173-237.
2. Aime, S., et al., NMR relaxometric studies of Gd(III) complexes with heptadentate macrocyclic ligands. *Magnetic Resonance in Chemistry*, 1998. 36: p. S200-S208.
3. Thompson, A.L., et al., On the role of the counter-ion in defining water structure and dynamics: order, structure and dynamics in hydrophilic and hydrophobic gadolinium salt complexes. *Dalton Trans*, 2006(47): p. 5605-16.
4. Terreno, E., et al., Determination of water permeability of paramagnetic liposomes of interest in MRI field. *J Inorg Biochem*, 2008. 102(5-6): p. 1112-9.

Acknowledgments

Looking back, I recon that the PhD thesis hereby presented is the outcome of a combined effort, not only mine but of all those that looked forward after my well-being and mental sanity.

First and foremost I want to acknowledge Prof. Carlos Geraldés. More than a teacher or a supervisor, he is a mentor. He taught me, consciously and unconsciously, how good science can do for you and his enthusiasm for research, motivated and kept me going through this tough endeavor, even during hard times. I doubt that I will ever be able to express fully my appreciation, but I owe him my gratitude.

I am also so very grateful to Prof. Silvio Aime, whose expertise, experience and vision added considerably value to the years spent in his group. I truly appreciate his vast knowledge and acknowledge him for all the opportunities he gave me.

A very special thanks goes to Prof. João Nuno Moreira, without whose motivation and encouragement I would not have reached this point. Under his tutelage I developed a more focused vision and he became more of a mentor and friend, than a professor.

I am particularly indebted with Prof. Enzo Terreno, who truly made a difference in my professional life. His suggestions, assistance and help along the way, as well as advice at critical times, allowed the achievement of the thesis hereby presented. He guided me not only in practical research but also gave me the capability and confidence to face many of this life frustrations. He kept me going even when I have been failed in journal's submissions (which was really hard). I learned a lot from his precious attitudes. Thank you Enzo.

This thesis would have remained a dream had it not been for the PhD programme organized by the Center for Neuroscience and Cell Biology that provided me with a tremendous education in emerging areas life sciences.

Moreover, I consider it an honor to work within the Department of Life Sciences from the Faculty of Sciences and Technology of

the University of Coimbra. It gave me great pleasure to enrich my knowledge in an institution established in 1290 that is still considered one Portugal's largest research institutions.

Appreciation also goes out to Dario Longo and Walter Dastrù for all of their computer and technical assistance throughout my graduate program.

I would also like to thank Daniela Delli Castelli, Eliana Gianolio, Giuseppe Digilio, Rachele Stefania, Simonetta Geninatti Crich and Valeria Menchise for our debates and exchanges of knowledge, as well as for venting out my frustrations during my PhD, helping the enrichment of the experience.

I owe my deepest gratitude to Juan Carlos Cutrin and to Elisa De Luca for sharing with me their expertise and technical support. It has been a great pleasure to work with you.

While writing the thesis acknowledgements I saw my self thinking on the many colleagues at the Molecular Biotechnology Center (but also at the Center for Neurosciences and Cell Biology) who offered me many suggestions and advices. Whiteout discriminating (I would certainly forget someone), to whom it may concern, many thanks. A special appreciation goes to BeB 6 for all the shared moments (Coms&BeBs always)!!

But three years in a long time in someone's life...and I cannot find words to express my gratitude to the people who have made my stay memorable and fun. Le ragazze del ufficio...mitiche Ele, Rizz, Eve, Puerto e Fra (quanto ci piace Ivrea)! Senza di voi il caffè non sarebbe oltre che una bevanda amara e ricca di caffeina!

Elena, mi sei stata vicina dal inizio fino alla fine e con te ho trovato una famiglia in Italia con tutto ciò che una ha di buono - la pizza della tua mamma e il tiramisù del tuo "babbo"!! Non avrei scelto un'altra persona con chi girare il mondo (quante storie ci sono da raccontare...che ridere!!!)...e rimarrai per sempre attaccata al mio frigo ed al mio cuore!!! Trust yourself girl!!!!!!

Rizz, mia Silvia! Sei stata l'eccezione alla mia regola "i colleghi sono colleghi, non amici"!!! Hai tante volte capito quello di cui avevo bisogno, senza alcuna richiesta...e mi sei stata sempre a fianco sia nei momenti belli che nelle avversità! Quanto mi hai sostenuto ed incoraggiato...quanti topi hai sacrificato (si dovrebbe leggere "ammazzato") a conto mio!!! Ti devo anche ringraziare per l'aiuto con il mio italiano (eheheh)!! Comunque...mi raccomando...le ciambelle!!!!!!!

Vorrei anche ringraziare gli "altri" amici...soprattutto quelli che mi sono stati accanto in questo ultimo difficile periodo - ho potuto, posso e potrò sempre contare con voi!!

Foi sem dúvida a minha família que me "sustentou" durante todo este percurso que culminou nestas últimas frases! Mãe, pai, Jorge e Rui...quantas vezes me foram buscar à escola, às explicações, às discotecas...Sei bem que foram noites e dias sem fim que culminam numa gratidão infinita que espero um dia recompensar! Nada disto teria sido possível sem a vossa presença continua! É a vocês que devo o facto de ser aquilo que sou hoje.

Last but not least, agradeço ao meu conselheiro gráfico que acompanhou de bem perto todo este meu percurso, colaborando de tantas maneiras e dando um sentido ao meu universo caótico - de que serve querer conquistar o mundo se não tiver alguém com quem festejar?! Para ti e por tudo, obrigada.

"Everybody is a genius.

But if you judge a fish by its ability to climb a tree, it will live its whole life believing that it is stupid."

Albert Einstein